DOE/NEER/PURDUE-C03-02

Annual Technical Report

for

THE MONTE CARLO-BASED DOSIMETRY OF BETA EMITTERS FOR INTRAVASCULAR BRACHYTHERAPY

For the Period of June 1, 2000 through May 31, 2001
(With no cost extension through May 31, 2002)

Under

DOE Contract Number: DE-PS07-99ID13730
R&D Project ID: DE-FG07-99ID13782

Submitted by

Professor Chan K. Choi
School of Nuclear Engineering, Purdue University
1290 Nuclear Engineering Building
W. Lafayette, IN 47907-1290

(765) 494-6789; e-mail: choi@purdue.edu

June 2002

The Monte Carlo-Based Dosimetry of Beta Emitters for Intravascular Brachytherapy

ABSTRACT: Monte Carlo techniques for radiation dosimetry and the experimental verifications of the Monte Carlo simulations have been developed for the treatment geometry of intravascular brachytherapy, a form of radionuclide therapy for occluded coronary disease (restenosis). Utilizing the recent version of the Monte Carlo code, MCNP4C, on both Sun workstations and Intel PC's, the radiation dose that is generated from the encapsulated array of β-emitting seeds (^{90}Sr/Y-source train) has been calculated in both linear and curved coronary vessels. At the total activity of 42 mCi (1.55×10^9 Bq), dose delivery varies from 32.05 to 0.63 Gy/min as the radial distance (r) from the source central axis increases from 0.5 to 5.0 mm in the linear vessel model. The dose rates at $r = 2$ mm in the lesion, which corresponds to the reference distance recommended by AAPM TG 60, are related to: 5.92 Gy/min in the central seed region of the ^{90}Sr/Y beta-source train, and 3.32 Gy/min in the last seed region at the edge of the source train. The present investigation attempted for the first time the effect of the seed curvatures on the actual dose delivery to the target area in coronary vessels. While the dose difference for the 5-degree curved vessel at the prescription point of r = 2.0 mm is 7.41%, within the 10 % guideline set by the AAPM, however, the difference increased dramatically to 16.85 % for the 10-degree case. This suggests the formation of the hot and cold areas of dose delivery in the curved coronary arteries. As the radial distance increases beyond $r =$ 3 mm, the degree of increase in dose in the region of inward curvature is further enhanced, while in the region of outward-curvature the change in dose remains less significant. Solid water phantoms have been fabricated to measure the dose on the radiochromic films that were exposed to the beta source train under linear and curved-vessel geometries ranging from 5 to 10 degrees. The radiochromic films were pre-exposed to the Gammacell irradiator for the constant exposure with 10 Gy. The experimental dose measurements are in good agreement with the simulation results for the r- θ iso-dose contours and the radial dose rates.

Keywords: Monte Carlo, intravascular brachytherapy, radiation dose, beta-emitters, GafChromic film.

ACKNOWLEDGEMENTS

The principal investigator would like to express his sincere appreciation to Dr. Prasanna Kumar, Chief of Medical Physics at the Deaconess Hospital in Evansville, Indiana, for his generosity and collaboration for our performing beta-dosimetry measurements for this current project. Support and encouragement from the NEER program manager, Ms. Nancy Elizondo at the DOE Idaho office, for the current project and the graduate students are gratefully acknowledged.

TABLE OF CONTENTS

I. INTRODUCTION

Intravascular radiation (or intravascular brachytherapy, IVBT) using γ - or β - emitters right after balloon angioplasty is the state-of-the-art radiotherapy modality to inhibit restenosis (reclosure of a blood vessel after angioplasty). Approximately 40% of patients undergoing the interventional coronary procedure (*i.e.*, over 160,000 annually in the United States) have angiographic evidence of restenosis by 12 months, which results in the need for repeated interventional procedure.[1] The economic impact from this re-procedure in the United States is estimated to be about $billion per year.

Among the isotopes for potential use in intracoronary irradiation, ^{90}Sr/Y appears to be an ideal source.[2] For this reason, a catheter-based β-emitter source (e.g., Beta-Cath, developed by Novoste Corp.) is one of the systems under clinical trials for IVBT. The radiation is supplied by a segmented-train source of encapsulated ^{90}Sr/Y seeds. This beta-emitter IVBT system is chosen for the current investigation of the Monte Carlo dosimetry analysis. In the current clinical trials, the dose calculation is based on either the vendor-provided measurement data or the recommendations by the Radiation Therapy Task Group No. 43 of the American Association of Physicists in Medicine (AAPM), or AAPM TG-43.[3] However, these protocols do not properly account for the complicated source geometries (e.g., guide wire, stent, and coronary vessel curvatures) and tissue inhomogeneity. The irradiated target site is generally located in a very complicated geometry that consists of both delicate human organs and source delivery components. In addition, there are significant contributions to dose from the secondary radiations such as fluorescent x-rays and atomic electrons. Due to the vicinity between a prescription point and the central axis of the seeds (2-3 mm), the measurement of dose variation is not

readily available at this scale. The Monte Carlo method is the only practical solution for difficulties described above; it is highly accurate and intrinsic for inhomogeneity, not subject to any geometrical constrain, and also includes all levels of electron/photon transport.

If this state-of-the-art radiotherapy is clinically justified, an established dosimetry routine for the treatment planning for individual patients will immediately be implemented. This is the primary motive of the project. Therefore, this project aims to develop the Monte Carlo-based dosimetry protocol for accurate calculations of absorbed dose in intravascular brachytherapy. The developed dosimetry package will efficiently account for the complicated treatment geometries such as the curvature of radioactive seeds, gold markers, a stent, and calcified plaque. This project also developed the experimental capabilities for measuring the 2-D doses with linear and curved coronary vessels using radiochromic film. Most of the computational tasks have been performed during the first year of the two-year project (with no cost extension into the third year) while the experimental verifications have been completed during the second/third year period.

This second-year annual report is to document the computational and experimental efforts and to analyze the initial results as detailed in the following sections. Firstly, the scheduled tasks for the current project period will be reviewed in Section II and then the corresponding tasks performed will be presented in detail in Section III. Further discussions of the current accomplishments of the project will follow in Section IV.

II. OBJECTIVES AND SCHEDULE OF TASKS

This project aimed at developing, in the first year, the Monte Carlo-based dosimetry protocol for accurate calculation of absorbed radiation dose for a catheter-based, beta-emitting intravascular brachytherapy system. During the current project period (June 1, 2000 through May 31, 2002), the experimental verifications of the Monte Carlo simulations have been performed. The Monte Carlo simulation for the dosimetry protocol and the experimental characterization of the catheter-based, beta-emitter brachytherapy have been accomplished in the following five distinct tasks during the current project period:

Task 6 (05/00–8/00): Phantom construction/fabrication; Review clinical treatment information and dosimetry protocols;

Task 7 (08/00–03/02): Experimental radiochromic film dosimetry and experimental measurements for linear vessel using solid water phantom;

Task 8 (08/00–03/02): Auxiliary calculation and experimental measurements for curved vessel geometries with phantom;

Task 9 (08/01–03/02): Possible development of treatment planning software – iso-dose contour development;

Task 10 (03/02–05/02): Complete MCNP dosimetry protocol; Project final report

The primary tasks of this project period were to simulate the various treatment geometries of the linear and curved coronary-vessel models, and to verify the MCNP(MCNP4C)[4] simulations with the corresponding experimental measurements.

In the following section, work performed during the second year of the current project period will be described in detail. Calculations of test dosimetry and the experimental measurements will be presented in section III. Experimental studies to verify the Monte Carlo dose calculations for trained beta-sources model and film

dosimetry using a densitometer and Gaf-Chromic films are documented for both linear and curved vessel geometries. The modeling of the linear and curved vessel models with the updated source compositions and 0.5-mm spatial resolution is documented in Section III-1, which complies with the most recent AAPM Task Group 60 recommendations.[5] The agreement between MCNP calculations and the measurements (provided by the vendor) in the region of r = 1.0–3.3 mm was fair (< 5%). Actually, this range corresponds to the region of interest for IVBT. In particular, the MCNP dose rate at r = 2 mm is determined to be 8.38 cGy/sec, which is almost equal to the vendor-provided data (8.4 cGy/sec). However, the large deviations appear in the region of r < 1.0 mm and r> 3.3 mm. The MCNP calculations show more exponential-like behavior of dose rate than the vendor-provided data. The higher dose of MCNP in r < 1.0 mm would be more reliable considering large potential errors from experimental difficulties at this sub-mm scales, while the higher dose of MCNP in r > 3.3 mm might be less reliable due to the artifacts of MCNP for extremely large Coulomb interactions in low energy (< 10 keV). The simulations for the curved vessel confirm that there exist the hot and cold areas in the treatment region because of a partially high degree of curvature in the coronary arteries. The inward curvature is noted to increase the dose level along the radial distance while the outward curvature is attributed to the reduction in the dose level. The dose variations are found to be directly proportional to the angles shifted between neighboring seeds as described in detail in section III-1.

Section III-2 describes in detail the experimental measurements for the linear and curved coronary vessel geometries with prefabricated solid water phantom. Experimental set-up, pre-measurement of the dose calibration with the Gaf-Chromic film,

and the measurement of actual dose rate are described in section III-2 in detail. The r- θ iso-dose contours and the dose rate comparisons between the Monte Carlo simulations and the experimental dose measurements have been analyzed in section III-2.

III. WORK PERFORMED DURING THE SECOND YEAR OF THE PROJECT

III-1. Monte Carlo Dosimetry Simulations

A. The Monte Carlo Code

The recent release of the MCNP4C, the Monte Carlo transport code upgrade originally developed by the Los Alamos National Laboratory (LANL) [4], provides a versatile treatment for the dosimetry calculations in brachytherapy, overcoming the complicated geometry. The new version of MCNP has a capability for a better electron transport, compared to the old version of MCNP4B.

The simulations are done with the MCNP4C code operated by the UNIX system on a Dell Precision-620 Minicomputer Workstation with Pentinum III Xeon. The linear vessel model with 1,000,000 particle histories in photon/electron transport mode takes cpu time of 377.47 min (6.3 hr), computing for 196 voxels. On the other hand, the curved vessel model simulation takes 2 days.

The *F8 tally is used to find out a deposited energy into the scoring voxels (in units of MeV per emitted beta). The statistical errors for all simulations are within 5%, for which the all ten statistical checks are passed. Some of the actual codes used in this study are shown in Appendix A and B.

B. Encapsulated β-emitter Source ^{90}Sr/Y (Beta-Cath System™ developed by Novoste Corp)

This source consists of a cylindrical train of 12 source seeds, a guide wire and proximal/distal gold markers (Fig.1), where each seed has 0.64 mm in diameter and 2.5 mm in length (Fig.2). From the vendor provided data, a total activity of 42 mCi

($1.55x10^9$ Bq) is specified for the entire source of 12 seeds, each seed having 3.5 mCi in the form of strontium titanate ceramic. The source is contained in a closed-end catheter, which is otherwise filled with a standard saline solution. The sources are delivered to the end of the single lumen catheter and withdrawn by hydraulic pressure using a device designed for this purpose, shown in Fig.3. When not in use, they are stored inside the delivery device, in which they are surrounded by acrylic plastic shielding.

Also, the decay schematic of this isotope is shown in Fig.4 [7,8]. Therapeutically useful electrons come from the higher energy β of ^{90}Y decay; its average β particle energy is 0.934 MeV with a range in water of 3.8 mm, and its maximum energy of 2.27 MeV has a range of 1.09 cm. Most of the betas from ^{90}Sr decays ($E_{ave}(Sr)$=0.18MeV, R=0.035 cm) are absorbed in the stainless steel wall of the source encapsulation.

The ranges discussed above are calculated by the following empirical equation for electrons in low-Z material relating the range in g/cm^2 to the kinetic energy T in MeV[6]:

For 0.01<T<2.5 MeV,

$$\mathbf{R=0.412T^{1.27-0.0954lnT}}.$$

This range of $^{90}Sr/Y$ is very ideal in that there would be less damage in surrounding healthy tissue, since the diameter of coronary arteries is about 2-4mm.

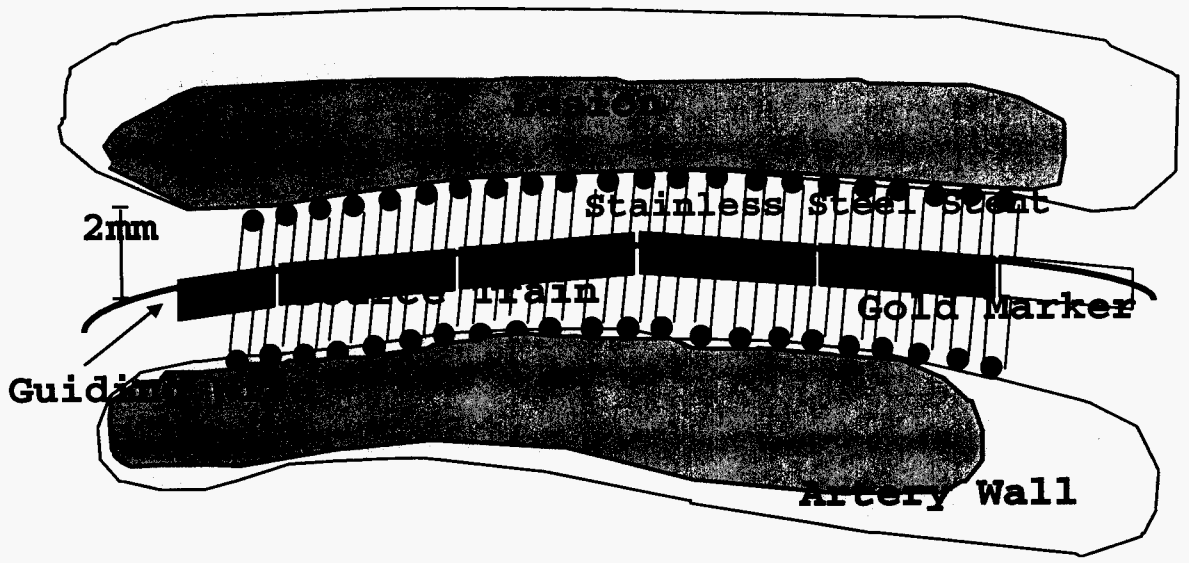

Figure 1. Schematic of complete treatment geometry of the intravascular brachytherapy using the catheter-based encapsulated β-emitter Source ^{90}Sr/Y and surrounding stent.

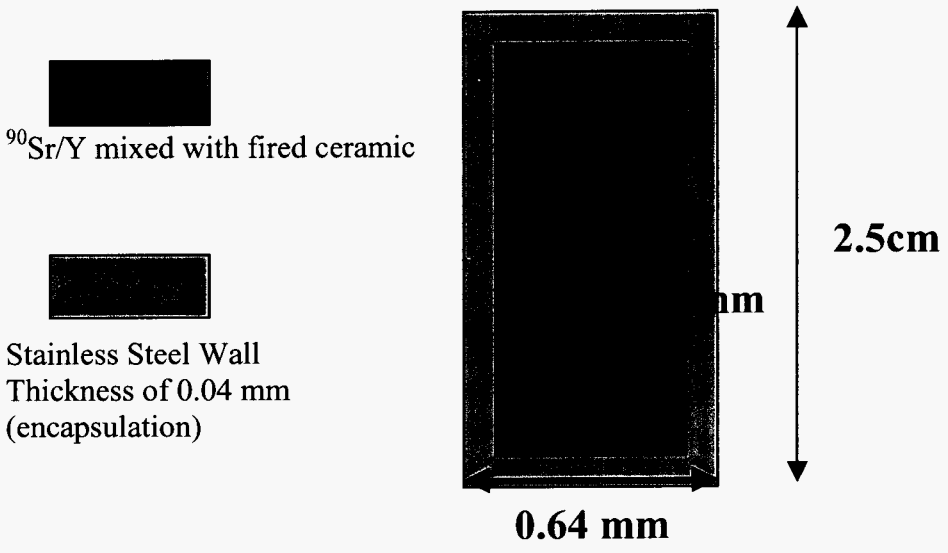

Figure 2. ^{90}Sr/Y Seed Description

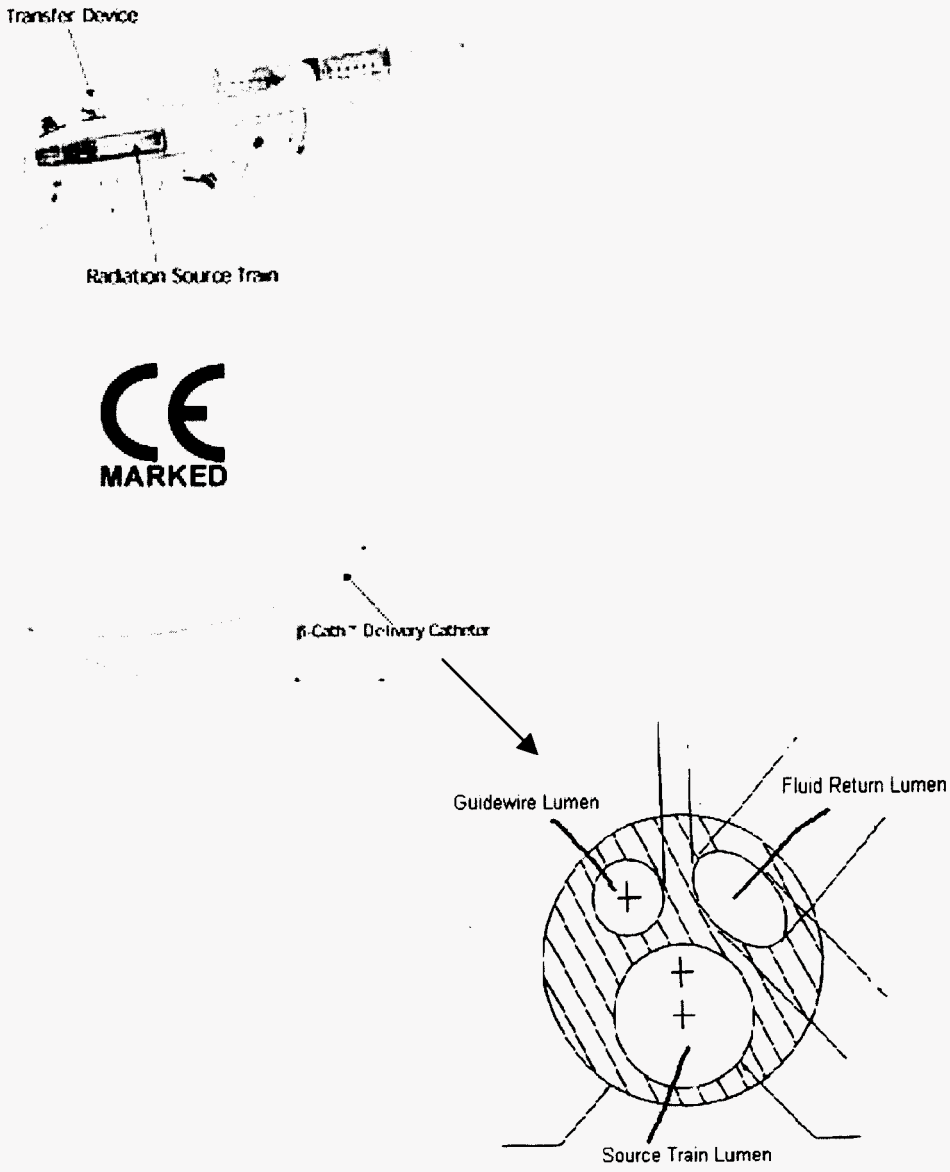

Figure 3. The Novoste beta-cath system™, and illustration of its catheter's cross section

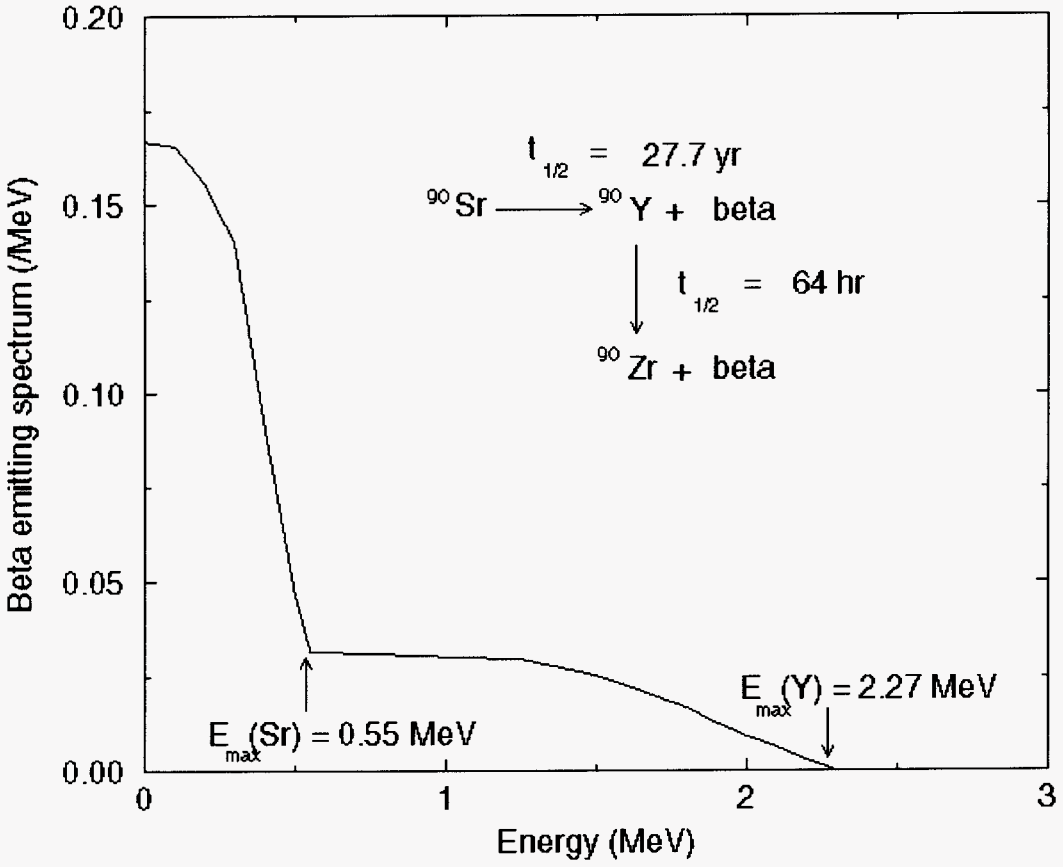

The electron range in water:
.35 mm at E_{ave}(Sr)=0.196MeV
3.8 mm at E_{ave}(Y)=0.934MeV

Figure 4. Energy Spectrum and Decay Scheme of β-emitter, ^{90}Sr/Y

C. The MCNP Simulation of the Linear Vessel Model

It is estimated that the contribution beyond the third neighboring seed, that is beyond ~5mm, is negligible[23]. Therefore, although the actual source consists of 12 seeds, only five seeds are explicitly modeled in our simulations. For the resolution of 0.5 mm recommended by AAPM Task Group (TG) No.60 [5], the surrounding water space is divided into 0.5 x 0.5 x 0.5 mm voxel lattices, to which the dose is computed. The MCNP modeling geometry for the linear vessel is shown in Fig.5.

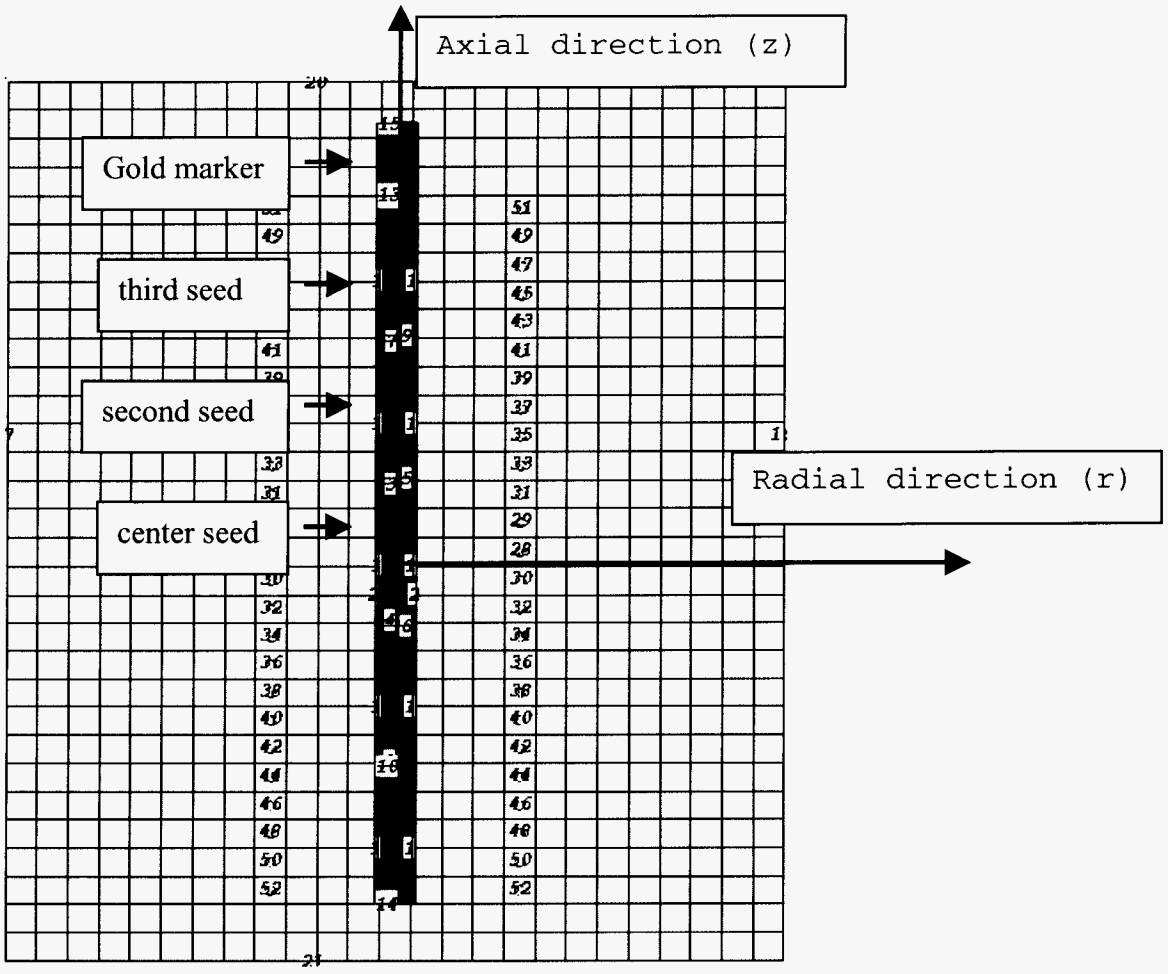

Figure 5. Schematic of the MCNP modeling geometry consisting of five seeds. Each voxel is 0.5 mm length in the axial and radial direction.

Furthermore, the region of interest in the simulations is normally not beyond 1 cm in the radial direction and 3 cm in the axial direction, due to a very short distance between the prescription point (2 mm) and the source centerline in IVBT.

In the simulation of the linear vessel model, all the five seeds are active. The radial dose distribution obtained for the linear vessel geometry is depicted in Fig.6. As the radial distance (r) increases from 1.5 mm to 6.0 mm, the dose rate drops very steeply from 8.99 to 0.27 Gy/min. At the prescription point of 2.0 mm, the result was 5.92 Gy/min.

Table 1 shows the dose rates in each voxel for the linear vessel model. It is found that the electron field at the edge of the last seeds and gold marker drops gradually along the source axis (z-axis). This reduced dose with the balloon induced trauma seems to cause restenosis in the region of the source end, called edge effect, and is shown explicitly in Fig. 7. For example, for r=2.0 mm, the dose rate decreases from 5.92 Gy/min to 3.32 Gy/min, as z changes from 0 mm to 6.0 mm. This is a decrease of 44% at the edge voxel (z=6.0 mm), compared to that of non-edge voxel (z=0 mm). Thus, the treatment length by the source train is always less than its physical length. Consequently, one has to consider this reduced radiation dose at source end for defining the real treatment length.

Also, for safe clinical usage, it is important to provide the equal dose regions around the source from the simulation data. An iso-dose curve is shown for the linear model in Fig. 7 [9]. This figure clearly depicts how the equal dose rate region changes in the coronary artery.

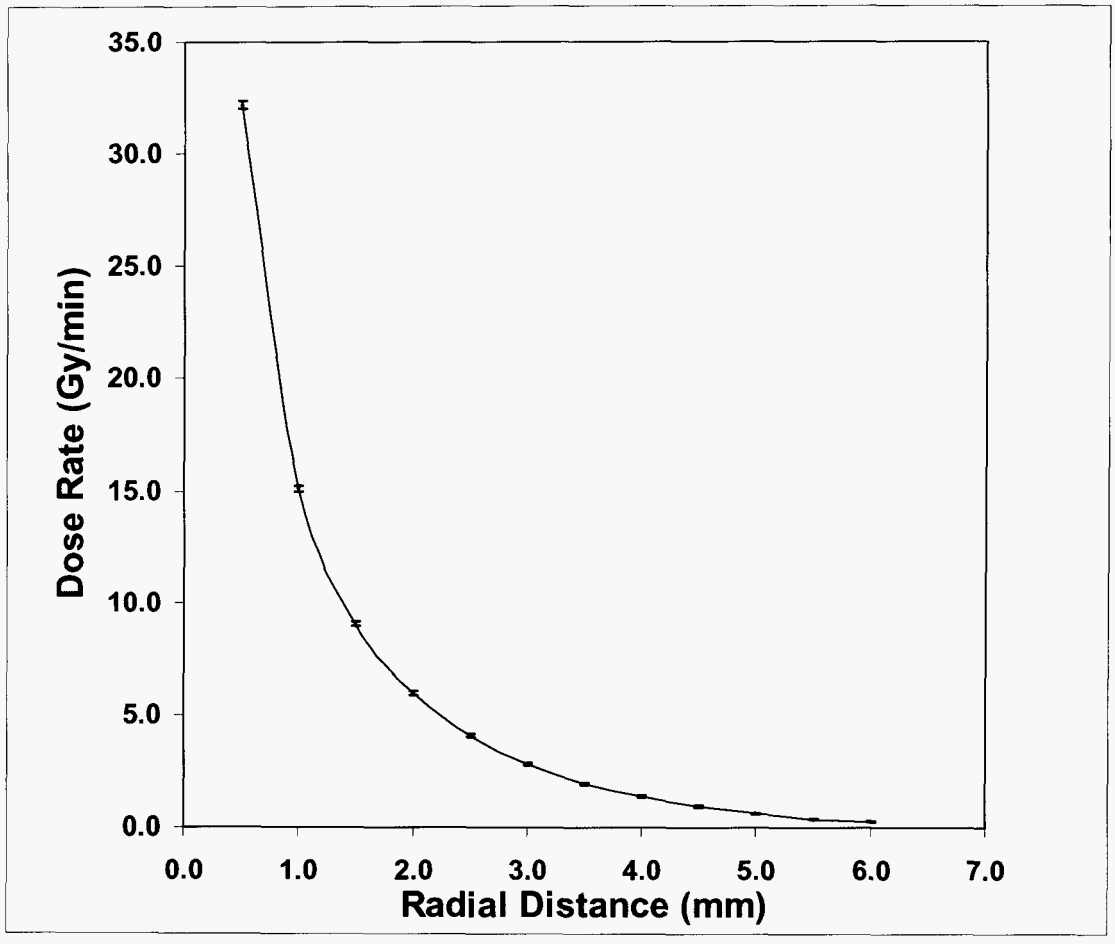

Figure 6. Dose rate distributions along the radial direction at z=0

Table 3. Dose rate distributions in the linear vessel model with the gold marker (Gy/sec). (z, r in mm)

z / r	*0.0*	*0.5*	*1.0*	*1.5*	*2.0*	*2.5*	*3.0*	*3.5*	*4.0*	*4.5*	*5.0*	*5.5*	*6.0*
0.5	32.05	31.48	29.39	29.27	31.32	31.81	31.39	29.55	29.10	30.77	30.95	29.32	22.68
1.0	15.06	15.16	14.77	14.67	15.20	15.23	14.98	14.66	14.18	14.20	13.83	12.45	9.52
1.5	8.99	8.88	8.68	8.82	8.84	8.85	8.76	8.63	8.26	8.02	7.62	6.54	5.37
2.0	5.92	5.81	5.73	5.70	5.72	5.67	5.68	5.60	5.29	4.99	4.79	4.13	3.32
2.5	4.04	4.00	3.99	3.99	3.86	3.94	3.98	3.79	3.63	3.43	3.11	2.80	2.25
3.0	2.79	2.93	2.91	2.75	2.74	2.67	2.71	2.63	2.60	2.35	2.12	1.87	1.58
3.5	1.95	1.95	1.98	1.88	1.91	1.94	1.88	1.86	1.64	1.60	1.43	1.32	1.14
4.0	1.38	1.39	1.39	1.32	1.32	1.34	1.31	1.22	1.20	1.11	1.03	0.91	0.79
4.5	0.95	0.87	0.94	0.96	0.96	0.84	0.81	0.80	0.77	0.76	0.71	0.63	0.55
5.0	0.63	0.63	0.61	0.60	0.62	0.54	0.53	0.55	0.51	0.52	0.51	0.41	0.32

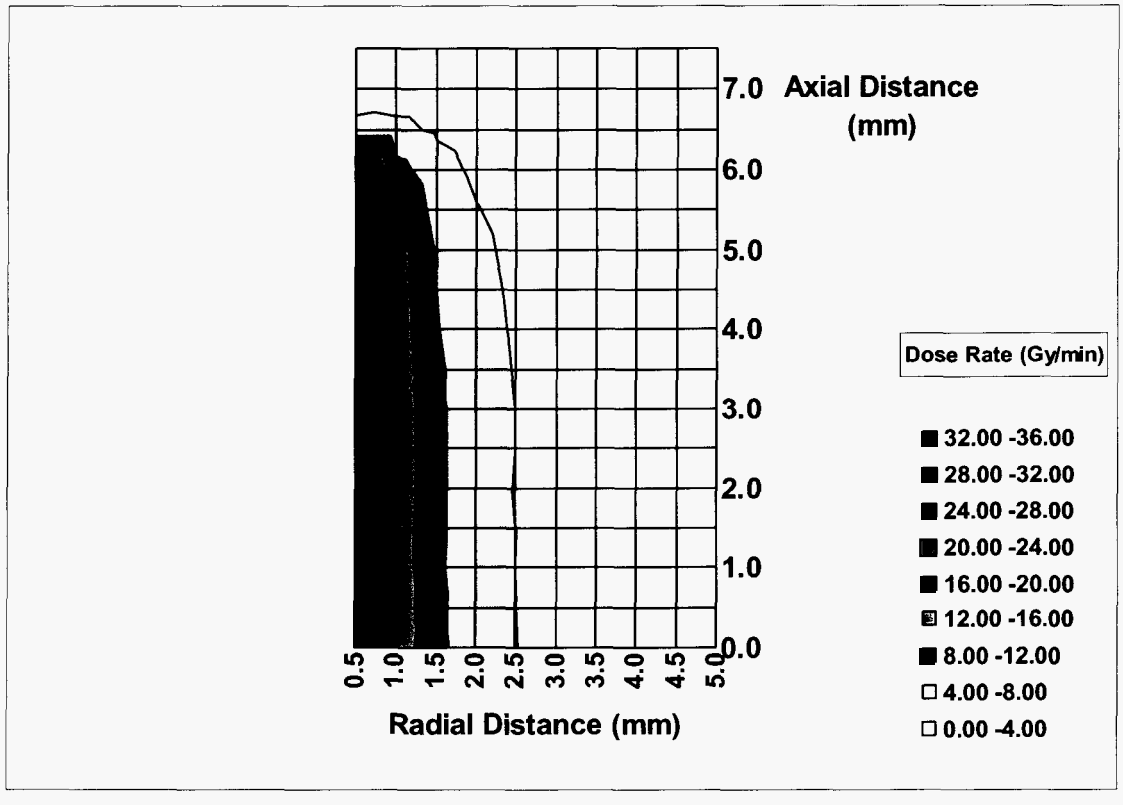

Figure 7. Iso-Dose curve for the linear model.

D. The MCNP Simulation of the Curved Vessel Model

AAPM TG60 also recommends the dose rate to the arterial wall to be uniform within 10% around the source and along the centered two-thirds of the treated length. The possible factors that affect dose uniformity to the arterial wall are:

1. Centering of the source in the artery
2. The cylindrical symmetry of the artery
3. The curvature of the artery.

The source centering effect is studied by several authors[10,11]. Chibani et al. [11] introduced Dose Perturbation Factor (DPF) = (dose with a source offset)/(dose with a centered source), and quantified the effect for the beta-cath system as follows:

Offset (mm)	-1	-0.5	0.5	1
At r=2.0 mm	0.47	0.68	1.53	2.63

Since the beta-cath system does not contain the centering device in itself, and in fact the source lumen within the delivery catheter is offset, this analysis of the source offset is critical. They concluded that the source offset effect need to be included in the dosimetry protocol for the beta-cath system™.

This research is focused to investigate the curvature effect, which has not been studied. It is important to know the dose non-uniformity caused by the curved source in terms of dose rates, since coronary vessels are very tortuous. Also, this study is interested in finding out how much of the source curvature causes the dose non-uniformity around the source larger than ±10%.

The curved vessel model is simulated in this study to estimate the amount of overdose and underdose caused by the curvature of coronary arteries. The MCNP

simulation geometry for the curved model is shown in Fig.8, in which each source seed is shifted by 5° with respect to the neighboring seed toward the positive r direction, resulting in the radius of the curvature of 2.86 cm. The 10° shift case is modeled as well (the radius of the curvature of 1.43 cm). In Fig.8, the expected overdose/underdose areas are defined: inside the curvature (inward) for overdose, and outside the curvature (outward) for underdose[12].

The dose rates, along radial direction at z=0, are compared with those of the linear model in Table 2. The dose rates found from the curved model is plotted with the dose rates of the linear model in Fig.9. Also, the percentage dose differences are shown in Table 3, and graphically in Fig.10. In particular, at the prescription point of r=2.0 mm, compared to the dose rate of the linear model, 5° model had +3.87% overdose for inward direction and −3.54% underdose for outward (minus sign indicates that it is less than the dose rate of the linear model)[13,14], where the 10° model had +9.95% overdose and -6.88% underdose. This implies that the current dosimetry protocols used for IVBT, which neglect the curvature effect, could not accurately deliver a prescription dose to the arteries. Therefore, the IBVT dosimetry has to take into account the curvature effect for its dosimetry planning.

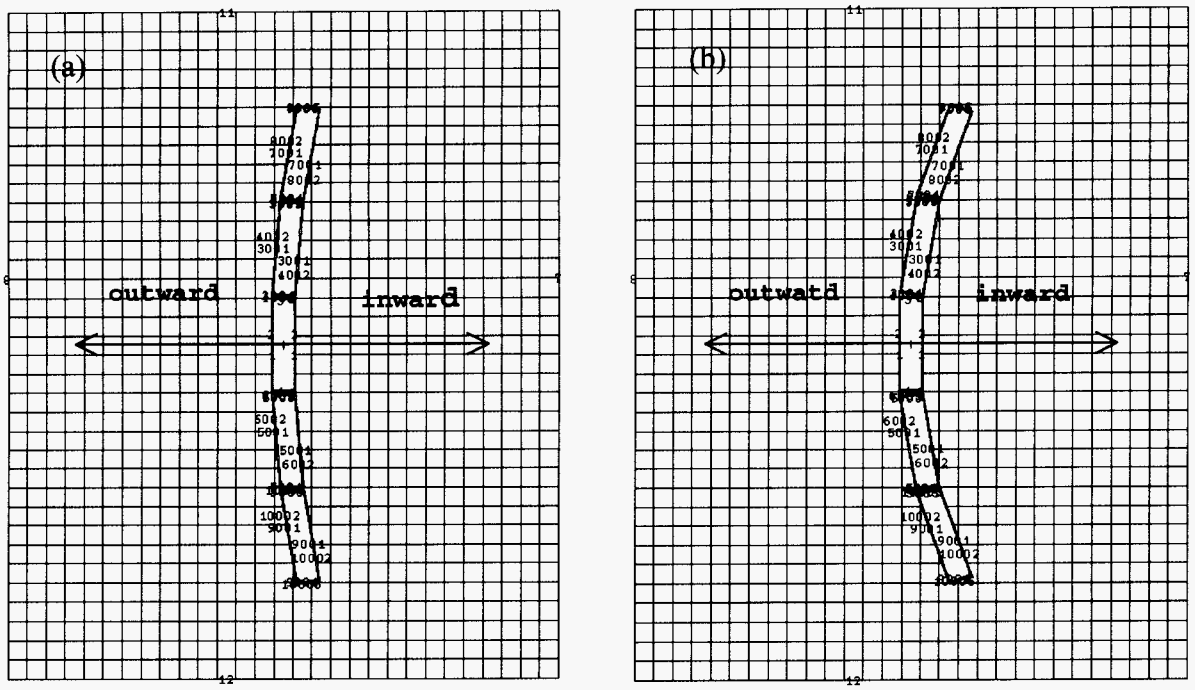

Figure 8. Schematic of the MCNP geometry for the curved vessel model; (a) 5 degree model, (b) 10 degree model.

Table 2. Radial dose rates (Gy/min) of the curved source trains for the total activity of 42 mCi (1.55×10^9 Bq). The simulations were performed for seeds shifted by 5° or 10° with respect to the neighboring seeds and thus, the radial doses inside or outside of the source curvature are different.

Distance (cm)	Linear Source	Inward 5°	Inward 10°	Outward 5°	Outward 10°
0.15	8.99	9.47	9.84	8.98	8.62
0.20	5.92	6.17	6.51	5.73	5.51
0.25	4.04	4.27	4.58	3.88	3.7
0.30	2.79	3.02	3.25	2.71	2.61
0.35	1.95	2.12	2.28	1.89	1.77
0.40	1.38	1.52	1.58	1.31	1.18
0.45	0.95	1.08	1.07	0.90	0.79
0.50	0.63	0.73	0.74	0.62	0.53

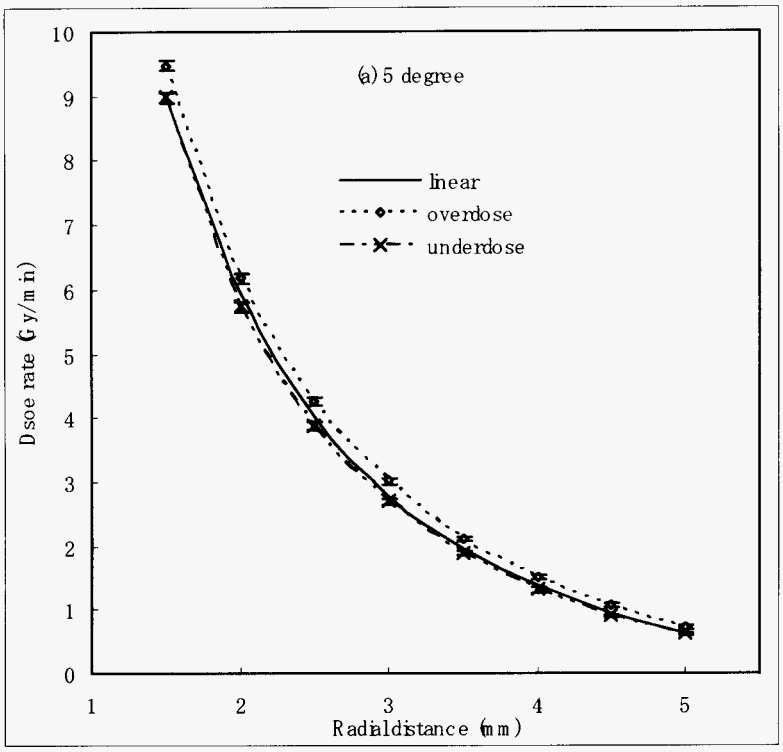

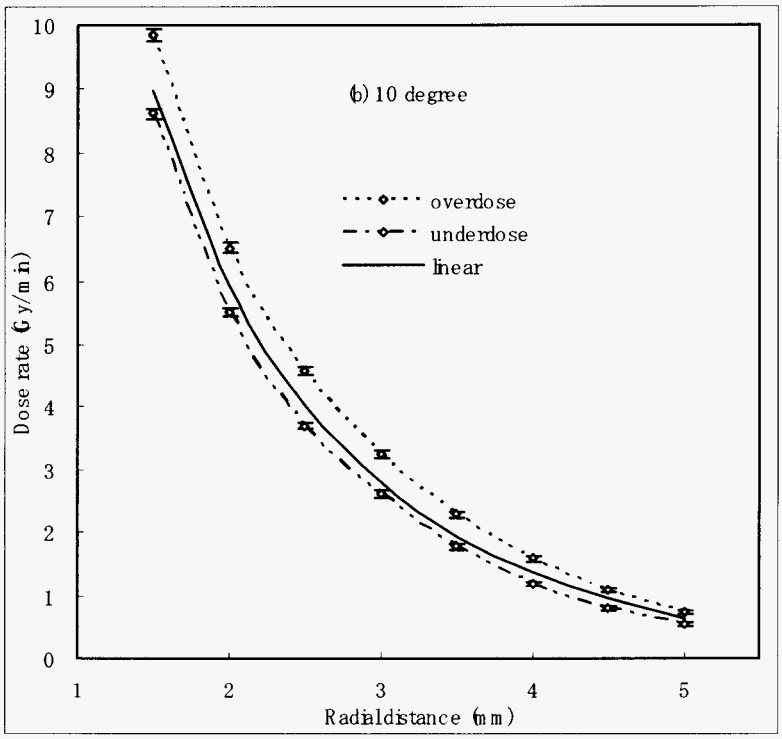

Figure 9. Comparison of the radial dose rate between the linear model and curved models: (a) 5 shift model, (b) 10 shift model.

Table 3. Dose difference (%) of the curved sources from those of the linear source.

Distance (cm)	Inward 5°	Inward 10°	Outward 5°	Outward 10°
0.15	4.99	9.49	-0.44	-4.06
0.20	**3.87**	**9.95**	**-3.54**	**-6.88**
0.25	5.43	13.35	-4.2	-8.4
0.30	7.86	16.63	-3.21	-6.43
0.35	8.16	17.18	-3.57	-9.09
0.40	9.35	14.53	-5.76	-14.18
0.45	13.68	12.96	-5.26	-16.92
0.50	15.87	17.57	-1.59	-16.14

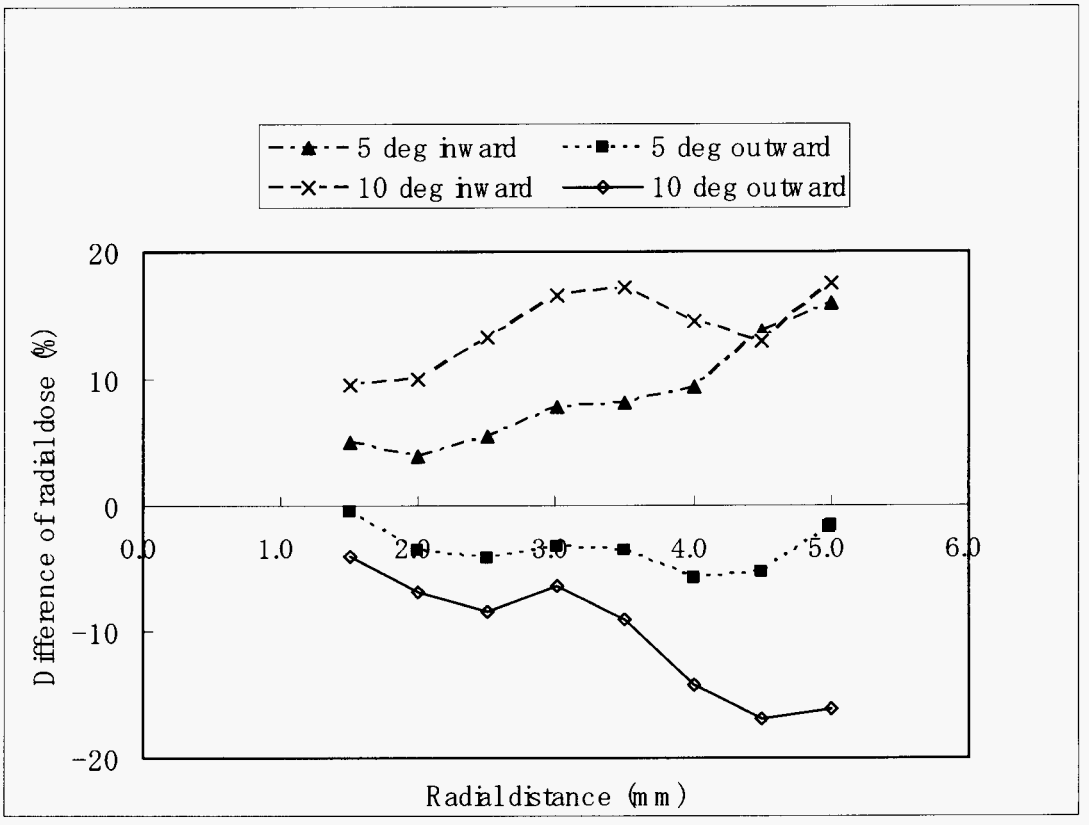

Figure 10. The % dose difference between the linear model and the 5° or 10° curved models.

III-2. Experimental Measurements

The first objective of this study is to develop the MCNP based dosimetry protocol for IBVT. Secondly, this project aims to verify the simulation data experimentally, using radiochromic film and scanning densitometer system. In radiation dosimetry especially for IVBT, there existed a number of difficulties with the measurement of dose distributions using conventional measuring systems, such as ionization chambers, thermoluminescent detectors (TLDs) and radiographic films. For instance, ionization chambers do not give enough spatial resolution, and radiographic films show different sensitivity depending on photon energies. These difficulties have resulted in finding a radiation measuring unit with high spatial resolution which does not require a special developmental procedure but still gives permanent absolute values of absorbed dose with accuracy and precision. The introduction of radiochromic film dosimeter has resolved some of the problems experienced with conventional radiation dosimeters[15].

The radiochromic film (RCF), a colorless transparent film, responds to ultraviolet light and ionizing radiation by turning blue, due to a polymerization of microcrystals of a radiation-sensitive monomer uniformly dispersed in the thin radiosensitive layer. It has characteristics of:

- High spatial resolution
- Insensitive to visible light
- Low spectral sensitivity (wide range of absorbed dose)
- No chemical processing
- Nearly tissue equivalent composition
- No significant energy dependence for photon energies above 100keV
- Ability to serve as archival radiographic imaging and data-storage media
- Ability to measure dose distributions in high-gradient regions of beam.

These properties of RCF make the dosimeter ideal for the brachytherapy. There are three types of films mainly used in medical applications: GafChromic HD-810 (also

known as DM-1260), MD-55-1 and MD-55-2. Since HD-810 absorbed dose range is 50-2500 Gy, MD-55-1 was next developed with the absorbed range of 10-100 Gy. HD-810 and MD-55-1 have a single sensitive layer of different thickness of 7μm and 15μm, respectively. Then, more sensitive RCF with double sensitive layers, MD-55-2 was introduced, which has the absorbed range of 3-100 Gy[16]. We will use this MD-55-2 type of radiochromic film in the experiment, since our dose range is 15-20 Gy and the MD-55-2 is the most sensitive film available[17,18].

Even though it is relatively easy to handle radiochromic films, there are a couple of things to pay attention to in order to assure the accurate measurements. It is sensitive to ultraviolet light; handling under incandescent light or using UV filter over windows and fluorescent light is needed. Another difficulty in using RCF for accurate dose measurement is its lack of immediate color stability upon irradiation[19]. That is, these films continues to darken at an ever-decreasing rate; for example, recently it was found that for MD-55-2 films optical density (OD) increases by 15% in the first 5 h, and after that less than 3% per week. In general, a 24hr period between irradiation and readout has been suggested for RCFs until relative stability of darkening is achieved. Since temperature and humidity during storage, readout, irradiation and post irradiation affect OD of films, it is best to keep them, at a constant temperature of around 20±2°C, throughout the storage and experiment[20].

Another component of radiochromic film dosimetry is a scanning densitometer system for two-dimensional data acquisition. In this scanning system, a uniform light source illuminates the object being scanned from the rear, and an imaging system (like a camera) is used to measure light transmission/reflection from many points on the sample

simultaneously. The resolution of the scan is primarily governed by the pixel size of the imaging system only [13].

A. Experimental Set-Up

Specifically, the linear model dose rates as well as the curvature effect need to be verified. Encapsulated β-emitter Source $^{90}Sr/Y$ (Beta-Cath System^{TM} developed by Novoste Corp) is inserted for dosimetry into a specially manufactured tissue equivalent phantom, which is cut so as to measure the dose rates for the linear model and curved model. A schematic illustration of phantom is shown in Fig.15 for the linear and curved source experiment set up[21, 22].

(a)

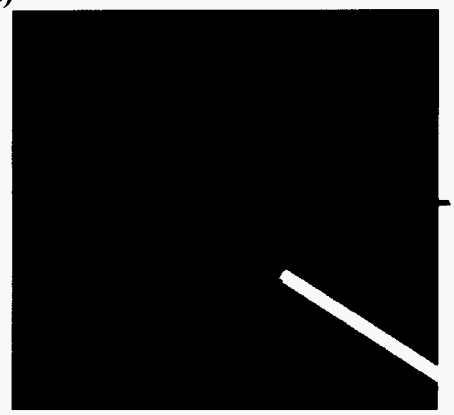

(b)

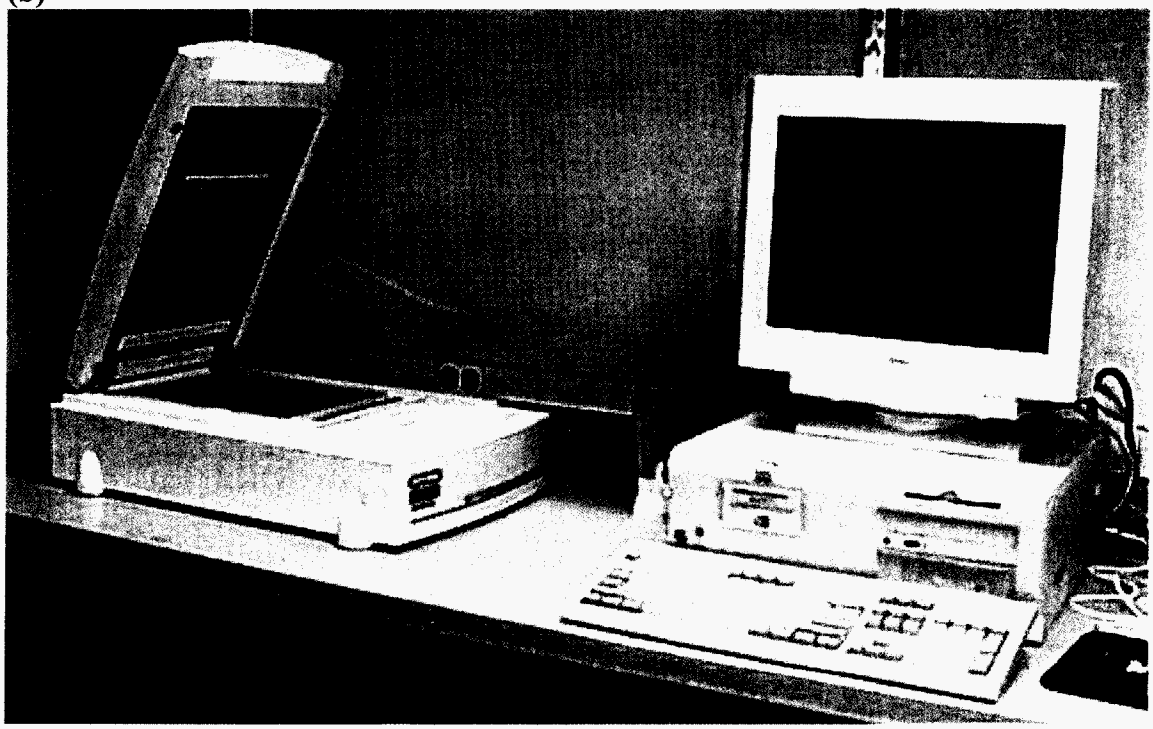

Figure 15 (a) Schematic illustration of radiochromic film (7μm thick) with β source train in a tissue-equivalent solid water for the curved model. (b) Scanning densitometer set up for analyzing dose rate of radiochromic film

This experimental measurement of the energy deposition into tissue equivalent used a block of solid water (Serial # 457100142), a filled epoxy with a density approximately that of water. To obtain a curved geometry, the solid water was cut using a CNC mill with a tolerance of +/- 0.001" (+/-25.4um). In this experiment, 4 different cases were cut, each designed to yield a specific curvature of blood vessel. The notation of degree measure used in reference to the cases illustrated the idea that the source seeds on a circular arc have an angle between them measuring as 5°, 7.5° or 10° (0° is the straight case, being used interchangeably). The cut geometry assumed that the radius of curvature was centered in the source train itself; thus, the cut was approximately centered in the catheter center, but with a slight deviation assuming that the source was centered toward the inner part of the arc. There is a negligible deviation between this radius and the actual distance of the source seed due to source lumen centering since there are tolerances in the cuts anyway due to the limitations of the CNC mill. Thus, any errors in the actual arc and the corresponding degree of that arc come completely from the error in accurately knowing what the rotational orientation the catheter takes inside the phantom. A sample cut is illustrated in Figures A1 and A2:

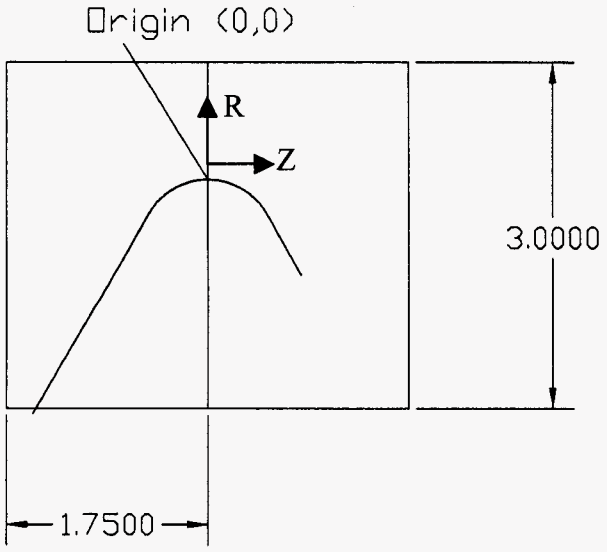

Figure A1. 10 Degree Phantom Cut Pattern

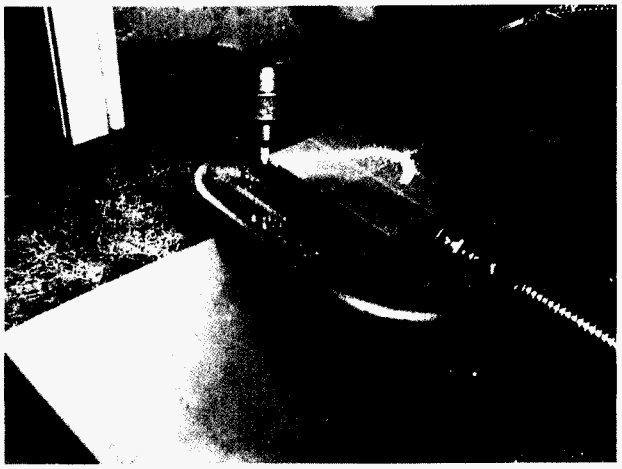

Figure A2. Cutting of the Phantom

First, the blocks were cut roughly into phantom quarters. These quarters were planed to a tight tolerance and then the channels were cut for the catheter to fit into.

Complimentary curves (i.e. mirror images) were cut into the phantom halves and were then brought together and bonded with super glue. Super glue was chosen for its low viscosity so that it would fill in the gap rather evenly and have a very thin coat to minimize the effect it would have on the beta slowing down spectrum (due mainly to difference in density between the glue layer and the solid water).

Since the Beta-Cath catheter has a 5 French (1.68mm) diameter (delivery catheter REF# DBC-0131, Lot# 424879), the hole needed to be cut with the smallest clearance possible. The nearest size mill bit that can cut this size hole is a 1/16" diameter ball end (1.59mm). This was designed originally to cut a hole closely approximating a circle using 3 passes. In cutting these passes, the catheter would fit through the hole until the curved part, where the catheter would continuously snag. The hole was enlarged incrementally until the catheter would fit through.

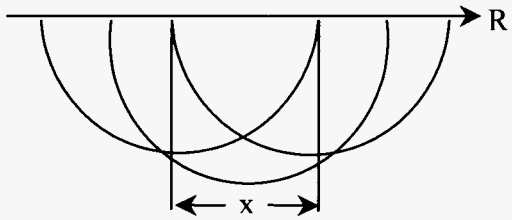

Figure A3. Spacing of the cuts

The passes cutting the channel through which the catheter would be fed through were cut approximating a circle using 3 passes with the ball end mill bit. The mid cut was lower in the material as well and the 3 passes were spaced by a distance "x". On the first phantom cuts, the mill diameter of 1.59mm plus x, which was 0.18mm (0.005"), approximated a circle of diameter 1.72mm. This should have been close enough for the catheter to fit through the 5° case phantom. However, the catheter would travel through the straight section of the channel, but would snag when the curve was reached. This was not due to a rough cut since the channel was cut using a CNC automated curve; rather, it was concluded that the catheter cross sectional area must be deforming due to the stresses in flexing along with frictional forces when trying to insert the catheter. Thus, attempts

to insert the catheter into the phantom proved to be impossible without damaging the catheter (by severely kinking it during insertion).

The distance x was increased by 1 mill incrementally, being the minimum resolution of the CNC stepper motors, until the minimum diameter hole could be found that allowed the catheter to pass through from the outside. The x value was increased to 6 mills, 7 mills, and finally, the value of 8 mills. At 8 mills, the diameter of the cut hole is very close to 5/64" so the decision was made to cut the channel with a 5/46" bit. The hole in the phantom allowing the catheter to pass through was 1.98mm in diameter, which is 120% of the catheter's 5 french diameter, and forcing a total gap distance on any given side of the catheter to be between 0um and 320um (depending on how the catheter is physically centered in the hole). These halves were bonded together and set aside for the experiment.

Most of the procedure involving film exposures loosely followed the recommendations found in the ***AAPM Task Group 55*** publication. In order to expose the film with a radial field, a hole was cut into the film using a jig. The film was protected from scratches and stray plastic or metal chips by being bolted down in a group of 4-10 films, sandwiched between protective paper or plastic (such as transparency acetate). The cuts were first made using a #53 carbide bit (1.50mm) and finished with a #51 bit (1.65mm). This size of hole snugly fits the catheter, ensuring that the catheter was centered perfectly inside the film's hole and eliminating the possibility of any off axis movement of the film relative to the catheter.

After drilling the hole, the film was given a pre-exposure irradiation in order to use the recommended double exposure technique. The initial irradiation was done in a Nordion International Gammacell 220 irradiator housed here on campus. The dose rate at exposure time (8:05am, November 28, 2001) of the film was 0.350Gy/s, and it was given a dose of 9.15 Gy via a 30s exposure. The film was then scanned in the following day beginning at 7:35pm. This was the approximate 36 hour wait time which was chosen as a minimum for our scans after exposure (although some wait times were longer than 36 hours). A Bio-Rad GS-710 Calibrated Imaging Densitometer (SN# 37S3797ETN) scanned all of the films for later analysis. This densitometer, with a resolution of 600dpi, yields a pixel size of 42.3um square on the scans. The actual film exposures occurred in

the afternoon on March 21, 2002 at the Deaconess Hospital in Evansville, Indiana. The exposures were scanned in late morning on March 25, 2002, giving the film about 93 hours to settle. This was within the guidelines for recommended minimum setting time of 24-48 hours. See examples of the before and after exposures in the following figure:

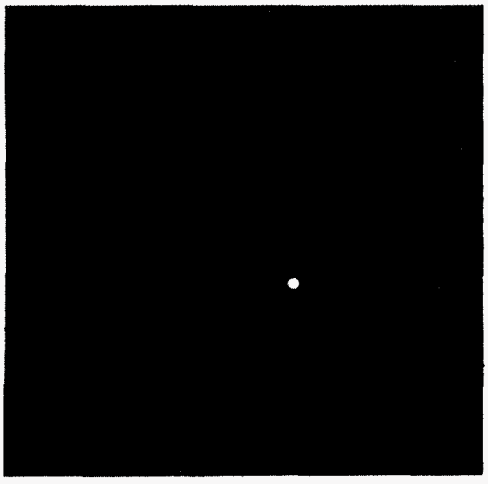

Figure A4. Uniform 10Gy exposure

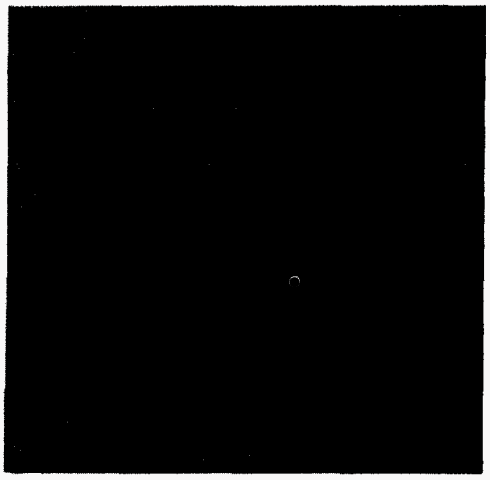

Figure A5. Film after beta field exposure

The alignment between the pre-exposure scans and the post-exposure scans relied on the film's corners, drilled circle and the written numerals at the top for alignment marks. This proved to be more challenging than expected because of the rough cuts in the film on the 40um scale, making pixel-to-pixel alignment on this scale very difficult. The films can roughly be aligned (+/- 2 pixels or so) though, but for the double exposure technique, that is not close enough. This caused problems that will be discussed later.

B. Pre-Measurement Work

The films used in the data acquisition were Gafchromic media type MD55-2 (Lot# H1146MD55, ISP Technologies). The sheets come packaged in packs of 5 sheets, each sheet being ~5" x 5". The films come packaged by the manufacturer inside black paper envelopes with each film separated from the adjacent film by a smooth paper spacer sheet; this protects the film surfaces from damaging each other as well as sticking together. The film taken from this lot was cut into pieces sized smaller for both the calibration data as well as the actual exposure data.

The first film cut and used was the calibration data set. The film was cut into squares roughly 1" x 1.5" and exposed in the Gammacell irradiator for given time intervals. They were elevated in the irradiator chamber on top of a hollow thin cardboard cylinder with a thin plastic lid to position the film in the center of the radiation field. The exposure in the irradiator is quite constant for our purposes, having a cosine distribution in the radial direction from the center of the chamber. In quantifying the chamber dose gradient (using Gafchromic film), the measured dose rose as the edges of the chamber were reached. Over the 2.5" square in the center of the 8" diameter chamber, the dose grew 10% between the center point and a point 1.25" away. Thus, we expect the distribution on the film to be very consistent since the sampled area of exposure was smaller than a square inch and was located in the approximate center of the chamber center itself.

A total of 34 calibration film exposures were actually used to determine the calibration curve for the experiment; some of these points were redundant exposures to monitor the consistency between films and ensure that the calibration technique was indeed reliable. The densitometer, upon completion of the scan, writes the data to a file in a vendor proprietary format. Thus, in order to measure the optical density of the film and analyze the data, an intermediate step of translation was made for the actual vendor data.

The GS-710 densitometer is a calibrated densitometer which uses fluorescent lamp motion synchronized with a linear CCD array to scan a film via transmission. The densitometer uses an internal step tablet for calibration whose values are provided by the vendor and measured for each individual device (the vendor assigned our tablet #911st110). The actual optical density value ranges for our film are 0.07 – 0.74 (Some arbitrary units that the vendor uses), while the densitometer is specified to measure over an approximate range of optical densities from 0.05 to 3.00. Over this range, only the first 4 of the 17+ steps in the step tablet are actually relevant to the measurements and the calibration, entering in some uncertainty in the step tablet calibration curve for the device.

Before the densitometer takes any data, it is necessary for it to first scan in the step tablet values and record these measurements (via hard copy which is kept by the

experimenter). This hard copy records the internal CCD response to the fluorescent lamp light passing through known optical densities. When the calibration films are scanned, step tablet scans are automatically performed every 20 minutes to ensure that the densitometer did not experience drift internally in the CCD sensor array (and if it did, the drift could be corrected). The first 4 values of the step tablet are relevant to this study because they provide the correlation between the digitized light flux values actually measured by the CCD array and the reference optical density values. Then, thess data fit to a polynomial and the optical density is found as a function of this light flux value itself. Since light flux or intensity is inversely proportional to the optical density, a nonlinear curve is expected for the step tablet values as measured directly by the CCD. A typical correlation plot is shown in the next figure, using a second order polynomial fit.

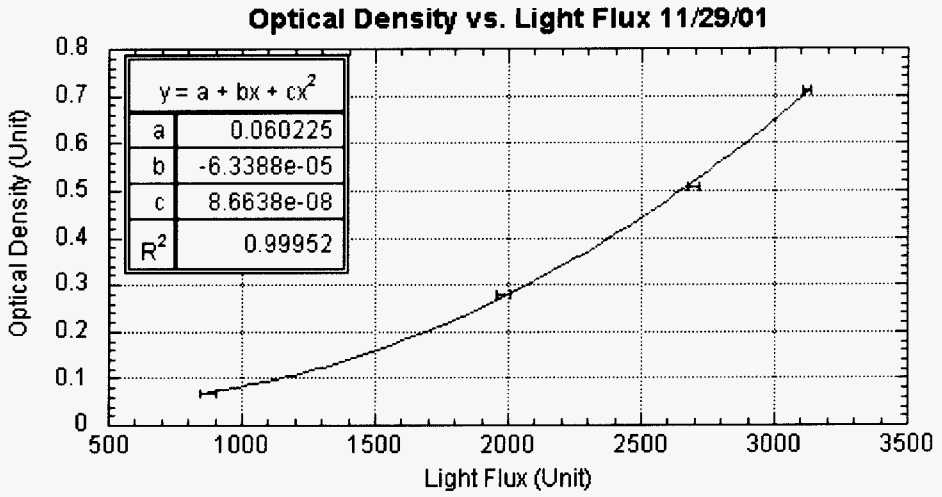

Figure A6. Correlation between optical density and CCD array measurements

The densitometer scans were acquired using Quantity One software provided by Bio-Rad and made to interface with the GS-710 denstometer. After the information is measured, it is entered into either a proprietary Quantity One format (*.1sc file) or can be exported to a TIFF file. In order to utilize the full 12bit resolution of the CCD array, the resulting matricies were output in a "12bit TIFF" according to the vendor. This actually ends up as a vendor modified format mimicking a 16bit TIFF image and can be opened in various programs such as MATLAB and Adobe Photoshop. It is these raw data that the data analysis techniques in MATLAB analyzed and compiled the results for this study.

The calibration scans acquired were cropped a distance from the film edge (3mm or more) to avoid edge effects reported in the literature. The scans were then exported

and saved in a TIFF format image. MATLAB read in the TIFF image and saved the values in a histogram for viewing, showing CCD flux values vs. Frequency. For a given calibration film, a histogram produced, exported and opened in a spreadsheet, where the flux values were converted using the appropriate step tablet calibration curve; and this distribution was then Gaussian fit. It was this Gaussian fit, providing a mean and a standard deviation, that compiled the dose vs. optical density calibration curve. See Figure A7 for a histogram from a sample cropped calibration film, the 42.7 Gray calibration film.

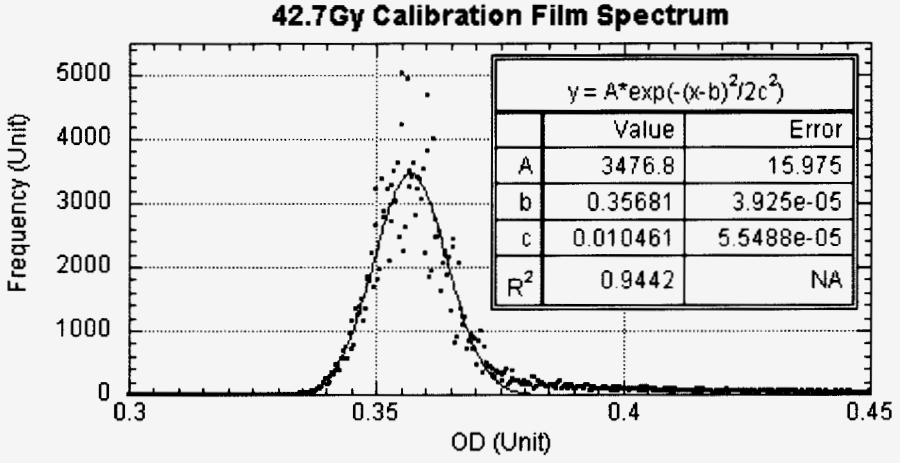

Figure A7. Histogram for the Optical Density (OD) spectrum of a calibration film

Note that this isn't exactly a Gaussian spectrum, but rather it is skewed toward the higher optical density values. This is, in our experience, an actual artifact of MD55-2 film. In close examination, the film is covered with dark spots very small in size (on the order of 50–100um, FWHM). These spots of radiation sensitive pigment seem to be conglomerated and artificially cause the optical density to be higher than the rest of the media which is roughly constant. As a result of these values, the correlation coefficient of the histogram to a Gaussian curve is lower than desired. However, this was the only systematic and repeatable method we could justify to make the film calibration. Dose with the optical density means are tabulated in the following figure, and again displayed in the calibration plot.

Table A8. Calibration measurements

Time (s)	Exposure (Gy)	OD Mean	OD Standard Deviation
0	0.0	0.1796	0.0059
5	1.5	0.1917	0.0082
10	3.1	0.1923	0.0065
15	4.6	0.1990	0.0077
20	6.1	0.2065	0.0072
25	7.6	0.2173	0.0098
30	9.2	0.2176	0.0098
35	10.7	0.2268	0.0081
40	12.2	0.2366	0.0078
45	13.7	0.2373	0.0076
50	15.3	0.2452	0.0075
60	18.3	0.2656	0.0096
70	21.4	0.2717	0.0095
80	24.4	0.2760	0.0087
90	27.5	0.2931	0.0080
100	30.5	0.3007	0.0079
120	36.6	0.3337	0.0103
140	42.7	0.3568	0.0105
160	48.8	0.3894	0.0122
180	54.9	0.4045	0.0123
200	61.0	0.4203	0.0129
210	64.1	0.4328	0.0116
210	64.1	0.4282	0.0113
210	64.1	0.4294	0.0114
230	70.2	0.4561	0.0127
250	76.3	0.4785	0.0116
285	86.9	0.4939	0.0109
290	88.5	0.5133	0.0150
295	90.0	0.5047	0.0118
300	91.5	0.5078	0.0140
300	91.5	0.5115	0.0129
350	106.8	0.5680	0.0132
400	122.0	0.6144	0.0118
450	137.3	0.6584	0.0112

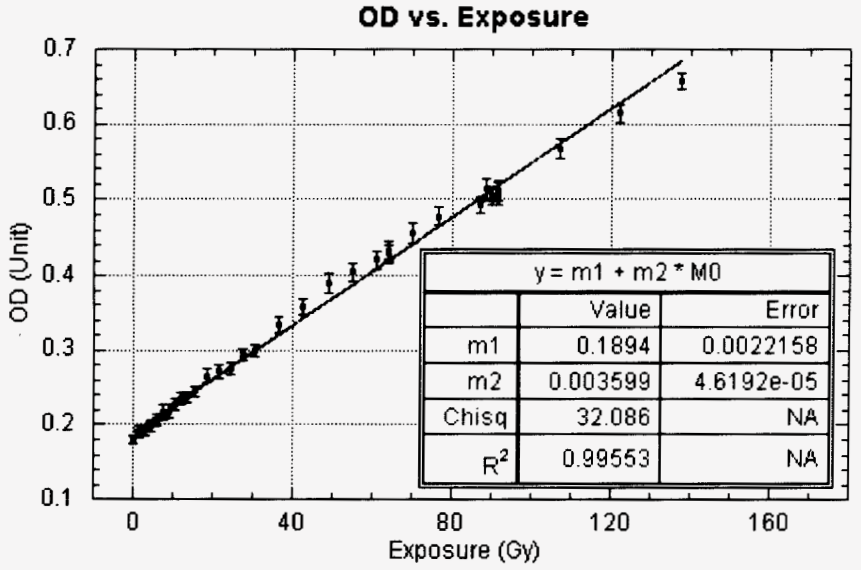

Figure A9. Optical density vs. Exposure calibration plot

C. Measurement Run

The data runs were conducted in a radiology surgery room, on a surgical table top. The phantoms themselves physically have no dimension (in 3D) in which the source seeds are not encased by at least 1" of solid water, so the position and composition of the tabletop surface was considered unimportant (but, it appeared to be made of a combination of carbon composite or fiberglass with steel supports). Before the exposure, the phantoms had the catheter inserted into the hole, then through the hole in the film and finally into the other phantom half. After full insertion, we placed the phantom into the acrylic holder designed to hold the phantom halves square and together. Nylon screws were used to tighten the 2 phantom halves together and keep the film from shifting during exposure. A fine tip permanent marker traced the top of the film where it contacted the phantom in order to give a reference line for the data set; this determines the orientation of the film relative to the phantom at the time of exposure, so that the radiation field orientation is known precisely (to account for small angle rotations of the film relative to the curved seeds).

A total of 2 exposures were taken for each curved case: one exposed for 5 minutes and the other for 15 minutes. We reasoned that since the field easily causes saturation close to the hole, the 15 minute case gives better dose values for distances further from

the catheter while the 5 minute case gives better resolution closer to the catheter. Thus, 8 films total were exposed to the Beta-Cath seed train. From the time of exposure to the scanning in at the densitometer, there was a gap of 93 hours. It was initially thought that the double exposure technique could be used after a matrix rotation was performed on these image scans. Yet, due to the small feature size of these noise spots, mathematical transforms on the data do not allow for this technique to work.

In order to attempt the double exposure measurements on the film, a second set of scans were preformed in early June of 2002 (June 4-5), months after the beta field exposure. These are the scans from which the data for this study were taken because they were oriented (in the densitometer) much closer to the original pre-exposure scans in angular orientation; this was intended to allow for background noise subtraction.

After exposure, the films were inserted into a small plastic zipper lock bag, each separated from the adjacent films by sections of the special slick paper included in the Gafchromic film package itself. This stack of films then was placed into an original black Gafchromic film envelope. This was then placed in a box (itself dark) for transport back to the lab for analysis. The best efforts were made to keep the film at room temperature for all transport to and from the exposure. In the lab, the films were stored in the same envelope inside of a light tight box. This lab was kept at a relatively constant room temperature.

When the time to scan came, the densitometer was cleaned using Bausch & Lomb disposable lens cleaner wipes (UPC# 0-10119-41503-9) purchased from a local store. These are designed for cleaning eyeglasses with antireflection coatings, so it was thought that they would perform well on the densitometer's optical surface. As stated in the **AAPM TASK55 Report**, there is a tendency for the gap caused by a thin layer of trapped air between the glass of the densitometer and the film to exhibit thin film interference (described as a sort of Newton's rings phenomenon). To overcome this, some black construction paper was cut so as to frame the film on the 2 side edges. Then the film pieces (2.5" x 2.5") would sit on the black frame, overlapping about 1-2mm on each of the sides but still leaving enough clearance to allow for the corners to be scanned in (as fiducials). Finally, on top of this setup, the GS-710's transmission diffuser plate was set and 9 scans were taken of each film. This technique did eliminate virtually all

traces of the thin-film interference underneath the film. It must be noted that the diffuser plate could also cause a thin film air gap and still exhibit the interference, and this was observed in the outer parts of the 10° data; it doesn't appear to actually alter the active region though.

The scanning in of the second image set provided the pixel information for the data analysis. When the films were given post-exposure scans, they were aligned as close as possible to the pre-exposure scans with the 9.1Gy background exposure alone so as to allow for the double exposure technique to be used. In this experiment, the double exposure technique was not eventually used in measurement because alignment of the pre-exposure and post-exposure films proved to be very difficult so as to allow for pixel-to-pixel comparisons. Even very small linear temperature coefficients in the film can cause linear dimensions to change such that noise pixels no longer align properly. Since it is virtually impossible to align a film exactly as it was in the pre-exposure scans, a better technique of pixel averaging or lower resolution scans must be utilized in future work.

The background exposure was measured by cropping a section of the film which was not affected by the Beta-Cath radiation field and this background value was measured using the same technique as used in the calibration measurements. In this set of scans, step tablet calibrations were taken frequently (usually immediately before and after the set of scans for each film were taken). Each of these step tablet calibrations was then used to obtain the optical densities to be used in the dose conversion and final analysis for that given film and to ensure a minimized drift effect.

The area of interest on the film itself is well within a 2cm square. For consistency, a square of 301 pixels by 301 pixels was cut from each film after averaging the 9 scans and this radiation field provided the raw data for the data analysis.

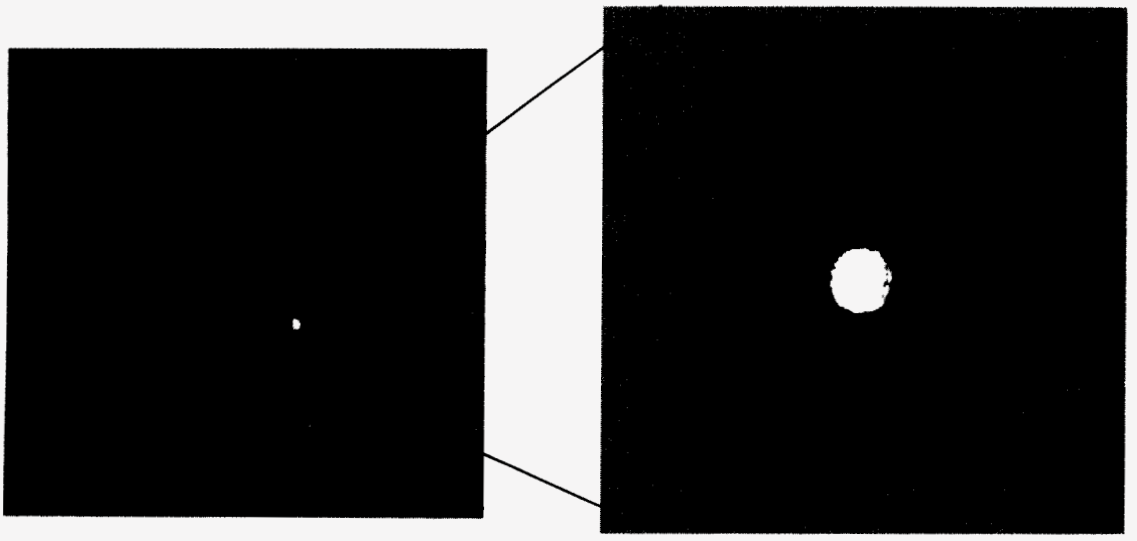

Figure A10. Sections of the film used

The background sample box was chosen for the large number of pixels and the fact that it is a substantial section of the film untouched by the experiment. The data set box is large enough (1.27cm x 1.27cm) that the entire radiation (within the error bars of the background noise) is enclosed within. Notice also that the film has a second artifact which is a dark line running directly through the data set (through the entire film). We determined that this was caused by a slight mismatch (~10um) is the aligning of the phantom halves. This is caused in the machining process where the phantoms must be secured and the mill planes the surface. In the tightening of the phantom in a vise of some kind, there is a slight bulge in the plastic due to the strains. As the surface is planed, the cut is in reality straight; however, when the phantom is removed from the vise, the stress is released and a warped surface results. This manifests itself in a very tiny gap between the phantom halves which introduces an impression on the film when it is sandwiched between the halves and then tightened down in preparation for the beta field exposure.

A factor important in measuring the radiation field after the exposure is locating the center of the lumen, which holds the radioactive source seeds. This lumen, as shown in the vendor documentation, is off centered in the catheter itself, for reasons the vendor chose. See the next figure for an illustration.

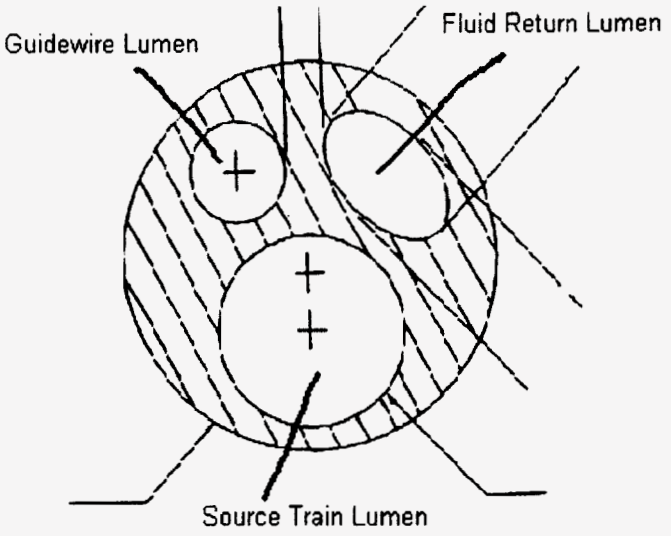

Figure A11. The cross section of the catheter (GA-1115-D-101-S Attachment 3)

There is a substantial off center distance between the catheter center and the source lumen center (about 20% of catheter diameter as seen in the figure, which ends up being 330um). Although this distance is "small", it is not negligible when figuring the actual source center because 300um is large in comparison to the distances in question for the study (0-3mm). Since the measurements are on a millimeter scale, this can introduce a fairly large bias in the data set. The error is systematic in nature and can be corrected for.

As of this time there is no way of knowing where inside the catheter the source lumen is actually located except by extrapolation or estimation, along with associated errors. Because the catheter is loose (in order to use it in multiple phantoms), it is a challenge to make the orientation of the catheter reproducible. It was not known at the time of experiment that this would be such an important effect. In future experiments, a means of controlling the angular orientation of the catheter inside of the phantom must be devised without attempting to use an adhesive to permanently bond the catheter inside of the phantom. This would mean phantom redesign and using some non-destructive and non-permanent means of orienting it

After measurement and analysis, measurements of the 4 different phantoms were scaled according to the appropriate step calibration curve and the film dose curve; the raw results are shown in the following plots (all of which were 15 minute exposures):

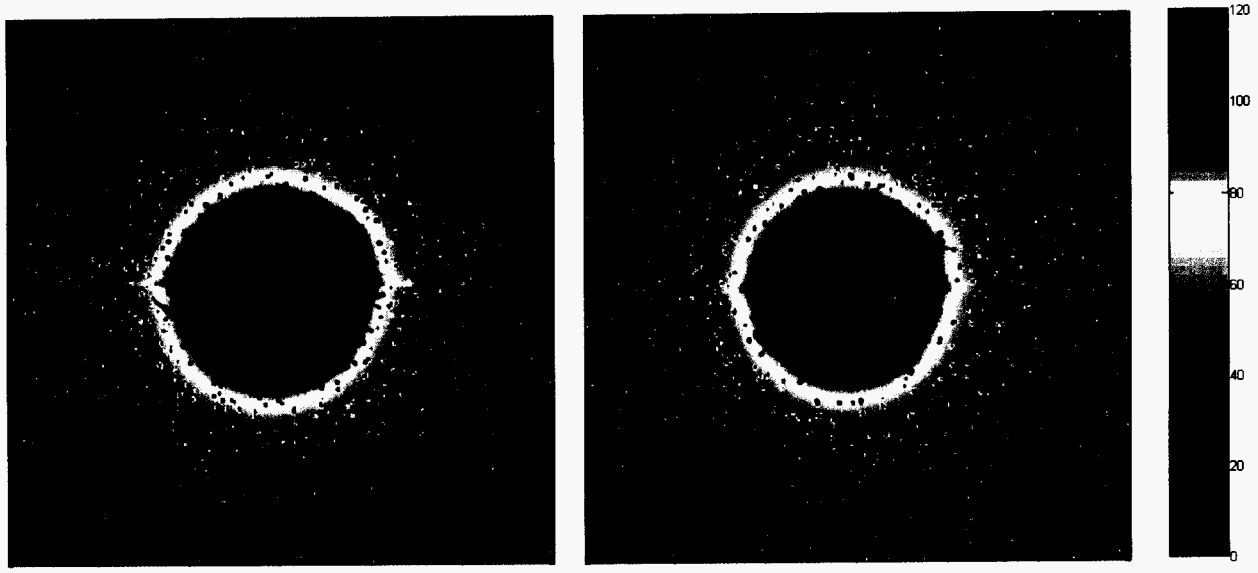

0° Case Exposure **5° Case Exposure**

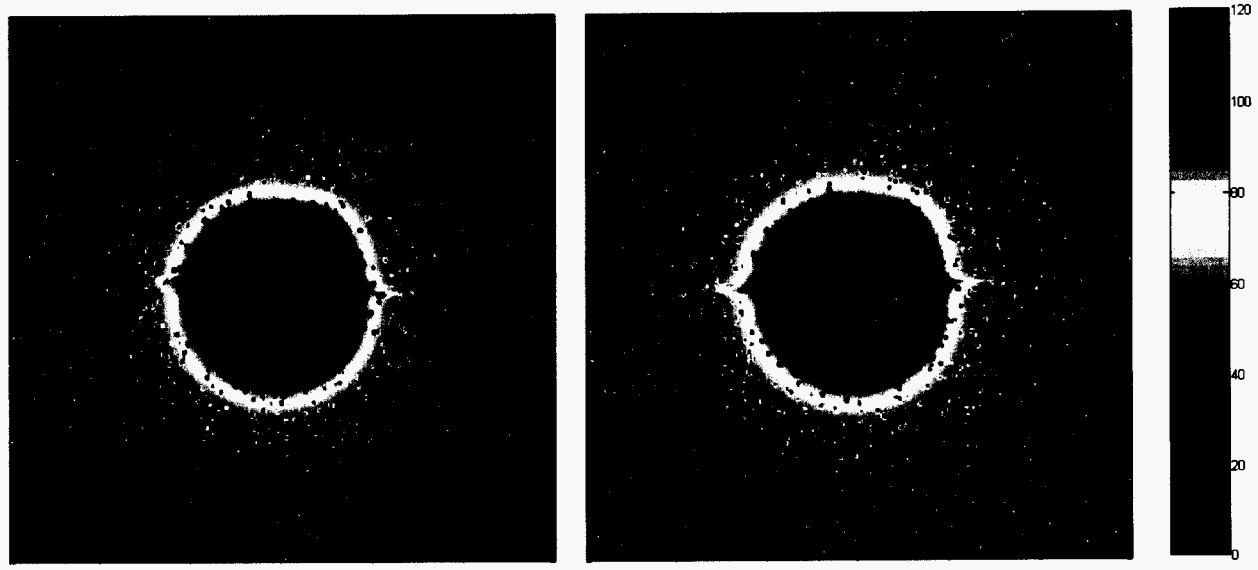

7.5° Case Exposure **10° Case Exposure** **Dose (Gy)**

Figure A12. False color plots of the 15 exposures on Gafchromic film for all cases

One can easily see from these plots that finding the dose through the spotted pepper noise inherent in the Gafchromic film is challenging. But even more challenging is locating the source lumen position itself. Because of the phantom hole oversized cut, there is always a void space near the catheter. Additionally, there is an angular degree of

freedom in which the lumen may be rotated. The first challenge in extracting useful data is to locate the lumen center for each case, so that the center of symmetry is known for the data set. Yet, the void near the catheter causes artificially high dose readings near the catheter in the film and does not mirror reality.

Initially, one analyzing the films may "eyeball" the dose distribution on the film and estimate, in the very least, what quadrant(s) is most likely for the source lumen to be in. This is especially easy in the 0° case where the radiation field should exhibit radial symmetry about the source center coordinate. Because of the tolerance in the phantom hole, the slack between the catheter and the phantom causes the close points to be artificially high, so it is critical to systematically find the most probable center of the source lumen. In order to do this, we extrapolate using the dose data along the y-axis, perpendicular to the data in question.

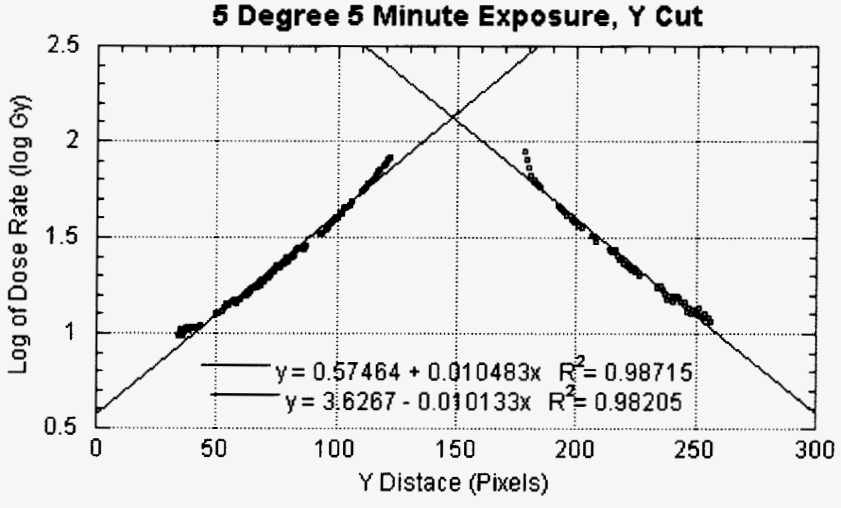

Figure A13. Extrapolation to find the axis of symmetry for the 2D dose distribution

This example extrapolation takes the logarithm of the dose, fits 2 lines and finds the crossover point. This crossover point locates the y-axis value of the source center; in the example, the center actually appears to be 3 pixels below the circle center, a distance corresponding to 0.127mm. This, therefore, tells us that the source is in the lower quadrants (III or IV) and that there are 2 or more possible positions that can be considered the source center. See the following illustration:

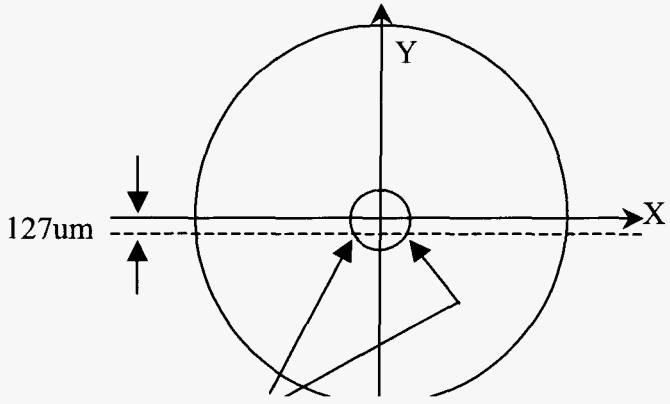

Figure A14. The effect of shifting the source seed center

The error associated with this center point choice is on the order of a pixel or 2, due to errors in the fit and the discrete nature of the measurements. The circle around which the seed must be located has a radius of ~250um, but this value itself has errors associated with it. Furthermore, the data within 2-3 pixels (0.08mm – 0.12mm) on either side of the x-axis is corrupt because of the damage done by the phantom crease artifact.

In aquiring the datasets, it was assumed that the seed was always at the furthest point down in the circle (the full 6 pixels) on the y axis. Then, samples were taken for the parallel rows here coinciding to this y coordinate, and the adjacent rows above and below this one. This was done because all the data runs (except for one, the 0° 5 minute case) had the source center in the lower 2 quadrants of the circle. This distance was far enough from the crease that it had no effect on the data. From this data had the background subtracted, then the mean and error (simple standard deviation formula) were used to quantify the measurement value and the standard deviation. A sample raw data set (before any of the previously described steps were performed) is shown below:

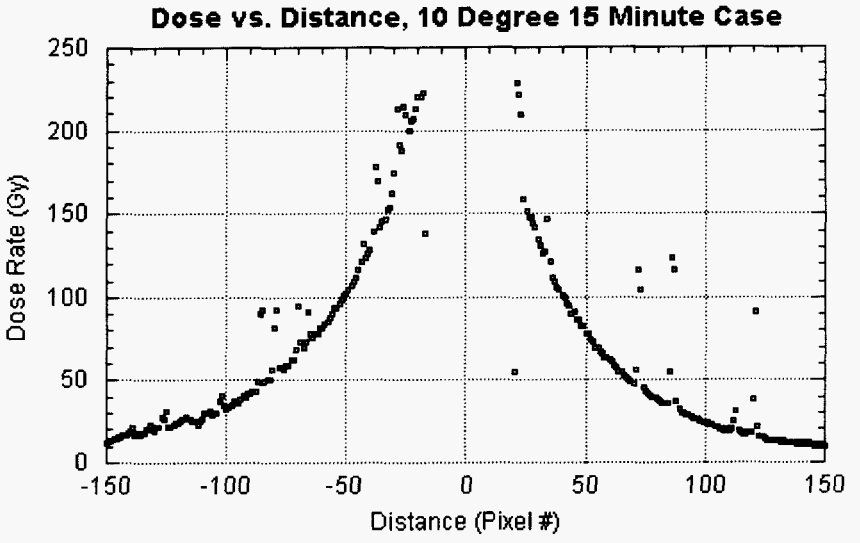

Figure A15. Raw data from the 10°, 15 minute case

On this plot you can see that the data, which is in the nonlinear range after about 120Gy, saturates between +/-40 pixels (+/- 1.69mm), which is to be expected. Additionally, you can see the manifestation of the pepper noise on the plot. It is not small, statistical noise. Rather, it is very large and biases the measurements very high, typically measuring in at 2-3 times the actual expected value itself. In order to analyze the data in a reasonable fashion, these known outlier points were eliminated by hand.

One last source of uncertainty is the gap between the oversized phantom catheter channel and the catheter itself. This gap is filled with air, so it is practically a void in comparison to the solid water. When the catheter is inserted into the phantom, there is a gap between the catheter surface and the hole in which is sits. The actual position of this gap is dependant on how the catheter sits inside the phantom. Thus, the actual position of this gap is unknown, but it appears that from the data, it can be inferred. Thus, there is an extra uncertainty in the effective distance between the data set and the possible source center coordinate due to an effective translational shifting of the data along the axis. This is justified because the void between the catheter and the phantom creates such an effect. It is not expected that the shifting be symmetric in both the positive and negative directions since the catheter is not necessarily situated symmetrically inside of the hole.

D. Data Analysis

1. Iso-dose contour around the source

The r- θ plane iso-dose contour figures illustrate the actual measured iso-dose rate in 2 dimensions on the film and overlays the theoretical iso-dose lines over the top. With the center of the theory aligned with the catheter center shown in Figure X1, one can see that the measured data overestimates on one side and underestimates on the other side. This is mainly because the source is not centered within the delivery catheter. In Beta-cath system™, the source lumen is not centered within the catheter, so the source train is always offset from the catheter center. Therefore, the measured contour map was shifted around until it seemed to match with the simulated contour lines, seen in Figure X2. In fact, these superimposed contour figures could be used to estimate the source center. Moreover, these figures point out that the offset of the source train within the catheter or even within the artery should be obtained for more accurate dose delivery.

All the iso-contour plots are shown below:

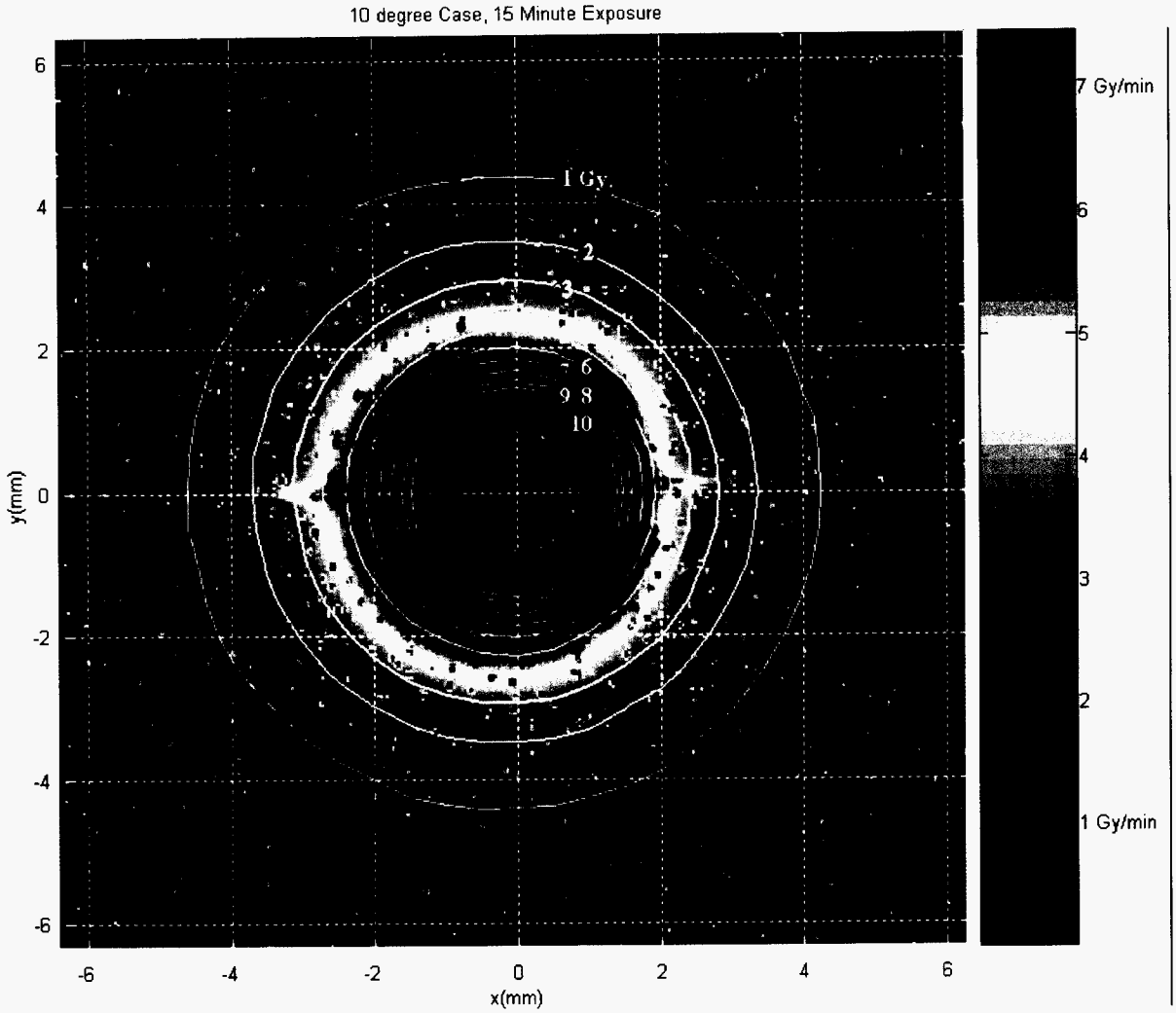

Figure X1. 10° 15 minute case, Catheter centered

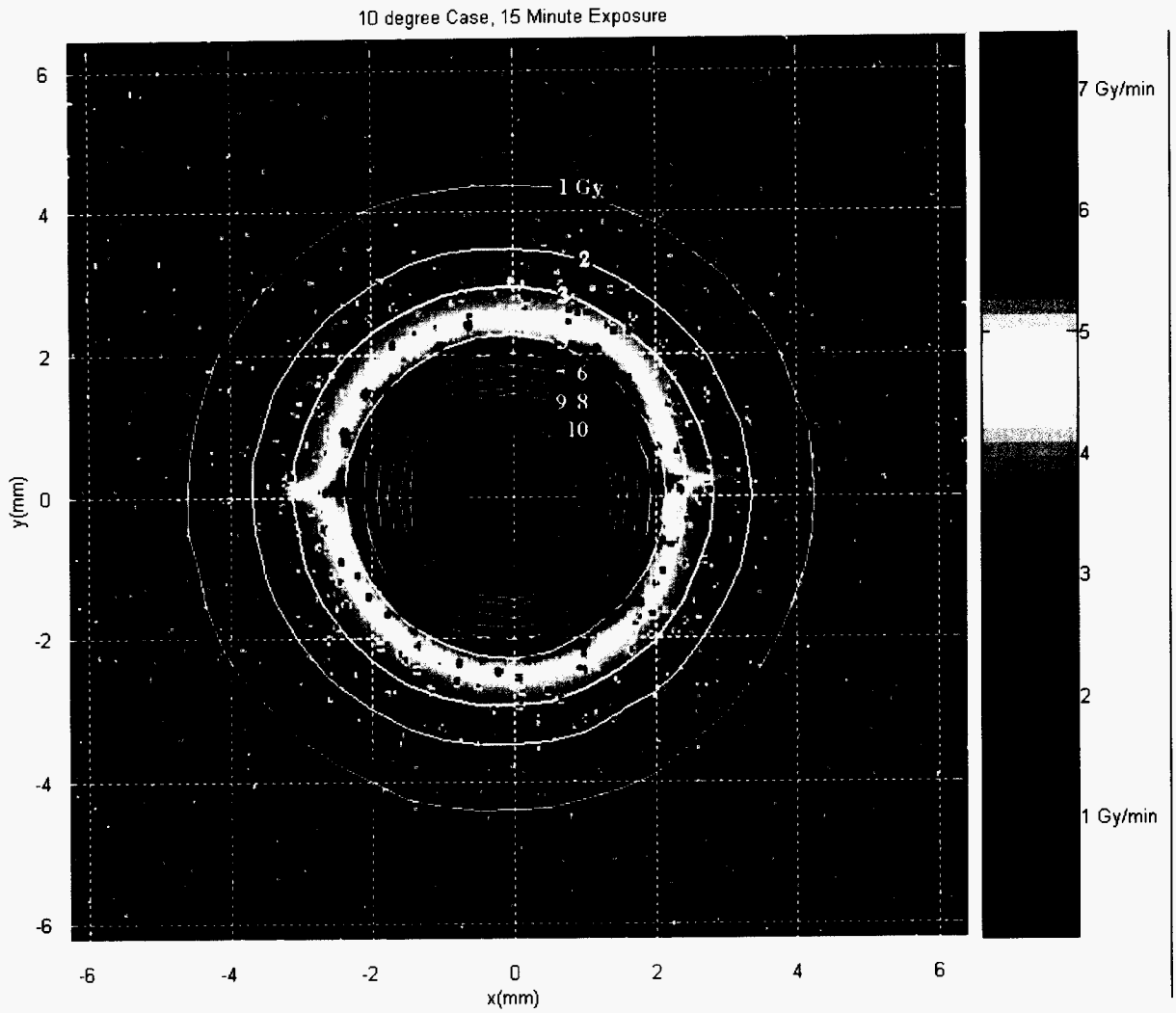

Figure X2. 10° 15 minute case, Field centered

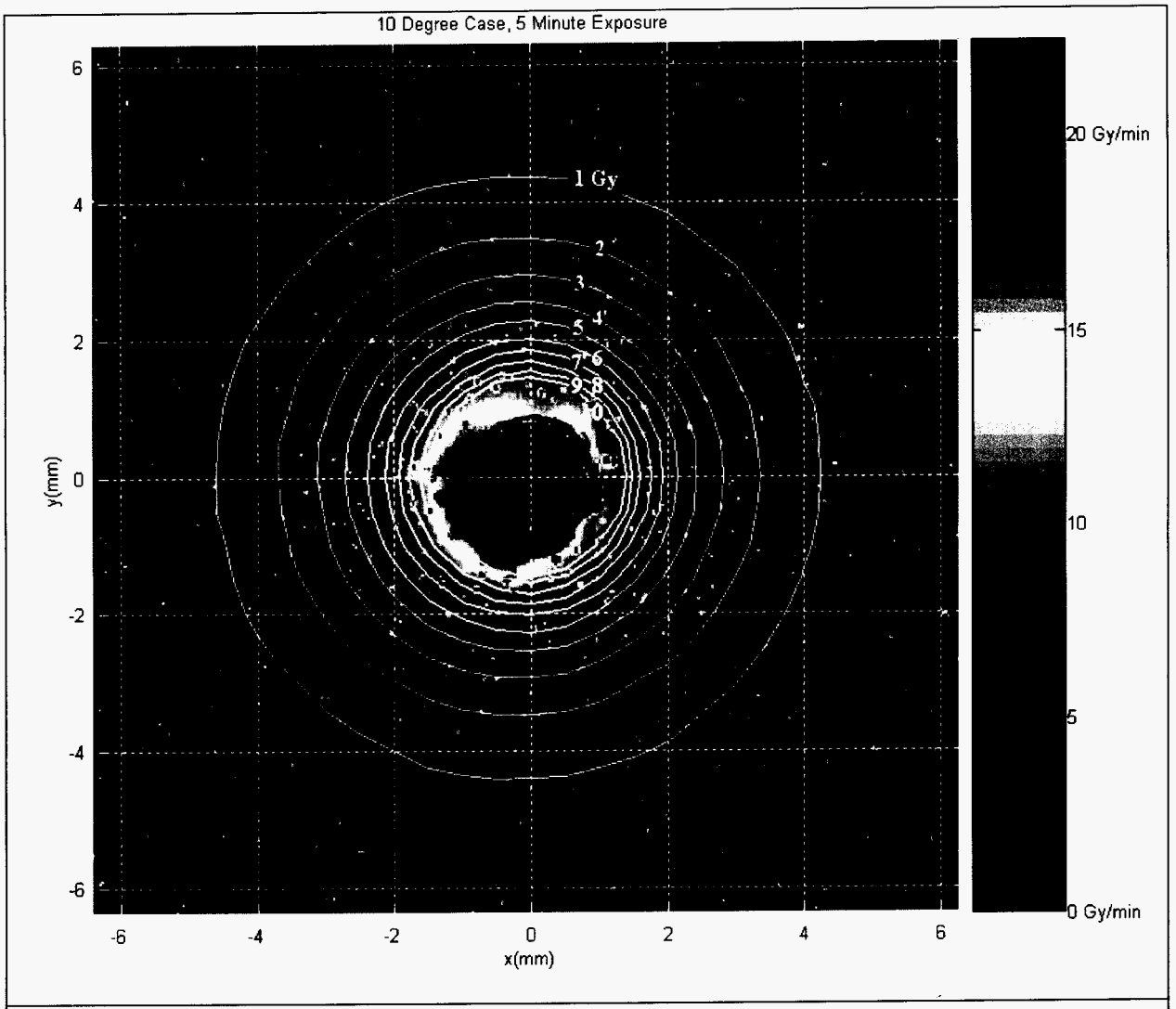

Figure X3. 10° 5 minute case, Catheter centered

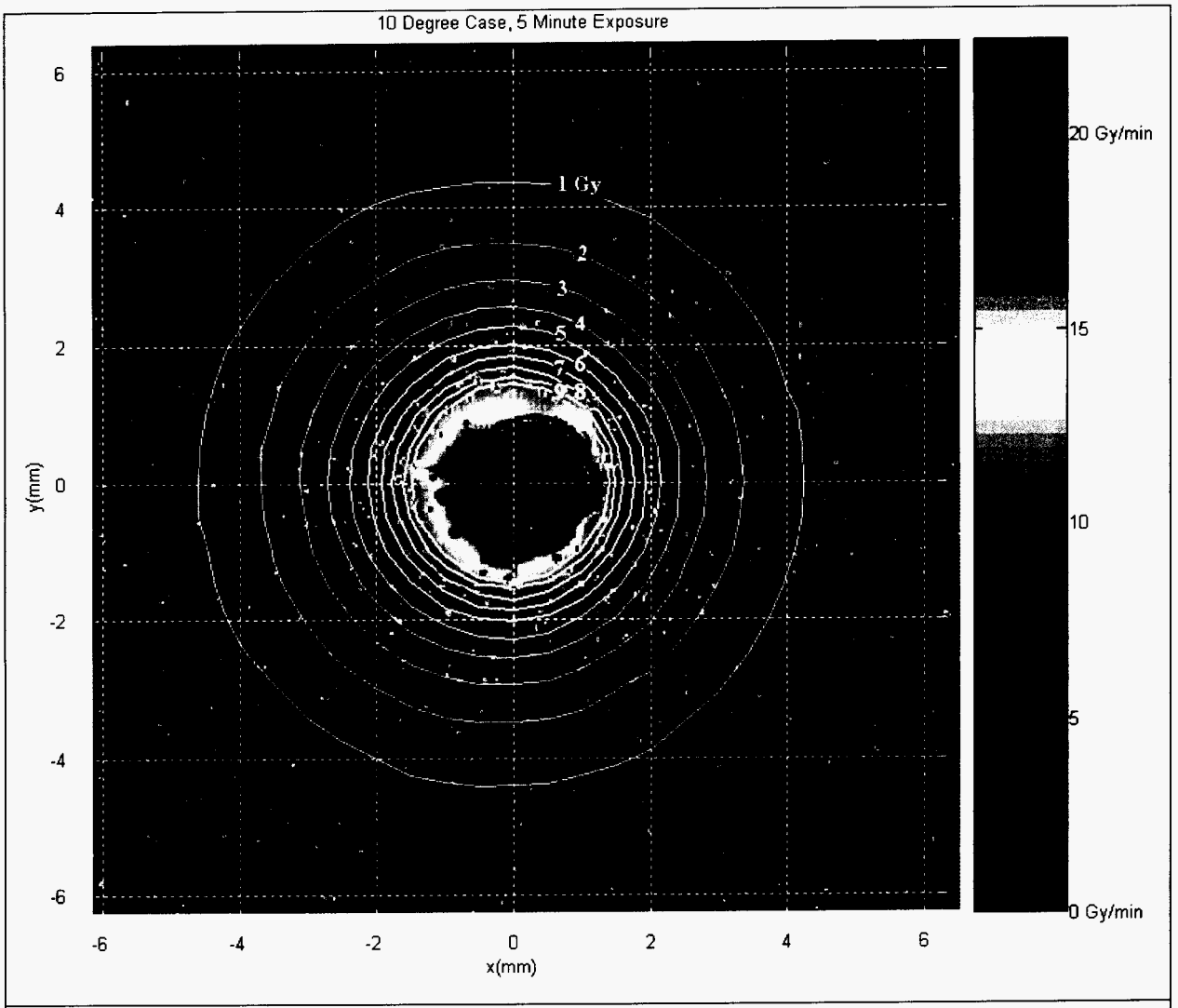

Figure X4. 10° 5 minute case, Field centered

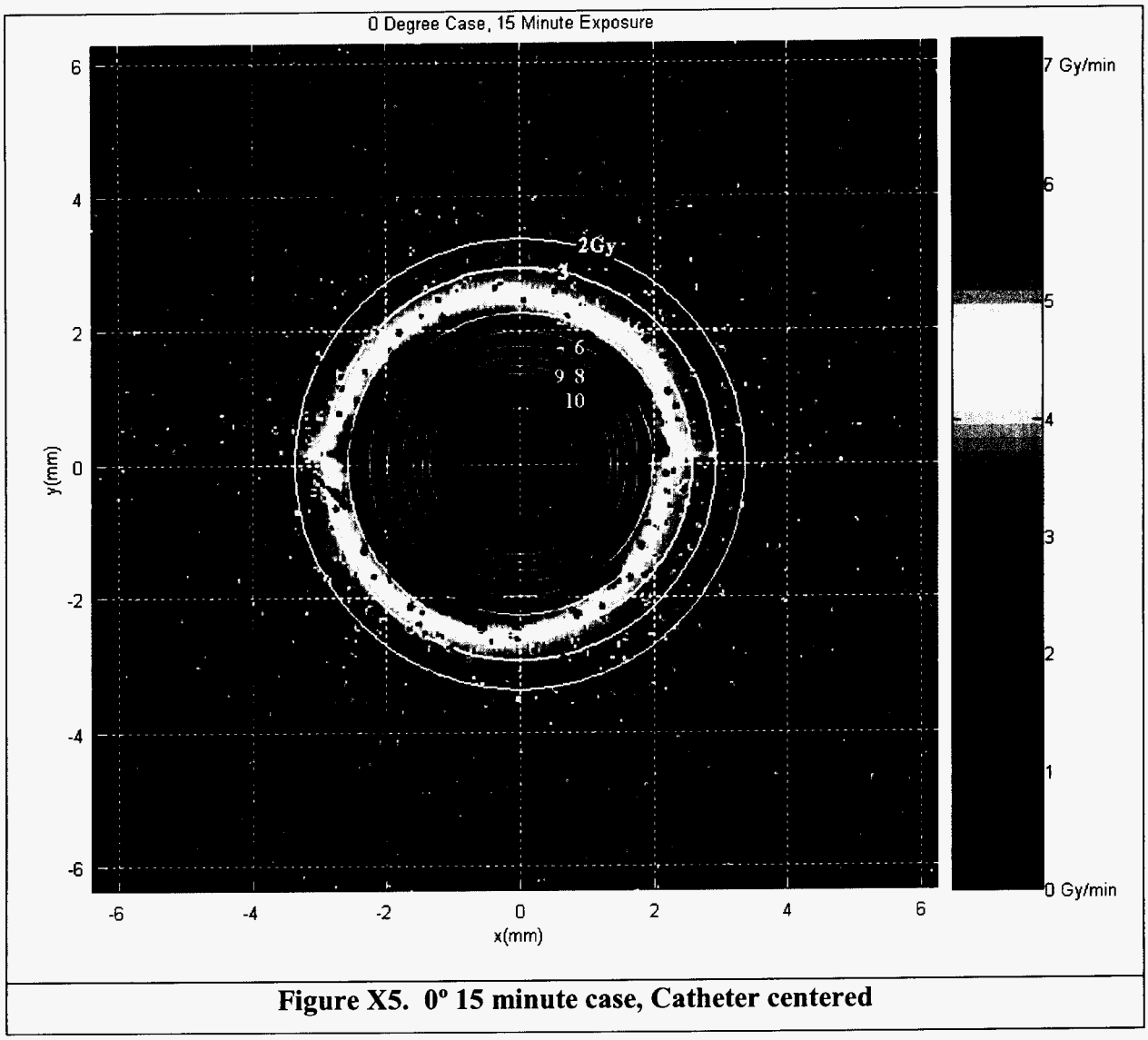

Figure X5. 0° 15 minute case, Catheter centered

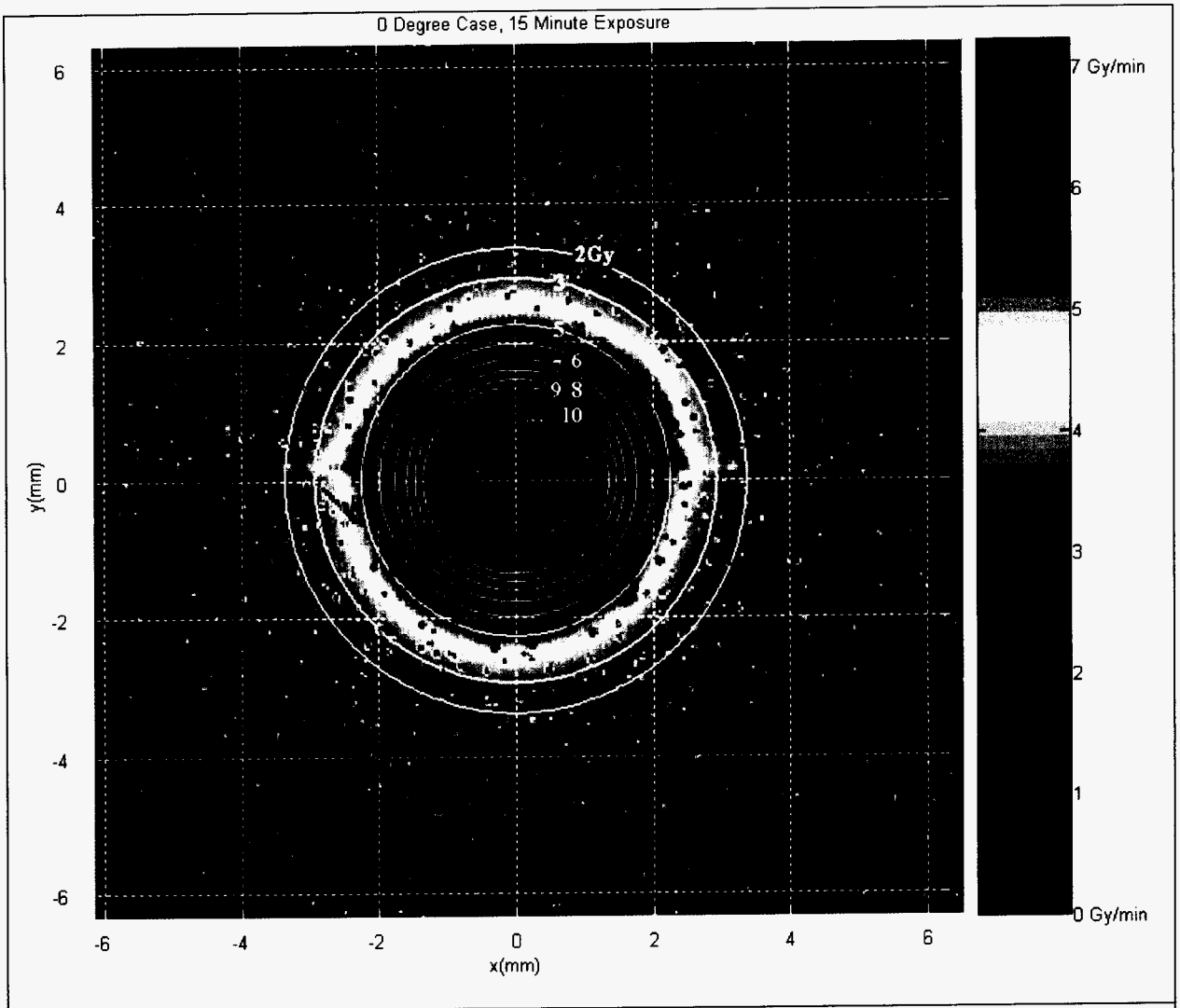

Figure X6. 0° 15 minute case, Field centered

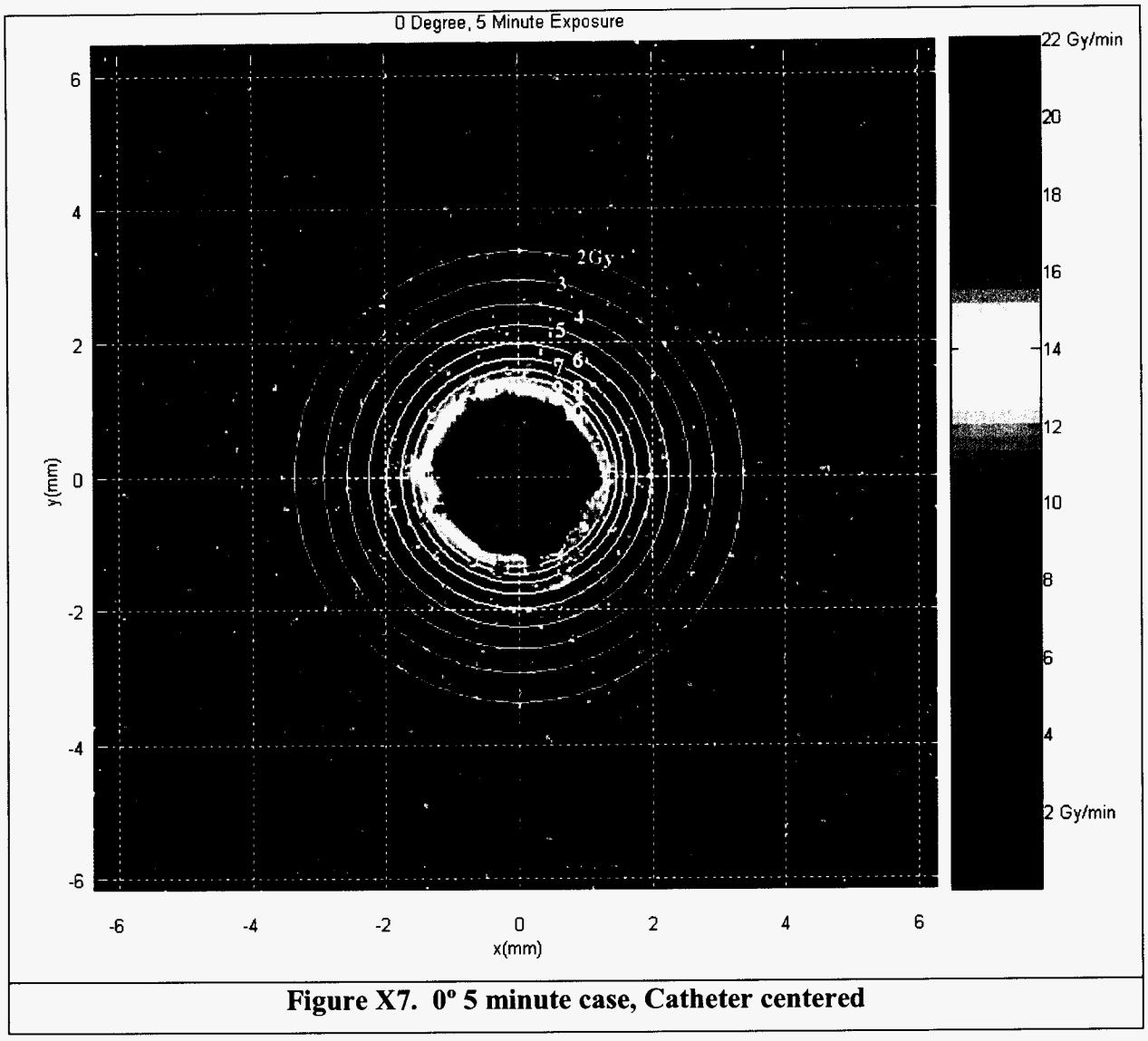

Figure X7. 0° 5 minute case, Catheter centered

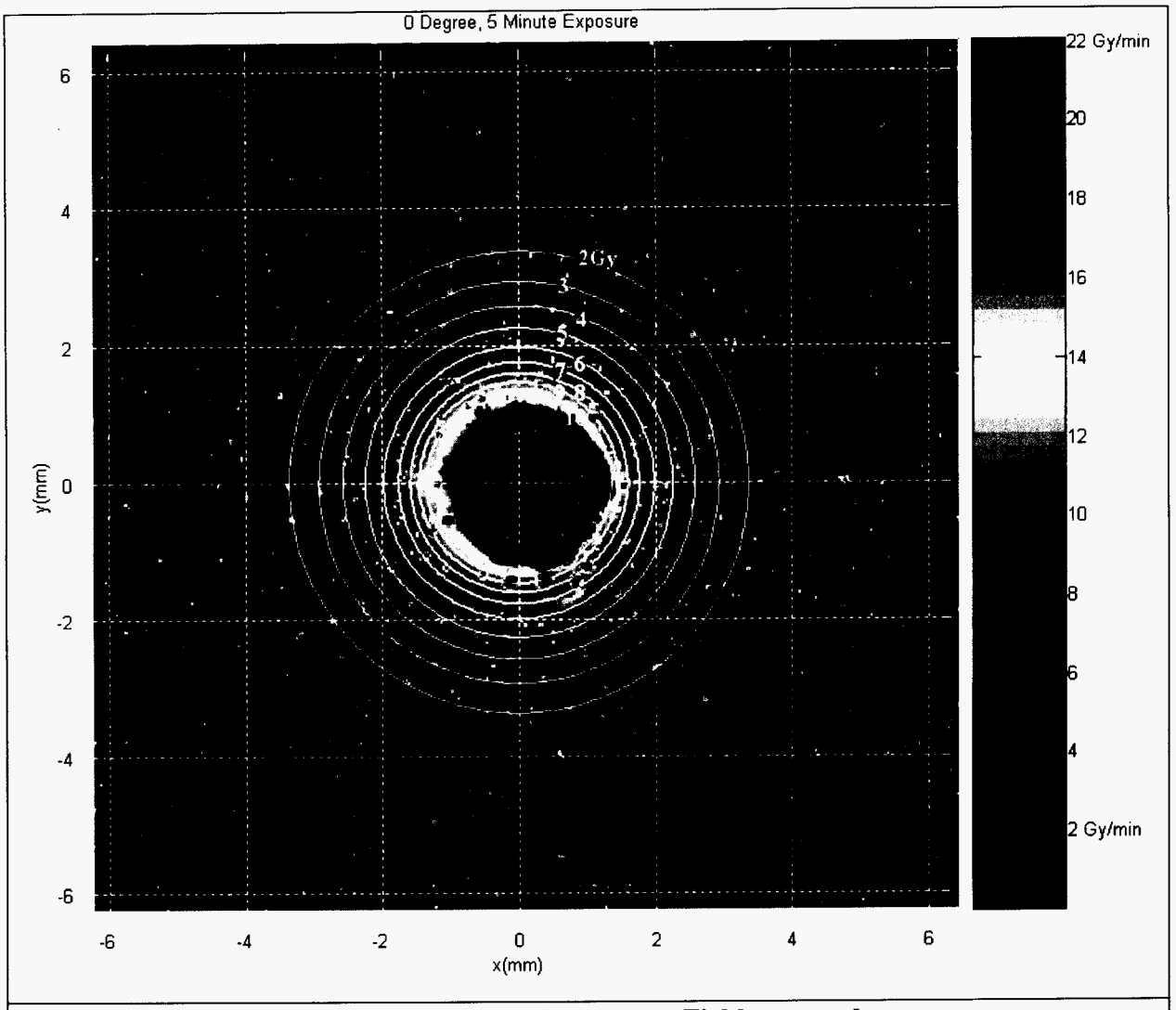

Figure X8. 0° 5 minute case, Field centered

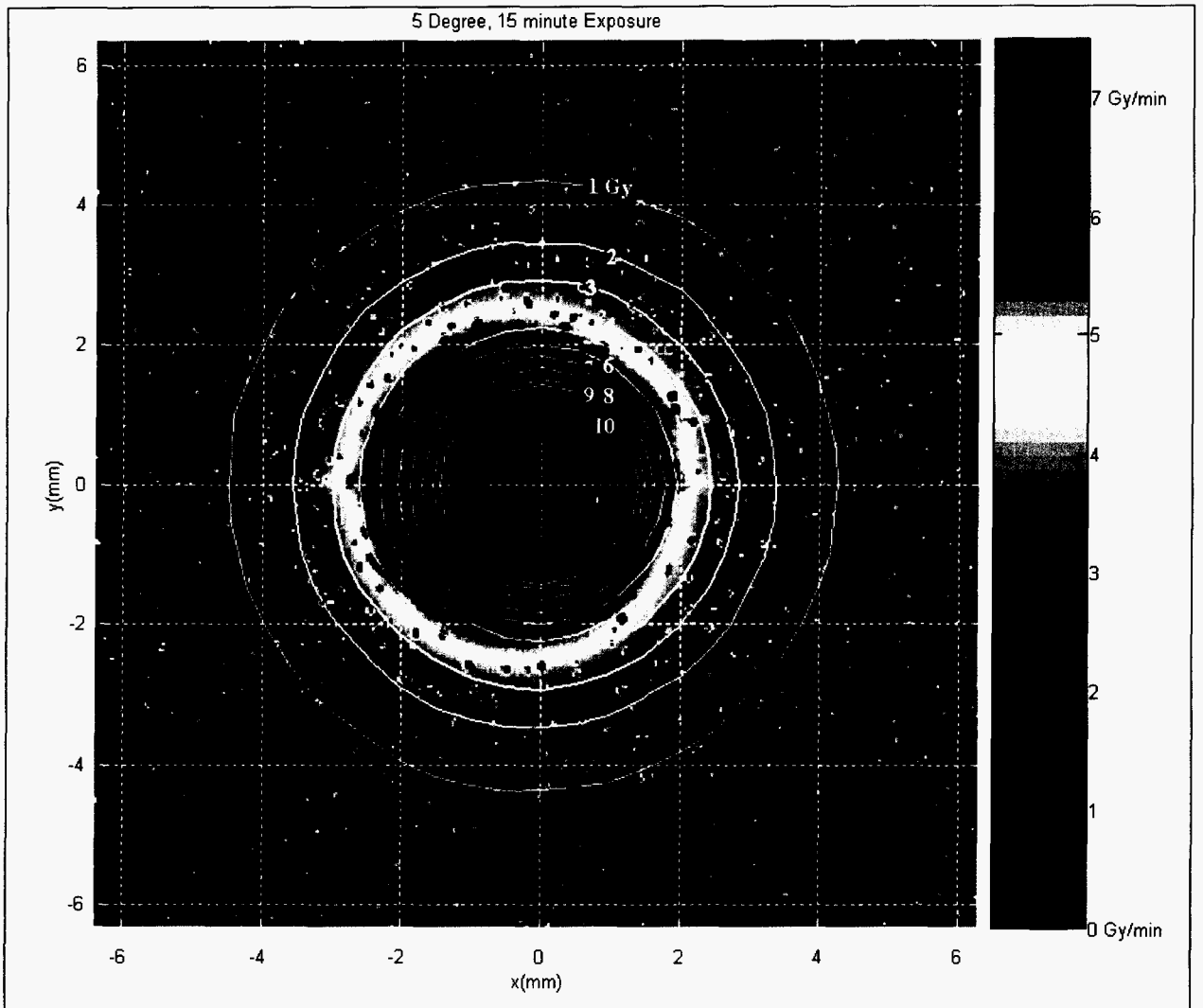

Figure X9. 5° 15 minute case, Catheter centered

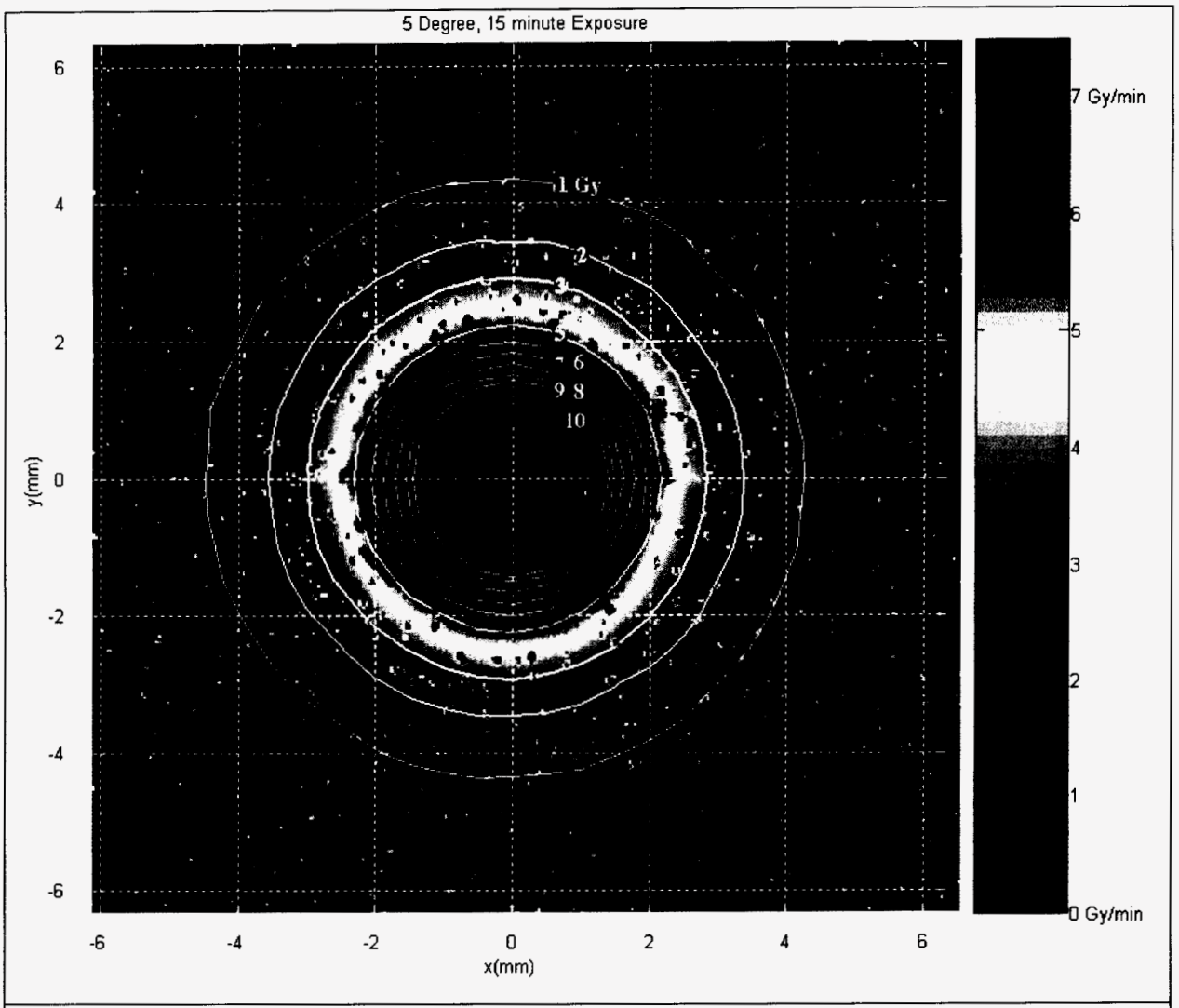

Figure X10. 5° 15 minute case, Field centered

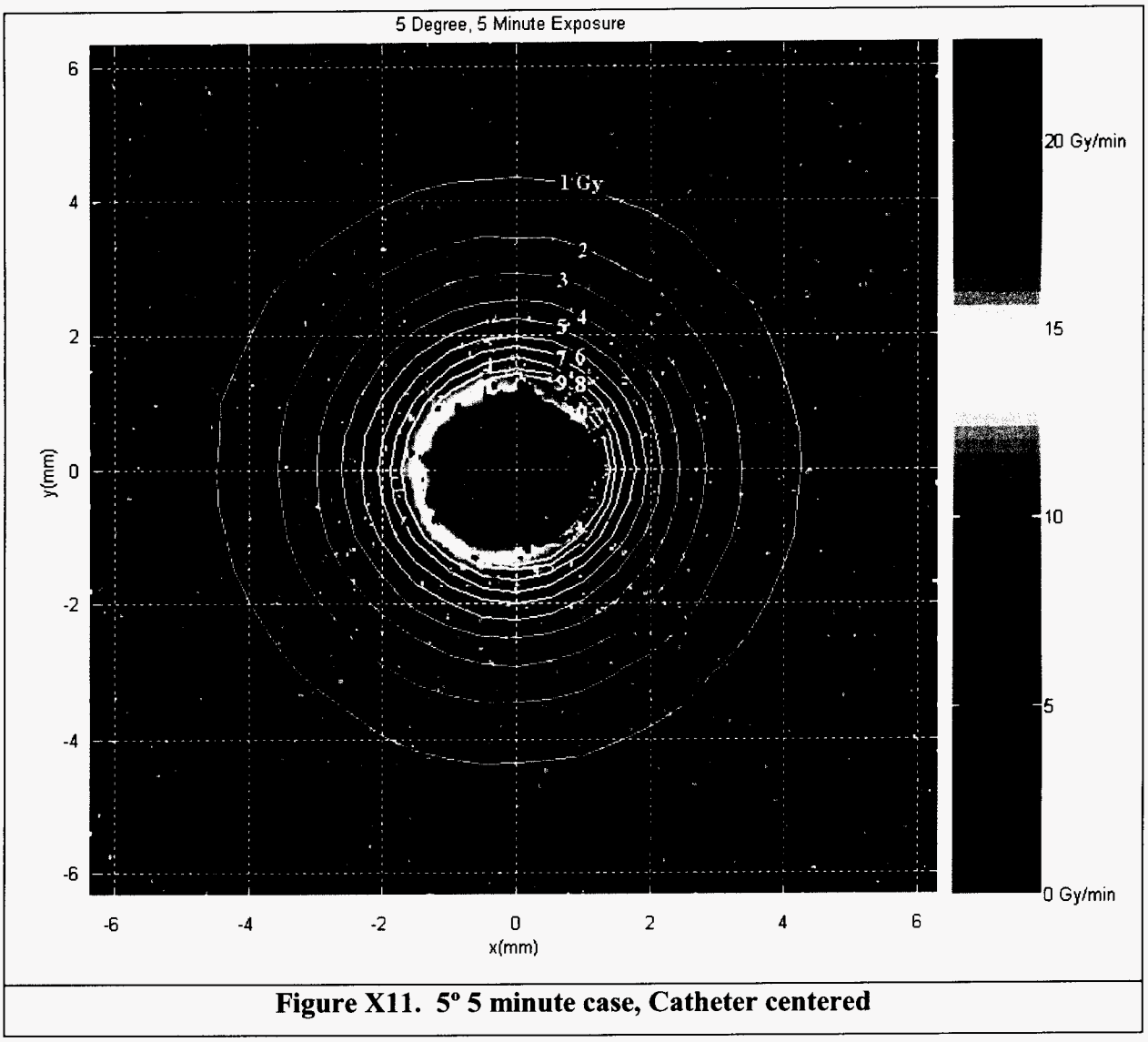

Figure X11. 5° 5 minute case, Catheter centered

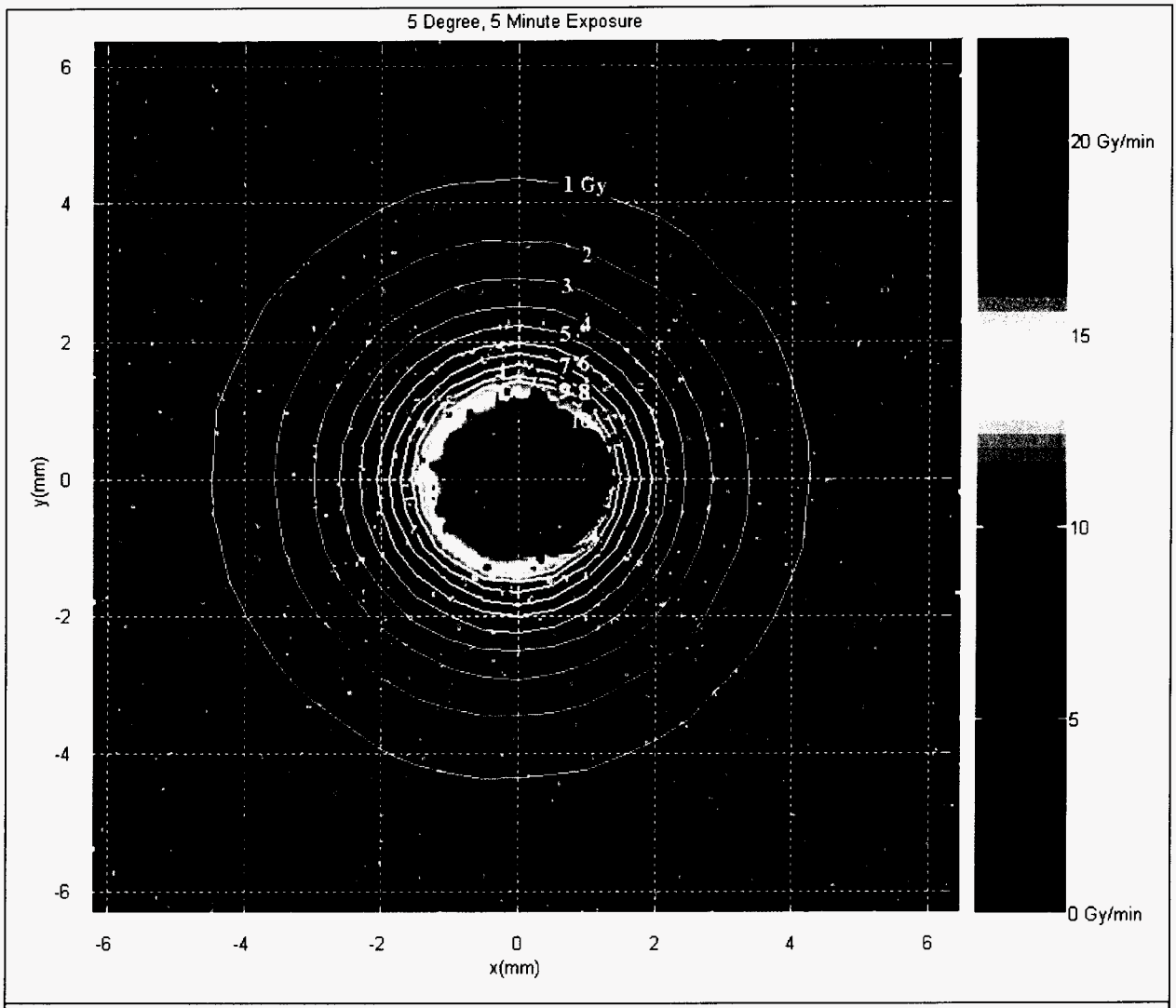

Figure X12. 5° 5 minute case, Field centered

2. Comparison of dose rate along the radial distance between the measured and simulated data:

The actual dose analysis along the axis of symmetry in the plane of the catheter curve was measured by mimicking the computer simulation voxel size. This voxel size of 0.50mm x 0.50mm is roughly equivalent to a 12 pixel x 12 pixel square on the film, yielding a distribution of 144 points for each voxel. Since the simulation integrates the dose over the voxel volume, this is, for purposes of the experiment, mathematically equivalent to taking the mean dose for the pixels on the film. This mean was found by fitting a Gaussian fit to the dose histogram for each individual voxel (24 voxels per data set, 6 on each side of the hole).

The first example of the results, Figure A16, shows the distribution for the 0° 5 minute case, illustrating the comparison between the actual measured voxel data Monte Carlo simulations.

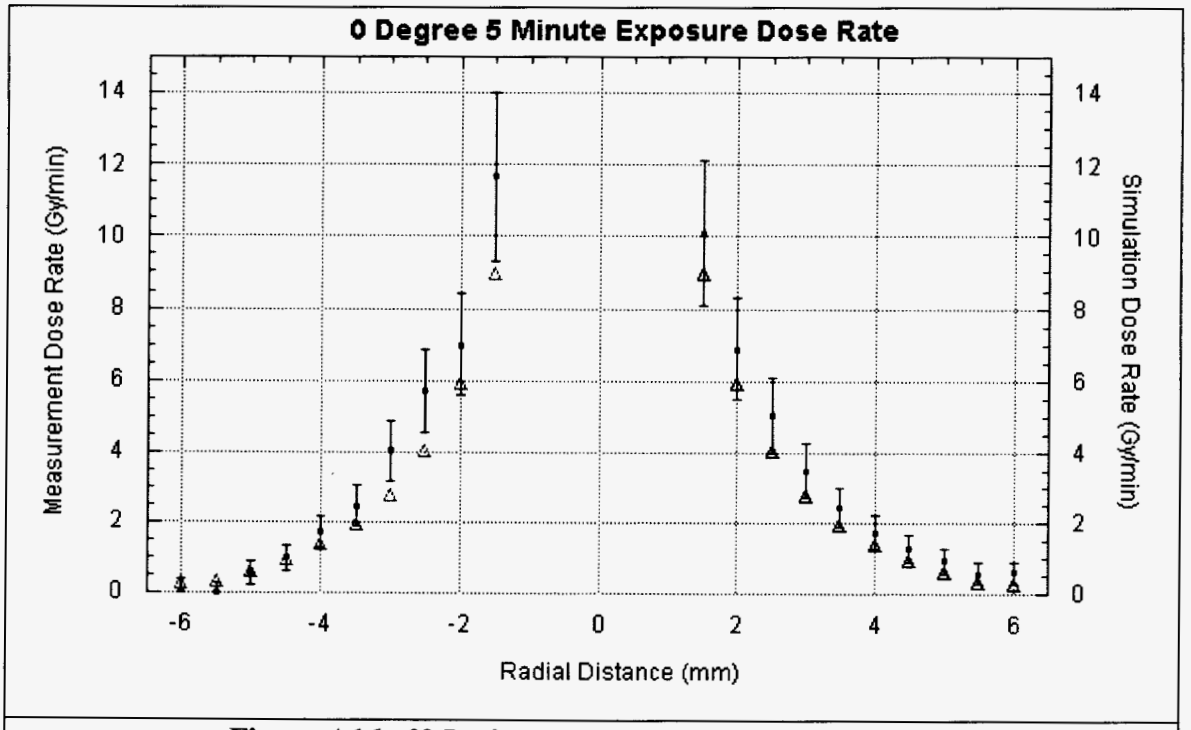

Figure A16. 0° 5 minute case, dose rate measurement

A semi-logarithmic examination of this plot shows the data appearing consistent with the simulation in the sense that the exponential "slope" of the simulation data is consistent with an exponential fit to the experimental data.

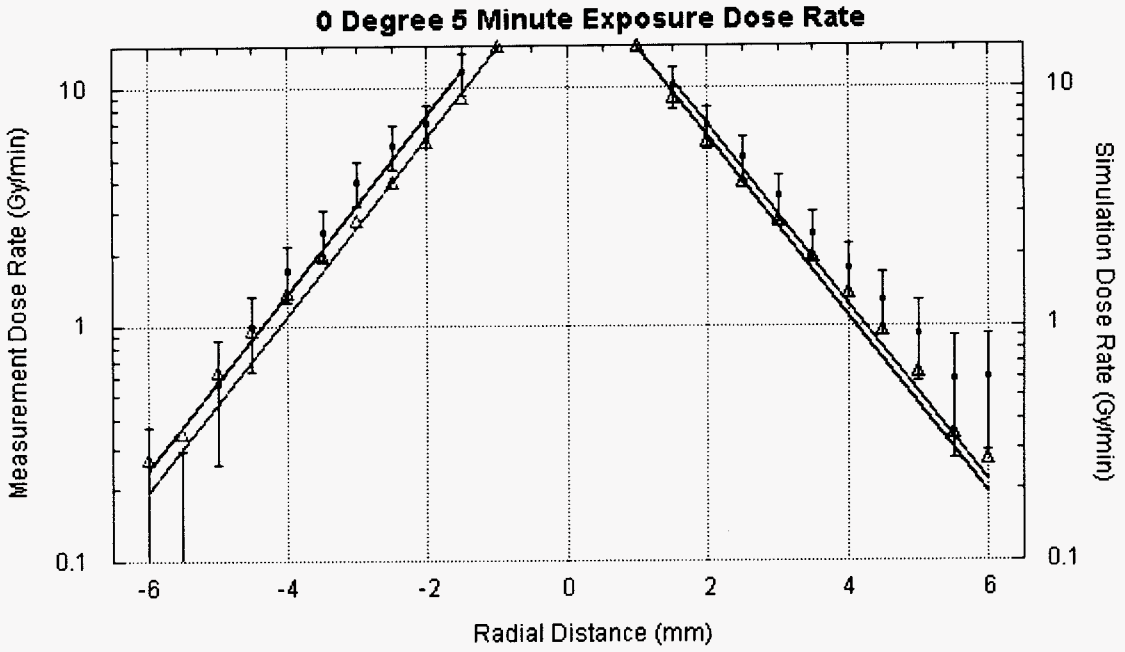

Figure A17. 0° 5 minute case, semi-log with exponential fits

The fits on the theoretical data were of the form $y = Ae^{r/b}$

and the fits of the experimental data were of the form $y = Ae^{(r-c)/b}$

where c is the effective radial shift distance of the data.

In the 5 minute linear case, the fit for both the right and the left side were the same, with A = 34.959 Gy/min and b = 1.1547mm. This results in a correlation of R^2 = 0.99632 for the theoretical data. Forcing these coefficients, the data on the left hand side fit with an R^2 = 0.98378 and c = 0.24978mm, while the right hand fit R^2 = 0.97583 and c = 0.13159mm. Thus the sum of the c values gives an effective shifting in the data of about 0.38mm.

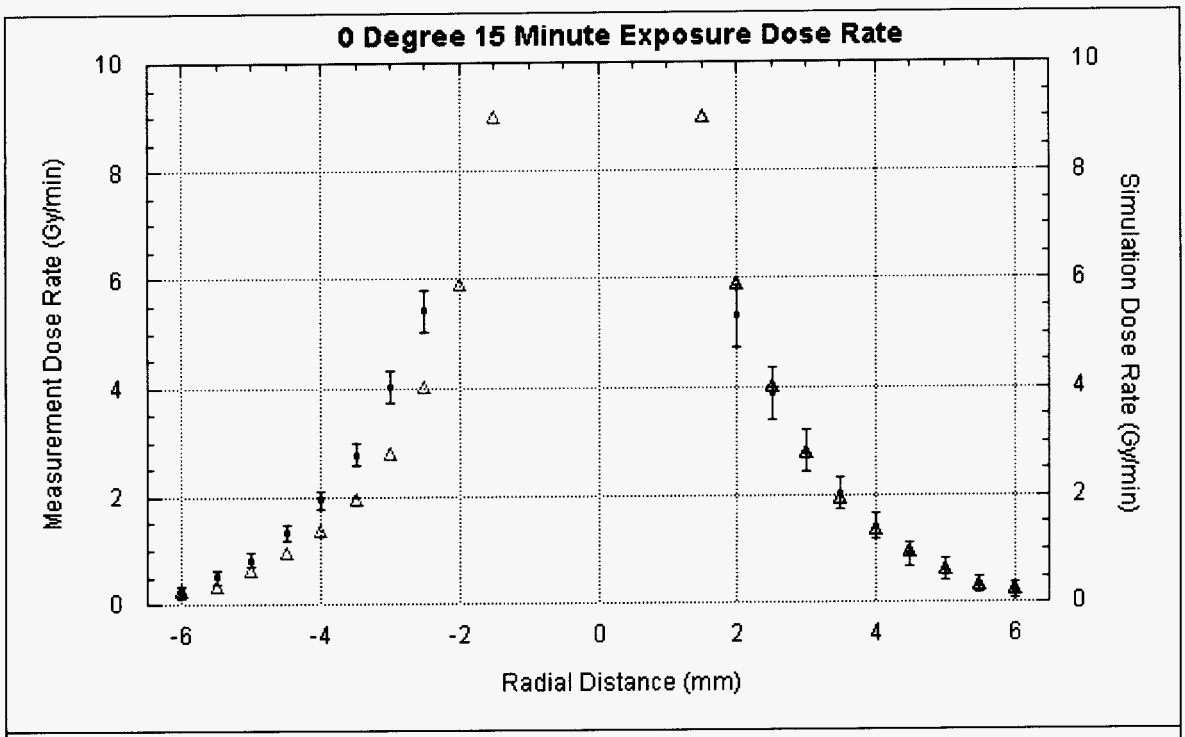

Figure A18. 0° 15 minute case, dose rate measurement

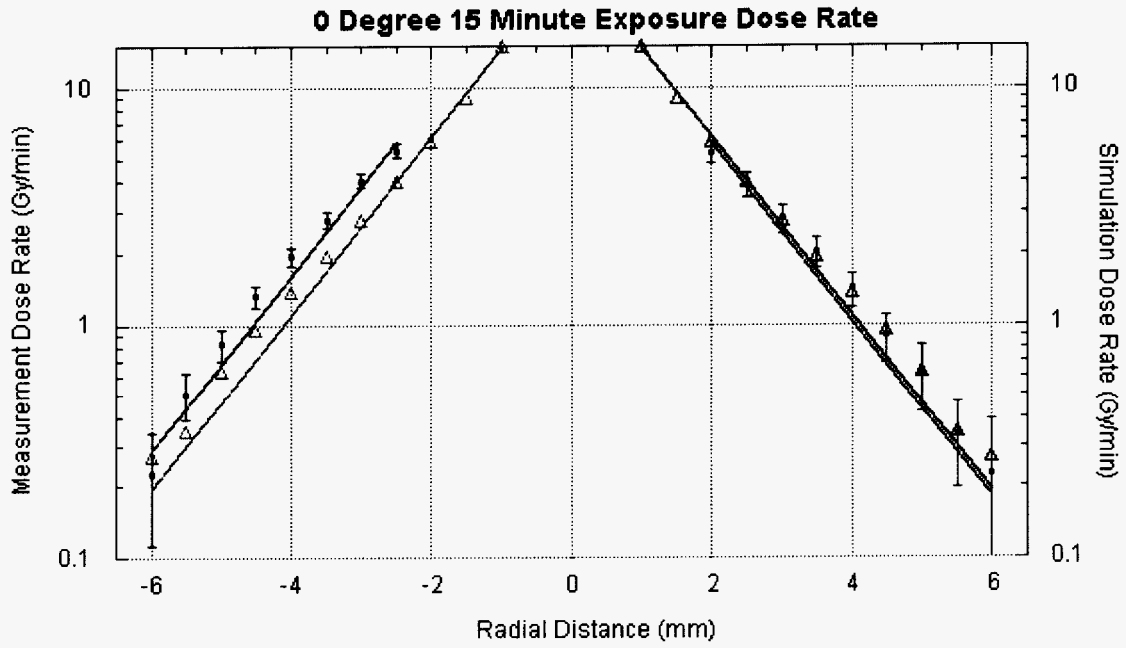

Figure A19. 0° 15 minute case, semi-log with exponential fits

In the 15 minute linear case, again the fit for both the right and the left side were the same with A = 34.959 Gy/min and b = 1.1547mm, R^2 = 0.99632. Forcing these coefficients, the data on the left hand side fit with an R^2 = 0.97462 and c = 0.438mm, while the right hand fit R^2 = 0.96519 and c = -0.077mm. Thus the sum of the c values gives an effective shifting in the data of about 0.36mm.

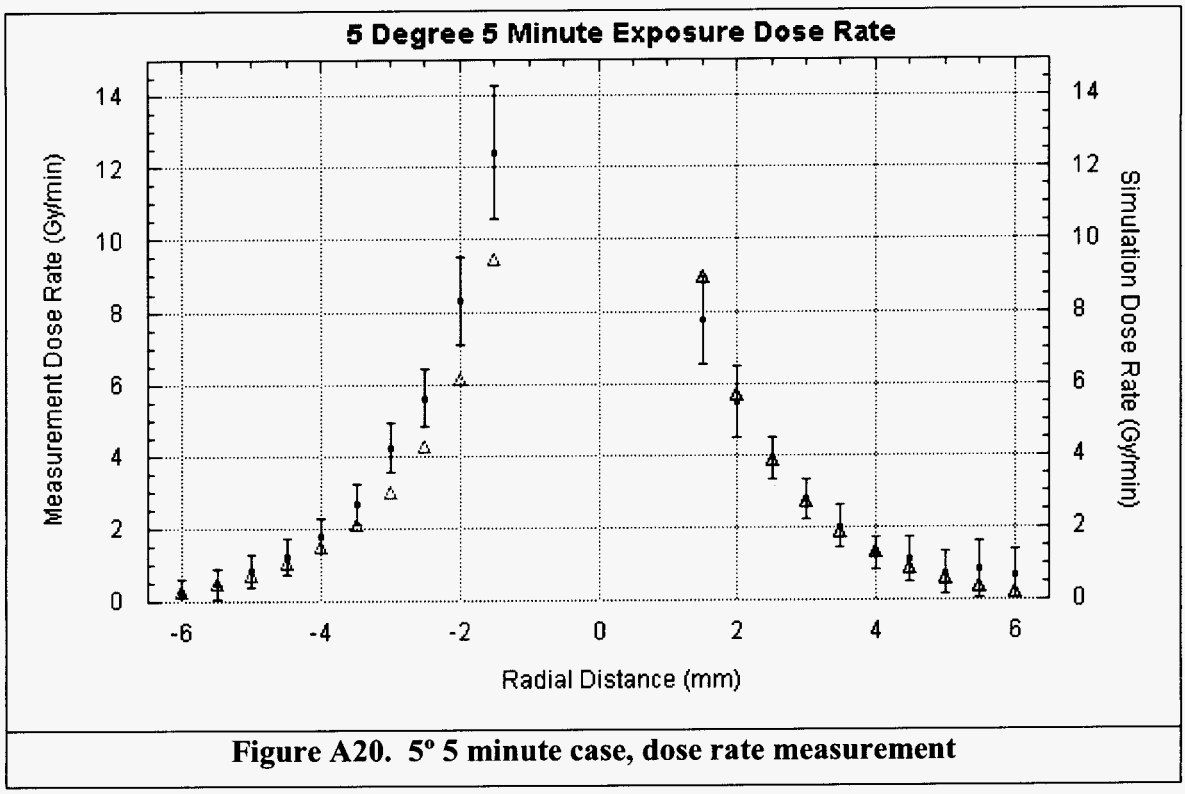

Figure A20. 5° 5 minute case, dose rate measurement

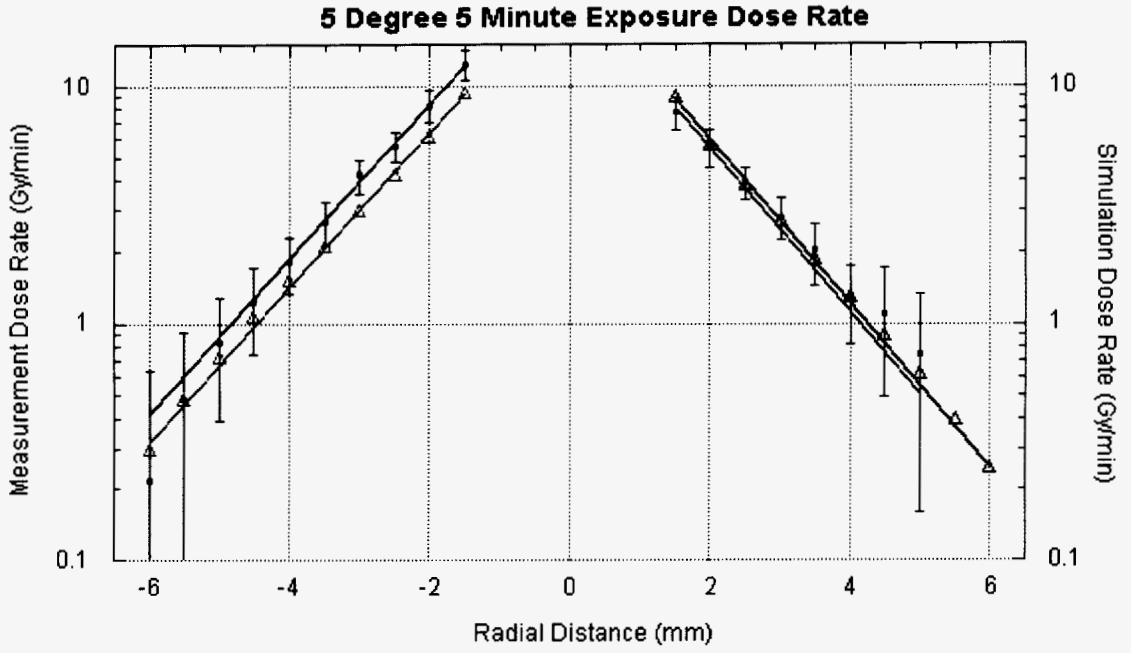

Figure A21. 5° 5 minute case, semi-log with exponential fits

In the 5° 5 minute case, the fit for the set on the left, the overdosed side, is given by A = 28.894 Gy/min and b = 1.3255mm with an R^2 = 0.99852. Forcing these coefficients for the data fit produces a fit giving an R^2 = 0.99867 and c = 0.367mm.

The right hand under-dosed simulation fits with A = 29.081 Gy/min and b = 1.2593mm with an R^2 = 0.99849. Forcing these coefficients for the experimental under-dosed data fit gives an R^2 = 0.98452 and c = -0.106mm. The sum of the c values gives an effective shifting in the data of about 0.26mm.

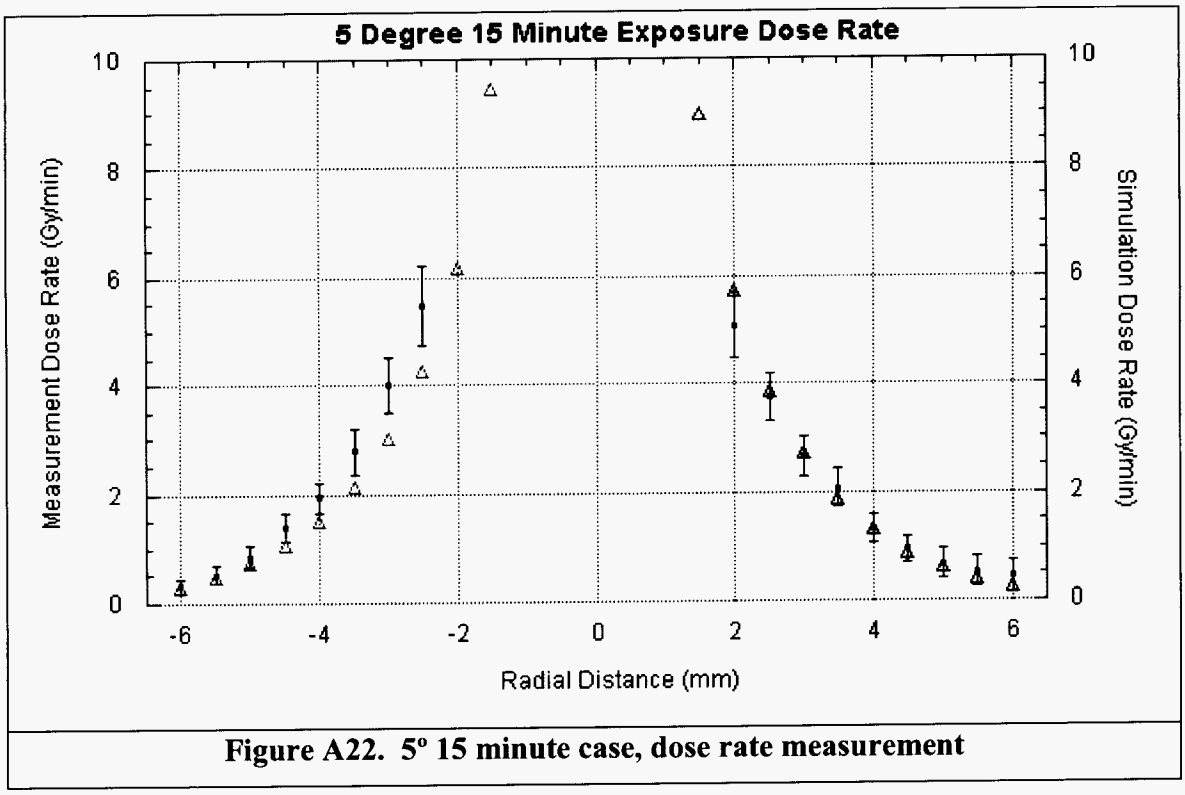

Figure A22. 5° 15 minute case, dose rate measurement

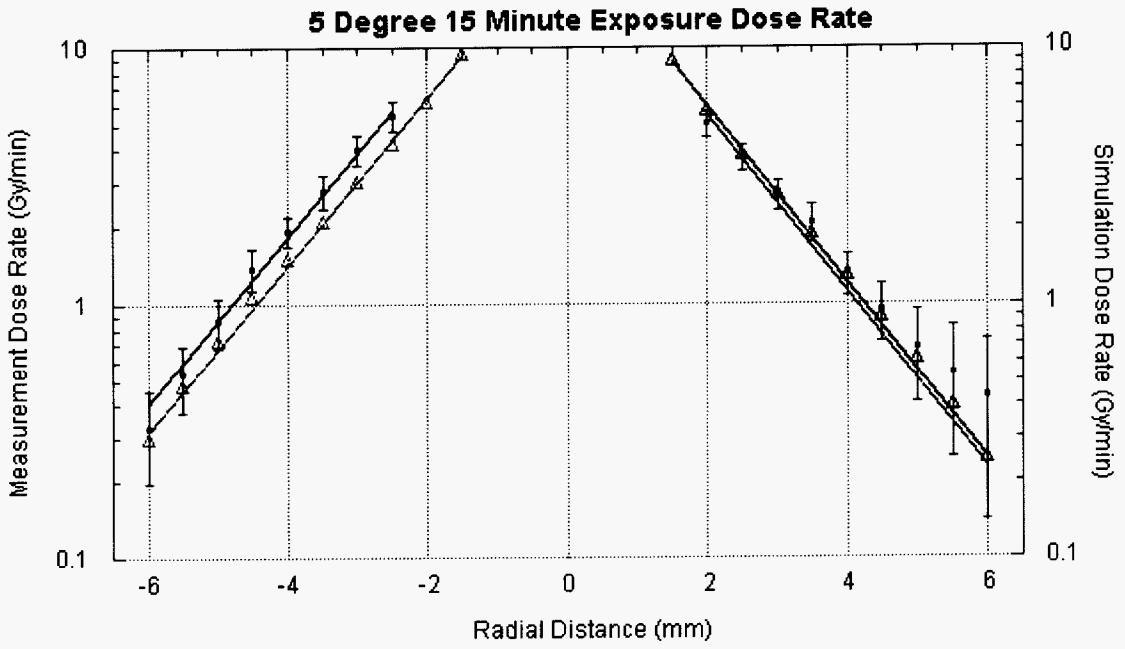

Figure A23. 5° 15 minute case, semi-log with exponential fits

In the 5° 15 minute case, again the fit for the set on the left, the overdosed side, is given by A = 28.894 Gy/min and b = 1.3255mm with an R^2 = 0.99852. Forcing these coefficients for the data fit produces a fit giving an R^2 = 0.9957 and c = 0.342mm.

The right hand under-dosed simulation fits with A = 29.081 Gy/min and b = 1.2593mm with an R^2 = 0.99849. Forcing these coefficients for the experimental under-dosed data fit gives an R^2 = 0.97336 and c = -0.106mm. The sum of the c values gives an effective shifting in the data of about 0.24mm.

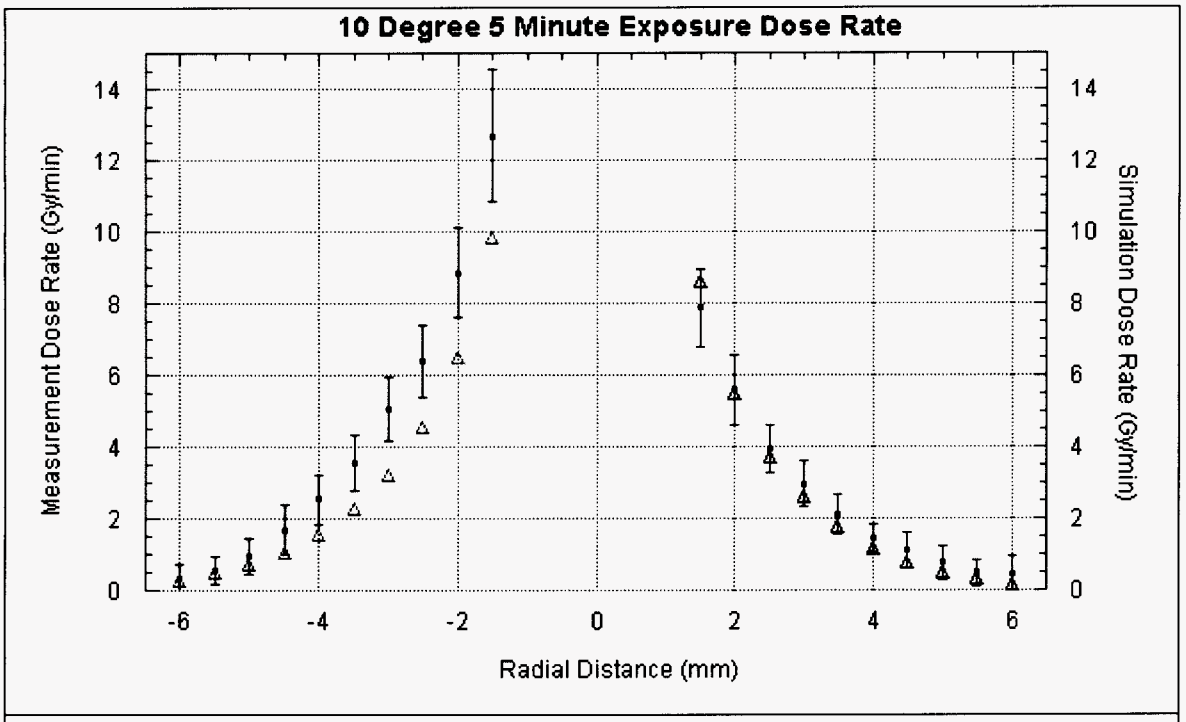

Figure A24. 10° 5 minute case, dose rate measurement

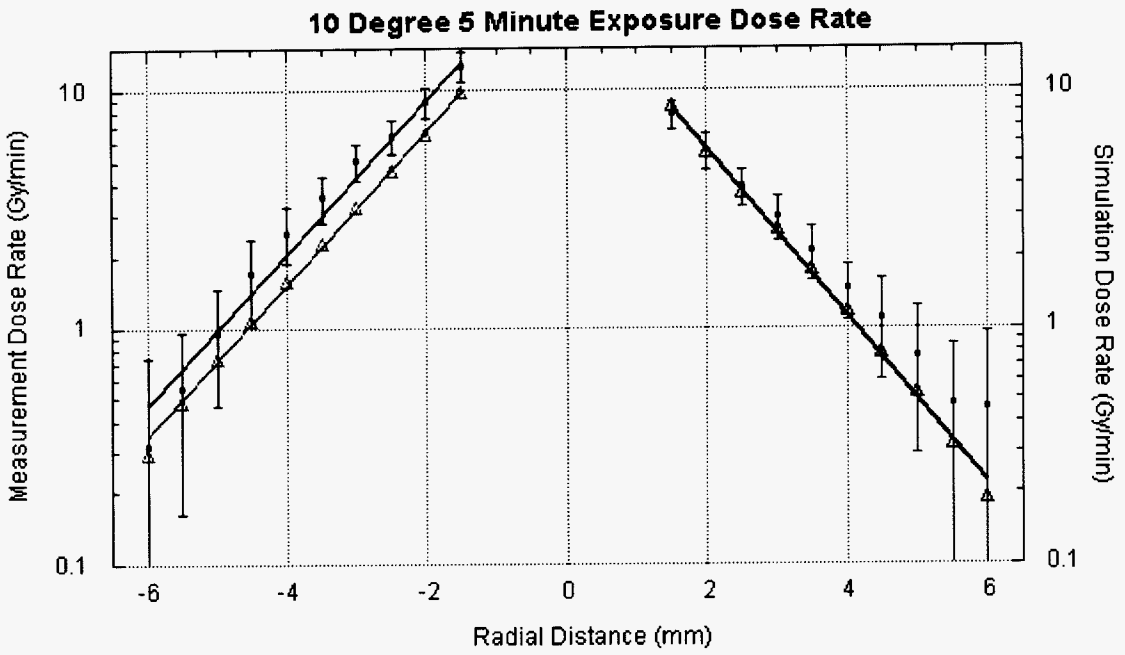

Figure A25. 10° 5 minute case, semi-log with exponential fits

In the 10° 5 minute case, the fit for the set on the left, the overdosed side, is given by A = 29.671 Gy/min and b = 1.3452mm with an R^2 = 0.99917. Forcing these coefficients for the data fit produces a fit giving an R^2 = 0.98967 and c = 0.403mm.

The right hand under-dosed simulation fits with A = 28.686 Gy/min and b = 1.2352mm with an R^2 = 0.99898. Forcing these coefficients for the experimental under-dosed data fit gives an R^2 = 0.97953 and c = -0.026mm. The sum of the c values gives an effective shifting in the data of about 0.38mm.

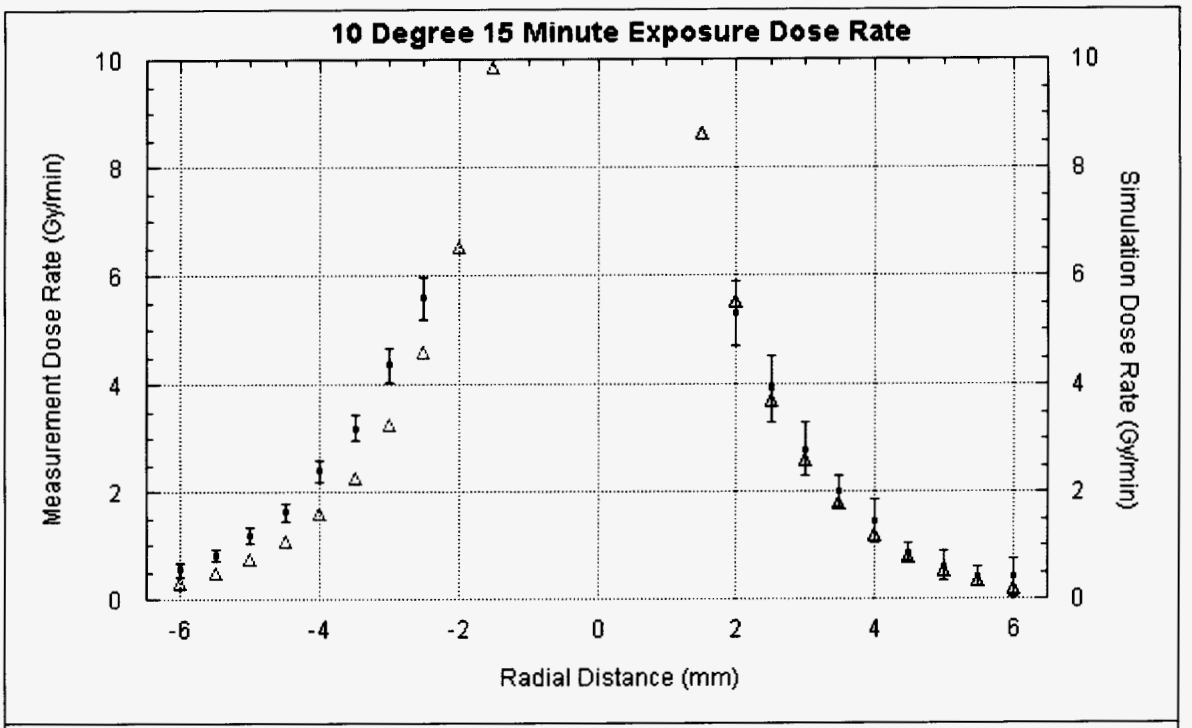

Figure A26. 10° 15 minute case, dose rate measurement

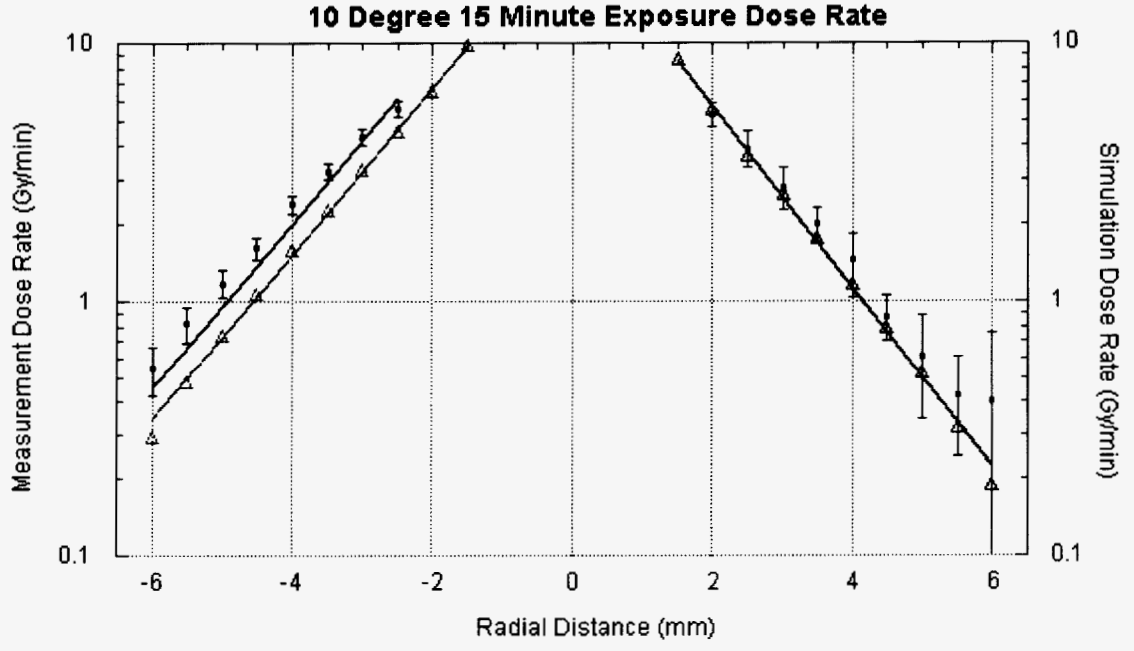

Figure A27. 10° 15 minute case, semi-log with exponential fits

In the 10° 15 minute case, again the fit for the set on the left, the overdosed side, is given by A = 29.671 Gy/min and b = 1.3452mm with an $R^2 = 0.99917$. Forcing these coefficients for the data fit produces a fit giving an $R^2 = 0.97012$ and c = 0.370mm.

The right hand under-dosed simulation fits with A = 28.686 Gy/min and b = 1.2352mm with an $R^2 = 0.99898$. Forcing these coefficients for the experimental under-dosed data fit gives an $R^2 = 0.97903$ and c = -0.002mm. The sum of the c values gives an effective shifting in the data of about 0.37mm.

IV. DISCUSSION AND CONCLUSIONS

The primary objectives of this project are: (i) to provide the Monte Carlo-based dosimetry protocol for intravascular brachytherapy with the catheter-based beta emitters, and (ii) to perform experimental measurements to verify the computational results.

During the first-year project period (June 1999 through May 2000), the computational set-ups and the test calculations of the electron dosimetry have been completed. The Monte Carlo simulations for the catheter-guiding beta sources in linear and curved coronary vessel models have been developed using the MCNP code (Monte Carlo N-Particle Tranport), MCNP4C. The experimental verification of the computational simulations were completed during the current project period (June 2000 through May 2002).

The dose rates in IVBT β-source for the linear and curved vessel model were investigated, and computed by MCNP simulations. As the radial distance (r) increases from 1.5 mm to 6.0 mm, the dose rate drops very steeply from 9.02 to 0.27 Gy/min. At the prescription point of 2.0 mm, the result was 5.92 Gy/min; a dwell time of 3.10 min delivers the Novoste prescription dose of 18.4 Gy.

Secondly, the dose rates are significantly less in the region of the last seed and gold marker. For example, for r=2.0 mm, the dose rate decreases from 5.92 Gy/min to 3.32 Gy/min, as z changes from 0 mm to 6.0 mm. This is a decrease of 44.1% at the edge voxel (z=6.0 mm), compared to that of non-edge voxel (z=0 mm). Thus, the treatment length by the source train is always less than its physical length. Consequently, one has to consider this reduced radiation field at source end for defining the real treatment length.

Moreover, the simulations for the curved vessel confirmed that there existed increased/decreased areas of the dose rates in the treatment region due to a degree of curvature in the coronary arteries. The inward curvature is attributed to an increase in the dose rate along the radial distances, while the outward curvature is responsible for the reduction in the dose level. At the prescription point of r=2.0 mm, compared to the dose rate of the linear model, 5° model had 3.87% overdose for inward direction and −3.54% underdose.

Normally, coronary arteries are mildly to severely tortuous and a simulations of the more curved model is needed to assess the necessity of the curvature effect for the more accurate dosimetry protocols of IVBT. Specifically, the 10° shift model with the radius of the curvature of 1.43 cm is planned.

We have developed the Monte Carlo based dosimetry protocol for IVBT simulating ^{90}Sr/Y source developed by Novoste Corporation. In order to verify the results from the computational simulations, the calibration procedure of both MD55-2 and HD810 radiochromic films has been performed. The obtained calibration curves between optical density and radiation dose will be used to convert the optical density map of films exposed to the source train to the iso-dose map. The special phantom for the curved vessel geometry has been fabricated. The calibrated range of dose to the films is between 10 and 150 Gy. We aim to deliver 100 Gy at the prescription distance (2mm from the source central axis) on the film so that the iso-dose curves should range from r=1.5 mm to r=5.5 mm (distance delivered by 10% of the dose to the prescription distance). However, we may possibly increase the calibration range of dose to obtain the iso-dose maps of a broader region.

Solid water phantom was fabricated to represent the same environment as the coronary fluids and the radiochromic film was employed to monitor the radiation dose. The iso-dose contours of the r-θ plane are in agreement with the simulation results for all cases of linear and curved coronary vessel geometries. The dose rates as a function of the radial distance illustrate the exponential behavior that is consistent with the simulations.

The experimental verifications for the dose rates computed by the simulations have been demonstrated and the experimental measurements are in good agreement with the Monte Carlo simulations. The developed computational algorithm will become the first Monte Carlo-based dosimetry protocol for intravascular brachytherapy.

V. BENEFITS TO STUDENTS IN NUCLEAR ENGINEERING EDUCATION RESEARCH (NEER)

A. M.S. Thesis

Clifford Racz is a second-year graduate student who has been a key person in the experimental dose measurements. Cliff is directly involved with the design and fabrication with the solid water phantom. He is expected to complete his M.S. thesis during the Fall 2002 semester.

B. Ph.D. Thesis

Ms. Jikkang Son has been involved with the NEER project during the last two years. She is mainly responsible for developing the Monte Carlo simulations and generating MCNP dosimetry protocol with developing iso-dose contours including experimental analysis. She has successfully completed her Ph.D. preliminary examination during the last Spring semester and is expected to complete her dissertation in May 2003.

VI. REFERENCES

[1] R. Waksman, S. B. King, and R. F. Mould, *Vascular Brachytherapy* (Nucletron B.V., The Netherland, 1996).

[2] H. I. Amols, M. Zaider, J. Weinberger, R. Ennis, P. B. Schiff, and L. E. Reinstein, "Dosimetric considerations for catheter-based beta and gamma emitters in the therapy of neointimal hyperplasia in human coronary arteries," Int. J. Radiat. Onc. Biol. Phys. **36**, 913–921 (1996).

[3] R. Nath, L. Anderson, G. Luxton, et al., "Dosimetry of interstitial brachytherapy sources: Recommendations of the AAPM Radiation Therapy Committee Task Group No. 43," Med. Phys. **22**, 209234 (1995).

[4] J. F. Briesmeister, "MCNP - A general purpose Monte Carlo *N*-Particle transport code, version 4B," LA-12625-M, Los Alamos National Laboratory, 1997.

[5] R. Nath, et al., "Intravascular brachytherapy physics: Report of the AAPM Radiation Therapy Committee Task Group No. 60," *Med. Phys.* **26**, 119152 (1999).

[6] J. E. Turner, Atoms, Radiation, and Radiation Protection (1995 by John Wiley & Sons, Inc., New York)

[7] S. Ye, X. A. Li, J. R. Zimmer, J. C. Chu, and C. K. Choi, "Dosimetric perturbations of linear array of β-emitter seeds and metallic stent in itravascular brachytherapy," Med.Phys. 27, 374-380 (2000).

[8] W.G.Cross, H.Ing, and N.Freedman, "A short atlas of beta-ray spectra," Phys.Med.Biol. 28, 1251-1260 (1983).

[9] Sung-Joon Ye, X. Allen Li, John R. Zimmer, James C. Chu, and Chan K. Choi, "Dose enhancement calculations due to neighboring β-emitter seeds and a stent in intravascular brachytherapy," Cardiovascular Radiation Therapy III, Washington, DC, February 1999.

[10] V. Sehgal, Z. Li, and J. R. Palta, "Dosimetric effect of source centering and residual plaque for β-emitting catheter based intravascular brachytherapy sources," Med.Phys. 28 (10), 2162-2171 (2001).

[11] O. Chibani, and X. A. Li, "Dosimetric effects of source–offset in intravascular brachytherapy," Med.Phys. 29 (4), 530-537 (2002)

[12] S. Ye, C. K. Choi, and S.Naqvi, "Non-uniformity of absorbed dose due to curvature of beta-emitter array in intravascular irradiation," World Congress on Medical Physics and Biomedical Engineering, Chicago, IL, July 2000.

[13] B. M. Coursey and R. Nath, "Radionuclide Therapy," Physics Today, April 2000.

[14] S. Ye, C. K. Choi, and S. Naqvi, "Monte Carlo dose calculations of curved β-emitter sources for intravscular brachytherapy," Cardiovascular Radiation Therapy IV, Washington, DC, February 2000.

[15] C. K. Choi, J. Son, S. J. Ye, "The Monte Carlo-Based Dosimetry of Beta Emitters for Intravascular Brachytherapy," U.S. Department of Energy's Nuclear Engineering Education Research: Hightlights of Recent and Current Research-I, 85-86 (2001)

[16] Azam Niroomand-Rad, et al., "Radiation film dosimetry: Recommendations of AAPM Radiation Therapy Committee Task Group 55," Med.Phys. 25, 2093-2115 (1998).

[17] A.S.Meigooni, M.F.Sanders, G.S.Ibbott, and S.R.Szeglin, "Dosimetric characteristics of an improved radiochromic film," Med.Phys. 23 (11), November 1996.

[18] M.Bambynek, D.Fluhs, U.Quast, D.Wegener, and C.G.Soares, "A high-precision, high-resolution and fast dosimetry system for beta source applied in cardiovascular brachytherapy," Med.Phys. 27 (4), April 2000.

[19] Y. Zhu, A. S. Kirov, V. Mishra, A. S. Meigooni, and J. F. Williamson, "Quantitative evaluation of radiochromic film response for two-dimensional dosimetry," Med.Phys. 24 (2), February 1997.

[20] L.E.Reinstein and G.R.Gluckman, "Optical density dependence on postirradiation temprature and time for MD-55-2 type radiochromic film," Med.Phys. 26 (3), March 1999.

[21] J. F. Demosey, D. A. S. Mutic, J. Markman, A. S. Kirov, G. H. Nussbaum, and J. F. Williamson, "Validation of a precision radiochromic film dosimetry system for quantitative two-dimensional imaging of acute exposure dose distributions," Med.Phys. 27 (10), October 2000.

[22] D.M.Duggan, C.W.Coffey II, John L. Lobdell, and Michael C. Schell, "Radiochromic film dosimetry of a high dose rate beta source for intravascular brachytherapy," Med.Phys. 26 (11), November 1999.

[23] C.G.Soares, D.G.Halpern, and C.K.Wang, "Calibration and characterization of beta-particle sources for intravascular brachytherapy," Med.Phys. 26, 339-346 (1998).

Appendix A

The Monte Carlo Code for the linear vessel model

```
A BLOOD VESSEL CONTAINS FIVE Sr-Y 90 CERAMIC SEEDS
1     1  -3.52   (-1 -3 4):(-1 5 -7):(-1 -6 8):(-1 9 -11):(-1 -10 12) $ CERAM
2     2  -7.92   -2 -13 14 #1                                  $ S.S.
3     0          (-15 16 -17 18 -19 20) (2:13:-14)     fill=1       $ WATER
4     0          15:-16:17:-18:19:-20                          $ VACUU
5     3  -1.0    -21 22 -23 24 -25 26 u=1 lat=1 vol=1.25e-04        $ LATTI

1     cz  0.028
2     cz  0.032
3     pz  0.12
4     pz  -0.12
5     pz  0.13
6     pz  -0.13
7     pz  0.37
8     pz  -0.37
9     pz  0.38
10    pz  -0.38
11    pz  0.62
12    pz  -0.62
13    pz  0.625
14    pz  -0.625
15    px  0.675
16    px  -0.675
17    py  0.675
18    py  -0.675
19    pz  0.675
20    pz  -0.675
21    px  0.025
22    px  -0.025
23    py  0.025
24    py  -0.025
25    pz  0.025
26    pz  -0.025

mode   e p                    $COUPLED ELECTRON/PHOTON TRANSPORT
C m1   CERAMIC
m1     1000  0.1
       8000  0.54
       25000 0.02
       14000 0.02
       20000 0.03
       22000 0.11
```

```
      26000  0.18
C m2    STAINLESS STEEL
m2      14000  1.93e-02
        24000  0.180
        25000  1.97e-02
        26000  0.669
        28000  0.112
C m3    WATER
m3      1001   0.667
        8016   0.333
imp:e   1 1 1 0 1
imp:p   1 1 1 0 1
C       ELECTRON DISTRIBUTION HOMOGENEOUSLY IN CELL 1 VOLUME
sdef    cel 1 par 3 erg d1 axs 0 0 1 rad d2 ext d3
sc1     INITIAL SOURCE SPECTRUM
si1     a 0.001 0.1 0.2 0.3 0.4 0.5 0.55 0.75 1.0 1.25 1.5
        1.6 1.7 1.8 1.9 2.0 2.1 2.2 2.3
sp1     0.1666 0.1652 0.1554 0.14 0.0896 0.0462 0.0314 0.0311 0.0302
        0.0294 0.0252 0.0224 0.0196 0.0168 0.0126 0.0092 0.0062 0.0028 0
sc2     UNIFORM IN SEED CROSS-SECTIONS
si2     0.028
sc3     UNIFORM IN SEED HEIGHT
si3     0.12
fc4     PHOTON FLUX [/CM**2] IN LATTICES ALONG RADIAL
f4:p    (5<5[0:13 0:0 0:0])
e4      0.025 0.05 0.075 0.1 0.2 0.3 0.4 0.5 0.6 0.7 0.8
fc14    ELECTRON FLUX [/CM**2] IN LATTICES ALONG RADIAL
f14:e   (5<5[0:13 0:0 0:0])
e14     0.0015 0.002 0.005 0.01 0.025 0.05 0.075 0.1 0.2 0.3 0.4 0.5 0.6
        0.7 0.8 0.9 1 1.1 1.2 1.3 1.4 1.5 1.6 1.7 1.8 1.9 2 2.1 2.2 2.3
fc6     PHOTON DOSE [cGy] IN LATTICES ON Z = 0 PLANE
f6:p    (5<5[0:13 0:0 0:0])
fm6:p   1.602e-08
fc8     ELECTRON/PHOTON DOSE [MeV] IN LATTICES ON Z = 0 PLANE
*f8:p,e (5<5[0:13 0:0 0:13])
nps     2.0e+06
print
```

Appendix B

The Monte Carlo Code for the 5 degree curved vessel model

```
A CURVED VESSEL (05 Degree)
1     1  -4.81  -1 -3 4
2     2  -7.92  -2 -5 6 (1:3:-4)
3     like 1 but trcl=1
4     like 2 but trcl=1
5     like 1 but trcl=2
6     like 2 but trcl=2
7     like 1 but trcl=3
8     like 2 but trcl=3
9     like 1 but trcl=4
10    like 2 but trcl=4
11    3  -1.0  13 -14 -41 42 -43 44 vol=1.25-4
12    3  -1.0  14 -15 -41 42 -43 44 vol=1.25-4
13    3  -1.0  15 -16 -41 42 -43 44 vol=1.25-4
14    3  -1.0  16 -17 -41 42 -43 44 vol=1.25-4
15    3  -1.0  17 -18 -41 42 -43 44 vol=1.25-4
16    3  -1.0  18 -19 -41 42 -43 44 vol=1.25-4
17    3  -1.0  19 -20 -41 42 -43 44 vol=1.25-4
18    3  -1.0  20 -21 -41 42 -43 44 vol=1.25-4
19    3  -1.0  21 -22 -41 42 -43 44 vol=1.25-4
20    3  -1.0  22 -23 -41 42 -43 44 vol=1.25-4
21    3  -1.0  23 -24 -41 42 -43 44 vol=1.25-4
22    3  -1.0  24 -25 -41 42 -43 44 vol=1.25-4
23    3  -1.0  25 -26 -41 42 -43 44 vol=1.25-4
24    3  -1.0  -27 28 -41 42 -43 44 vol=1.25-4
25    3  -1.0  -28 29 -41 42 -43 44 vol=1.25-4
26    3  -1.0  -29 30 -41 42 -43 44 vol=1.25-4
27    3  -1.0  -30 31 -41 42 -43 44 vol=1.25-4
28    3  -1.0  -31 32 -41 42 -43 44 vol=1.25-4
29    3  -1.0  -32 33 -41 42 -43 44 vol=1.25-4
30    3  -1.0  -33 34 -41 42 -43 44 vol=1.25-4
31    3  -1.0  -34 35 -41 42 -43 44 vol=1.25-4
32    3  -1.0  -35 36 -41 42 -43 44 vol=1.25-4
33    3  -1.0  -36 37 -41 42 -43 44 vol=1.25-4
34    3  -1.0  -37 38 -41 42 -43 44 vol=1.25-4
35    3  -1.0  -38 39 -41 42 -43 44 vol=1.25-4
36    3  -1.0  -39 40 -41 42 -43 44 vol=1.25-4
37    3  -1.0  -7 8 -9 10 -11 12 #1 #2 #3 #4 #5 #6 #7 #8 #9 #10 #11
            #12 #13 #14 #15 #16 #17 #18 #19 #20 #21 #22 #23 #24
            #25 #26 #27 #28 #29 #30 #31 #32 #33 #34 #35 #36
38    0  7:-8:9:-10:11:-12
```

```
1     cz  0.028
2     cz  0.032
3     pz  0.12
4     pz  -0.12
5     pz  0.125
6     pz  -0.125
7     px  0.725
8     px  -0.725
9     py  0.725
10    py  -0.725
11    pz  0.775
12    pz  -0.775
13    px  0.05
14    px  0.1
15    px  0.15
16    px  0.2
17    px  0.25
18    px  0.3
19    px  0.35
20    px  0.4
21    px  0.45
22    px  0.5
23    px  0.55
24    px  0.6
25    px  0.65
26    px  0.7
27    px  -0.05
28    px  -0.1
29    px  -0.15
30    px  -0.2
31    px  -0.25
32    px  -0.3
33    px  -0.35
34    px  -0.4
35    px  -0.45
36    px  -0.5
37    px  -0.55
38    px  -0.6
39    px  -0.65
40    px  -0.7
41    py  0.025
42    py  -0.025
43    pz  0.025
44    pz  -0.025

mode   e p                    $COUPLED ELECTRON/PHOTON TRANSPORT
```

```
C m1   CERAMIC
m1     8000  0.6
       22000  0.2
       38000  0.2
C m2   STAINLESS STEEL
m2     14000  1.93e-02
       24000  0.180
       25000  1.97e-02
       26000  0.669
       28000  0.112
C m3   WATER
m3     1001   0.667
       8016   0.333
imp:e   1 36r 0
imp:p   1 36r 0
C      TRANSFORMATIONS
tr1    1.1016-2 0 2.5231-1 .99619 0 -.08716 0 1 0 .08716 0 .99619
tr2    1.1016-2 0 -2.5231-1 .99619 0 .08716 0 1 0 -.08716 0 .99619
tr3    4.3981-2 0 5.0271-1 .98481 0 -.17365 0 1 0 .17365 0 .98481
tr4    4.3981-2 0 -5.0271-1 .98481 0 .17365 0 1 0 -.17365 0 .98481
C      ELECTRON DISTRIBUTION HOMOGENEOUSLY IN VOLUME OF SEEDS
sdef   cel 1 par 3 erg d1 pos 0 0 0 axs 0 0 1 rad d2 ext d3
sc1    INITIAL SOURCE SPECTRUM
si1    a 0.001 0.1 0.2 0.3 0.4 0.5 0.55 0.75 1.0 1.25 1.5
       1.6 1.7 1.8 1.9 2.0 2.1 2.2 2.3
sp1    0.1666 0.1652 0.1554 0.14 0.0896 0.0462 0.0314 0.0311 0.0302
      0.0294 0.0252 0.0224 0.0196 0.0168 0.0126 0.0092 0.0062 0.0028 0
sc2    UNIFORM IN SEED CROSS-SECTIONS
si2    0.028
sc3    UNIFORM IN SEED HEIGHT
si3    0.12
fc8    ELECTRON/PHOTON DOSE [MeV] IN LATTICES ON Y = 0 PLANE
*f8:p,e 11 12 13 14 15 16 17 18 19 20 21 22 23 24 25 26 27 28 29 30
      31 32 33 34 35 36
nps    1.0+6
prdmp  5.0+5 5.0+5 0 0 0
print
```

Chicago 2000 World Congress on Medical Physics and Biomedical Engineering
Chicago, Illinois, July 23–28, 2000; Session Number MO-G 309-4, Intravascular/Prostate 1

Non-Uniformity of Absorbed Dose Due to Curvature of β-Emitter Array In Intravascular Irradiation

Sung-Joon Ye[1], Chan K. Choi[2], and Shahid A. Naqvi[3]

Abstract – **The uniformity of dose delivered to the lesion could be broken in the region of curved coronary vessel. We present the Monte Carlo dose calculations to account for the curvature of vessel and trained seeds. A catheter-based β-emitter system (^{90}Sr/Y) is modeled using the Monte Carlo code, MCNP4B2. Dose distributions are calculated for linear and curved (10° shift between neighboring seeds) cylindrical vessels and then compared along inward-curvature and outward-curvature directions. At the total activity of 70 mCi (2.59×10^9 Bq), the dose in the linear vessel varies from 40.0 to 0.53 cGy/sec as the radial distance (r) from the central axis of seeds increases from 0.64 to 5.4 mm. In the curved vessel, it varies from 41.8 to 0.91 cGy/sec for inward-curvature direction and 39.6 to 0.50 cGy/sec for outward-curvature direction at the same radial distance. In particular, the dose rates at r = 2 mm are: 8.1 cGy/sec in the linear vessel, 10.1 cGy/sec in the inward-curvature (25% overdose compared to that of the linear vessel), and 7.8 cGy/sec in the outward-curvature (4% underdose compared to that of the linear vessel). In the region of interest, r = 2–4 mm, the average inward-overdose and outward-underdose are 28% and 10%, respectively, with respect to those of the linear vessel. The overdose inside the curved seeds is more significant than the underdose outside them. This non-uniformity of dose should be taken into account in both the treatment planning and the design of radioactive seed delivery systems.**

Key words – **Non-uniformity of dose, β-emitter, Monte Carlo, coronary vessel curvature**

I. Introduction

Intravascular brachytherapy (IVBT) is under clinical trials to prevent restenosis following interventional coronary angioplasty.[i] Among the isotopes for potential use in intracoronary irradiation, ^{90}Sr/Y appears to be an ideal source.[ii] For this reason, a catheter-based β-emitter source (e.g., Beta-Cath System, developed by Novoste Corp.) is one of the systems under clinical trials for IVBT. The radiation is supplied by a train source of encapsulated ^{90}Sr/Y seeds. This system is chosen for the investigation, but the methods developed in this project can be generally applied to others. If this state-of-the-art radiotherapy is clinically justified, an established dosimetry routine for the treatment planning of individual patients will immediately be implemented. For the last decade, both analytical and experimental methods have been developed to determine dose distributions in complex treatment geometry such as curvature of vessel, edge of trained seeds, and stent.[iii] However, there are still large uncertainties in the dose calculation due to such complicated treatment geometry. As a preliminary study for Monte Carlo-based dosimetry planning for IVBT, Monte Carlo dose calculations for a simplified linear vessel model with surrounding stent and proximal/distal gold markers were described in the authors' earlier paper.[iv] The actual geometry of the source train is not linear, but rather always curved along the coronary artery. However, current dosimetry protocols do not account for the curvature of vessel and seeds. Due to such simplified calculations, overdose and underdose are expected along inward-curvature and outward-curvature directions, respectively. In this paper, we first calculate this non-uniformity of dose delivery using Monte Carlo simulations.

II. Material and Computational Techniques

The Monte Carlo code, MCNP4,[v] is an excellent choice for the dosimetry calculation of IVBT because it facilitates modeling of complicated geometrical structure to a greater extent than other transport programs. This code has been in development, originally for neutron/photon transport in the Los

[1] Department of Medical Physics, Rush University, Chicago, IL 60612 USA
yesj@therad.rpslmc.edu
[2] School of Nuclear Engineering, Purdue University, West Lafayette, IN 47907 USA
choi@purdue.edu
[3] Department of Radiation Oncology, University of Maryland School of Medicine, Baltimore, MD 21201 USA

Alamos National Laboratory, since the 1940's. It is now applied for coupled neutron/photon/electron transport. A recent release of MCNP, MCNP4B2, uses an improved electron transport algorithm of ITS3.0 (Integrated Tiger Series Version 3.0) to correct the underestimated mean electron energy-loss in the earlier version of ITS1.0.[vi] Its utility for many applications has been already demonstrated in the fields of nuclear and material sciences, high-energy physics, and medical physics.

The actual treatment geometry consists of an encapsulated train of seeds, a guide wire, and a stent in a curved vessel. The source is a cylindrical train of 12 source seeds, each having dimensions of 0.64 mm in diameter and 2.5 mm in length, and proximal/distal gold markers. Each seed contains ^{90}Sr/Y mixed with fired ceramic encapsulated in a 0.04 mm stainless steel wall (Fig. 1). The total activity (sum of activities from the parent isotope, ^{90}Sr, and the daughter isotope, ^{90}Y) of the source train is about 70 mCi (2.59×10^9 Bq).

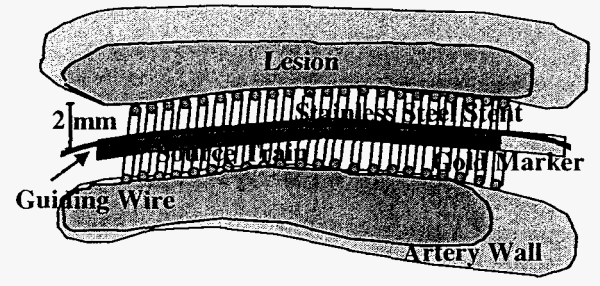

FIGURE 1. Schematic of complete treatment geometry of intravascular brachytherapy using the catheter-based β-emitter source and a surrounding stent.

In this paper, we focus on investigating the dosimetric variations inside and outside the curvature of seeds. The edge effect around the last seed and gold markers and the screening effect from the metallic stent are found in the authors' earlier paper.[iv] Figure 2 shows the MCNP simulation geometry for the curved train of seeds, of which the shift angle between neighboring seeds is 10° toward the positive r-direction. For comparison, a straight linear array of seeds was also simulated to yield the dose in the same size voxels of Fig. 2.

III. RESULTS AND DISCUSSION

The dose in voxels of Fig. 2 was normalized by the total activity of 70 mCi (2.59×10^9 Bq). The radial dose rate distributions of inward- and outward-curvature directions are compared with that of the straight linear vessel model (see Fig. 3). At the total activity of 70 mCi (2.59×10^9 Bq), the dose delivery in the linear vessel varies from 40.0 to 0.53 cGy/sec as the radial distance (r) from the central axis of seeds increases from 0.64 to 5.4 mm. In the curved vessel, they vary from 41.8 to 0.91 cGy/sec for inward-curvature direction and 39.6 to 0.50 cGy/sec for outward-curvature direction at the same radial distance. In particular, the dose rates at $r = 2$ mm are: 8.1 cGy/sec in the linear vessel, 10.1 cGy/sec in the inward-curvature (25% overdose compared to that of the linear vessel), and 7.8 cGy/sec in the outward-curvature (4% underdose compared to that of the linear vessel). The calculated dose rate of the linear vessel model at $r = 2$ mm is only 4% smaller than the vendor-provided value (8.4 cGy/sec), which determined by the source calibration. In the region of interest, r = 2–4 mm, the averaged inward-overdose and outward-underdose are 28% and 10%, respectively, compared to those of the linear vessel. This means that current dosimetry protocols for IVBT neglecting the curvature of vessel could not accurately deliver a prescription dose (15–20 Gy) to the lesion site.

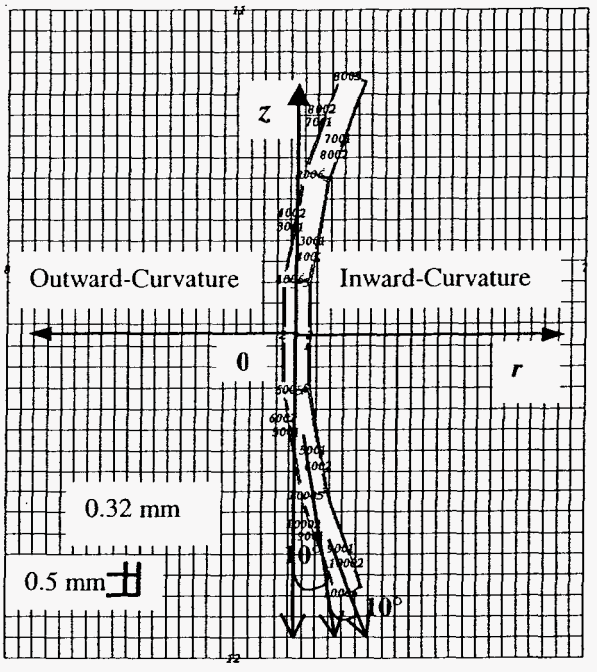

FIGURE 2. Schematic of the MCNP modeling geometry consisting of five seeds (^{90}Sr/Y) and stainless steel wall. Each seed is shifted by 10° from neighboring seeds.

Figure 4 shows the axial dose rate distributions of the linear vessel model (on r-z plane). The dosimetric edge effect started from z = 0.3 cm, which approximately corresponds to the center of the second last seed. The dose at r = 0.2 cm and z = 0.5 cm (at the center of the last seed) is only about 75% of the corresponding non-edge dose. This is because the

voxels in front of the last two seeds could not receive the full dose contribution from neighboring seeds (so called "train effect").

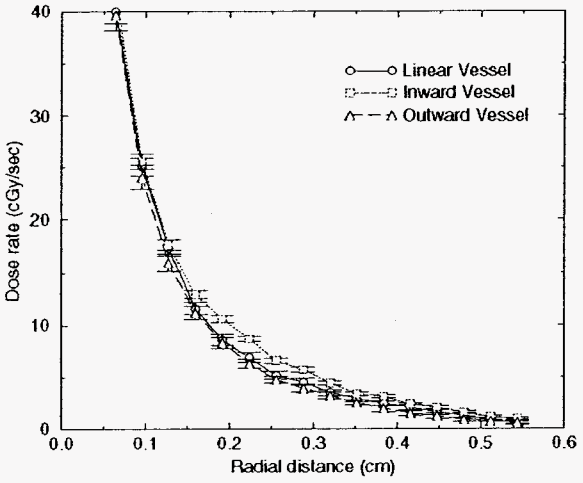

FIGURE 3. Comparison of radial dose rate distributions from the MCNP simulations for both linear and curved vessel models.

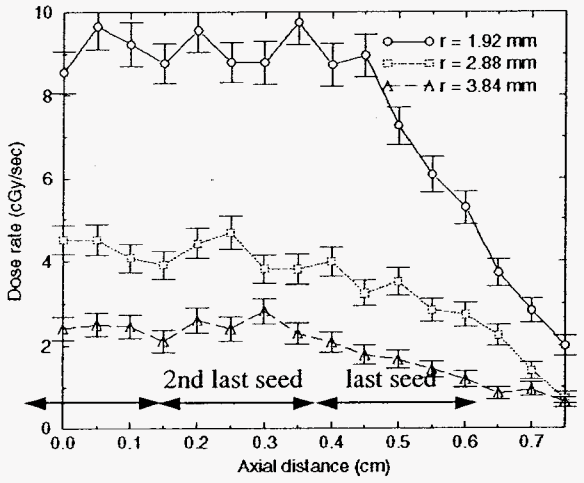

FIGURE 4. Axial dose rate distributions at three different radial distance of linear vessel model.

IV. CONCLUSIONS

The Monte Carlo simulations for the curved or linear geometry in intravascular brachytherapy were very successful in improving the accuracy of the dosimetry. In addition, the dose calculated for the linear vessel model is in a good agreement with the vendor-provided data. The overdose and underdose from the curved structure of the seeds and vessel are significant in the inward- and outward-curvature directions, respectively. The edge effect should be considered in the treatment of lesions site, for which the length is comparable to the source train. A new design study of radiation delivery system will be required to eliminate the dose non-uniformity caused by the curvature of seeds and the edge field.

REFERENCES

[i] R. Waksman, S. B. King, and R. F. Mould, *Vascular Brachytherapy* (Nucletron B.V., The Netherland, 1996).

[ii] H. I. Amols, M. Zaider, J. Weinberger, R. Ennis, P. B. Schiff, and L. E. Reinstein, "Dosimetric considerations for catheter-based beta and gamma emitters in the therapy of neointimal hyperplasia in human coronary arteries," Int. J. Radiat. Onc. Biol. Phys. **36**, 913–921 (1996).

[iii] R. Nath, et al., "Intravascular brachytherapy physics: Report of the AAPM Radiation Therapy Committee Task Group No. 60," Med. Phys. **26**, 119–152 (1998).

[iv] Sung-Joon Ye, X. Allen Li, John R. Zimmer, James C. Chu, and Chan K. Choi, "Dosimetric perturbations of linear array of β-emitter seeds and metallic stent in intravascular brachytherapy," Med. Phys. **27**, 374–380 (2000).

[v] J. F. Briesmeister, "MCNP - A general purpose Monte Carlo *N*-Particle transport code, version 4B," LA-12625-M, Los Alamos National Laboratory, 1997.

[vi] D. W. O. Rogers and A. F. Bielajew, "A comparison of EGS and ETRAN," in *Monte Carlo Transport of Electrons and Photons*, edited by T. M. Jenkins, W. R. Nelson, and A. Rindi (Plenum, New York, 1998).

U.S. DEPARTMENT OF ENERGY'S NUCLEAR ENGINEERING EDUCATION RESEARCH: HIGHLIGHTS OF RECENT AND CURRENT RESEARCH—I

Sponsored by the Fusion Energy Division

Cosponsored by the Isotopes and Radiation Division

Session Organizer: Kathryn McCarthy (INEEL/BWXT)

All Papers Invited

4. The Monte Carlo–Based Dosimetry of Beta Emitters for Intravascular Brachytherapy, *C. K. Choi, J. Son, (Purdue Univ), S. J. Ye (Med Coll of Ohio)*

Intravascular brachytherapy (IVBT) is a new radiotherapy modality to prevent restenosis (re-blockage of the coronary artery) following interventional coronary angioplasty. It is estimated that the restenosis rate may drop from ~35 to 40% to well below 10% if radiation is delivered to the obstruction site during or after angioplasty.

In traditional brachytherapy, the dose is typically specified at 1 cm from the source, and the effects of low-energy photons and secondary electrons are essentially ignored. In IVBT, however, the entire lesion may be 1 to 3 mm in thickness. A better understanding of dosimetry in the millimetre range will help in the development of optimum clinical devices and their efficacious use in different institutions using different radionuclides and devices.

The actual treatment geometry consists of an encapsulated train of seeds, a guide wire, and a stent in a curved vessel. The source is a cylindrical train of 12 source seeds, each having dimensions of 0.64 mm in diameter and 2.5 mm in length, and proximal/distal gold markers. Each seed contains $^{90}Sr/Y$ mixed with fired ceramic encapsulated in a 0.04-mm stainless steel wall. The Monte Carlo simulations are carried out for the trained source geometries in the linear and curved vessels with and without a stent. The stent structure is approximately modeled as a set of tori with a rotational radius of 1.92 mm from the source axis and a circular radius of 0.08 mm in cross section. Five tori are equally spaced for each seed. The stent shadows 31% of the total area of the source surface. The total activity of 70 mCi (2.59×10^9 Bq) was chosen from manufacturer data. The corresponding mass fraction of $^{90}Sr/Y$ in the source ceramic is negligible and was not explicitly included in the MCNP simulations.[1] All tallies were multiplied with 5.83 mCi/seed $\times$ 3.7×10^7 s/mCi for one active seed, and then the tallies that made contributions to the dose in a voxel of interest were summed over to obtain the actual dose for the total activity.

For IVBT with catheter-based systems, the American Association of Physicists in Medicine Task Group 60 (AAPM TG 60) (Ref. 2) recommended that the radiation dose rate be measured at a reference point located at a radial distance of 2 mm from the center of the catheter. The AAPM TG 60 further recommended that the dose rate at that distance be uniform to within ±10% over the centered two-thirds of the treated length and that the relative dose rate in the plane perpendicular to the catheter axis through the center of the source be measured at the distances from the center ranging from 0.5 mm to R_{90} (the distance in water within which 90% of the energy from a point source is absorbed) at intervals of 0.5 mm.

The actual geometry of the source train is not linear but rather always curved along the coronary artery. However, the current dosimetry protocols do not account for the curvature of vessel and seeds. Because of such simplified protocols, the possible overdose and underdose are expected along the inward-curvature and outward-curvature directions, respectively. Figure 1 shows the MCNP simulation geometry for the curved source trains, of which the shifted angles between the neighboring seeds are 5 and 10 deg toward the positive r direction. Thus, two directions are defined as the inward and outward curvatures, respectively.

At the total activity of 70 mCi (2.59×10^9 Bq), the dose delivery in the linear vessel varies from 12.0 to 0.38 cGy/s as the radial distance r from the central axis of seeds increases from 1.5 to 6.0 mm. In the curved vessel, as shown in Fig. 1 for the 10-deg case, the doses vary from 13.5 to 0.54 cGy/s for the inward-curvature direction and 11.8 to 0.37 cGy/s for the outward-curvature direction at the same radial distance. In particular, the dose rates at r = 2 mm are: 8.4 cGy/s in the linear vessel, 8.9 cGy/s in the inward curvature (7% overdose compared to that of the linear vessel), and 7.7 cGy/s in the outward curvature (8% underdose compared to that of the linear vessel). In the region of interest, r = 2 to 5 mm, the averaged inward overdose and outward underdose are 13 and 12%, respectively, compared to those of the linear vessel. This implies that the current dosimetry protocols for IVBT that neglect the curvature of the vessel could not accurately deliver a prescription dose (15 to 20 Gy) to the target site.

The degree of increase and reduction in a 5-deg-shifted vessel is about ±4% at the prescription point (r = 2 mm). However, to achieve the accuracy of ±5% in dosimetry of radiotherapy, the variation by a small degree of curvature (~5 deg) also should be taken into account for dosimetry planning. As mentioned before, in the 10-deg-shifted vessel, the dose levels increase at about ±8% at the prescription point. Therefore, the hot and cold areas will be found because of a partially high degree of curvature in the coronary artery. Figure 2 shows the trend of dose increase and reduction of two-shifted vessel geometries versus radial distance. As radial distance increases beyond r = 3 mm, the degree of increase in the inward curvature is likely to be enhanced, while the degree of reduction in outward curvature is not significant. This is due to a very short range of betas in water (4 mm for 1-MeV electrons).

The simulations for the curved vessel confirm that there exist the hot and cold areas in the treatment region because of a partially high degree of curvature in the coronary arteries. The inward curvature is attributed to an increase in the dose level along the radial distance, while the outward curvature is responsible

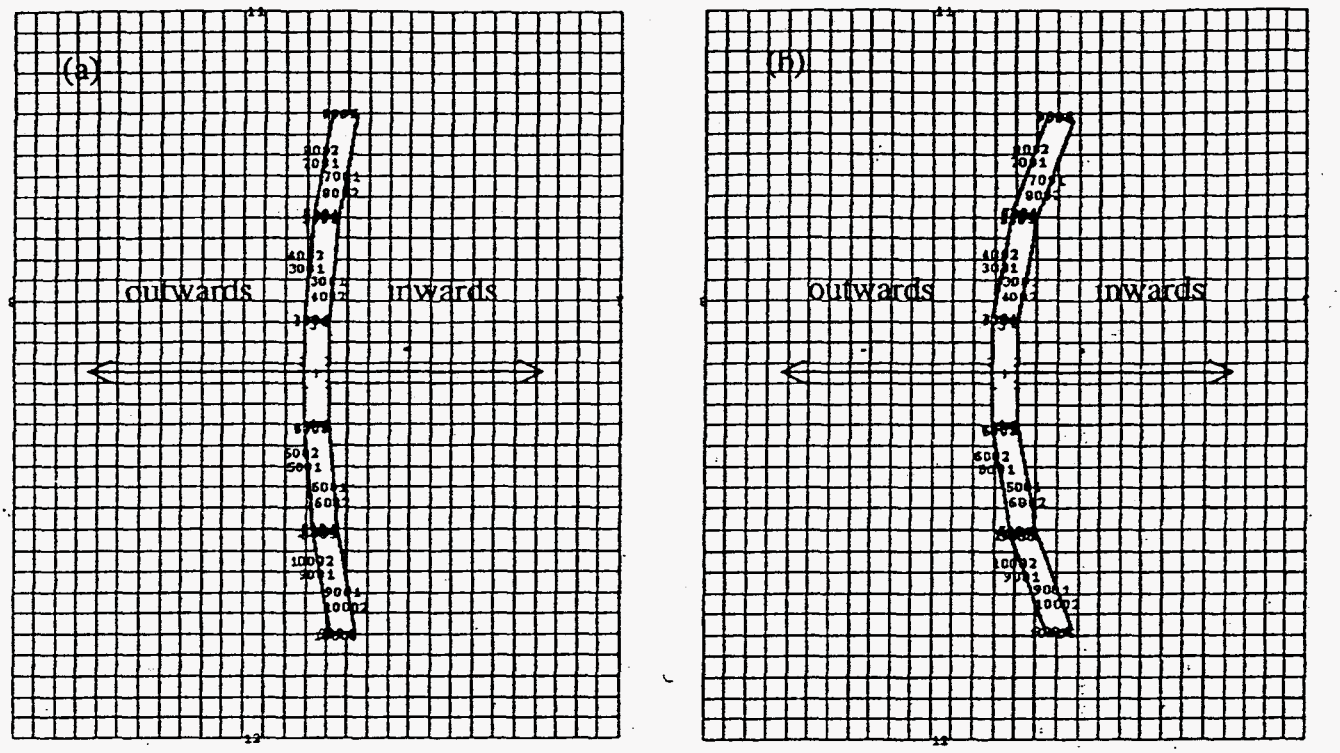

Fig. 1. Schematic of the MCNP modeling geometry for the curved source trains, of which seeds are consecutively shifted by (a) 5 deg and (b) 10 deg, with respect to the neighboring seeds.

for the reduction in the dose level. The dose variations were found to be directly proportional to the angles shifted (e.g., 5 and 10 deg) between the neighboring seeds. Along with the iso-dose distributions in the region of interest, the developed computational algorithm will become the first Monte Carlo–based dosimetry protocol for IVBT for an actual treatment planning platform.

1. "MCNP—A General Purpose Monte Carlo *N*-Particle Transport Code, Version 4B," LA-12625-M, J. F. BRIESMEISTER, Ed., Los Alamos National Lab. (1997).

2. R. NATH et al., "Intravascular Brachytherapy Physics: Report of the AAPM Radiation Therapy Committee Task Group No. 60," *Med. Phys.*, 26, 119 (1999).

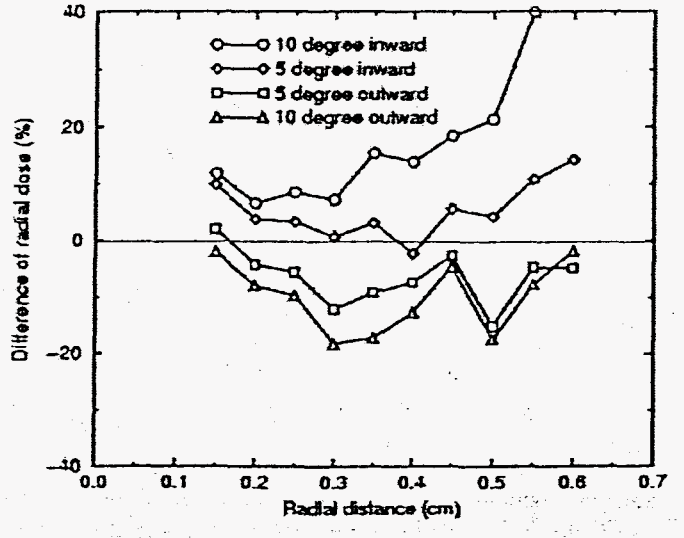

Fig. 2. Radial dose difference of the curved sources from those of the linear source. The dose increase and decrease are expected in the directions inward and outward from the curvature, respectively.